UNIVERSITÀ POLITECNICA DELLE MARCHE

DIPARTIMENTO SCIENZE DELLA VITA E DELL'AMBIENTE

Corso di Dottorato della Facoltà di Scienze
Curriculum Biologia ed Ecologia Marina
XXX Cycle (2014 – 2017)

METABOLIC and REPRODUCTIVE AGING in TELEOSTS

Tesi di dottorato di:

Martina Api

Supervisor:

Prof.ssa Oliana Carnevali

To Davide and my family,

for their endless and priceless support.

Abstract

Aging is defined as a general biological decline with increasing age, caused by an irreversible time-progressive decay in organisms. The phenomenon of aging appears to be a direct function of the metabolic rate and this largely depends on the different animal species, which, in turn, can reflect their reproductive strategy. Much of the research on aging process is focused on a single species however, lifespan in animals varies significantly across different species, and therefore, studies on different short and long-lived species are necessary to shed light on the biological signatures associated to aging.

In the present PhD thesis, focus was addressed on two different fish species: the African killifish, *Nothobranchius furzeri*, considered the shortest-lived vertebrate and to one of the most long-lived pelagic fish, the Atlantic Bluefin tuna (ABFT), *Thunnus thynnus*.

Using annual killifish *N. furzeri* as model to identify the effects of parental aging, in this study was demonstrated that phenotypic plasticity during the embryonic development was affected by parental age influencing the growth process during adult life. Reproductive performance from different-age breeder groups were also studied. Maternal contribution was relevant in terms of embryos quality, resulting in poorest success of embryonic survival and hatching rate from old females. In this species, the results obtained demonstrated that not only the environmental conditions and food availability but also parental age could be a key factor for embryo development as well as for the reproductive process during the adult life.

In the long lifespan species, *Thunnus thynnus*, the growth-at-age was evaluated with different approaches to gain information on aging process during their life. These studies evidenced that in long-lived teleost the ABFT growth rate was higher during the first 8 years of life after which this species use their metabolic energies mainly for adding fat.

Finally, an update on the length/weight relationship of ABFT was provided for stock assessment analysis.

Contents

Introduction

Nature includes an amazing diversity in the lifespan of species with a remarkably diverse trait ranging from insects living one day (e.g. mayflies called "one-day insects") and longest-lived species such as African elephant and Galapagos Giant tortoise which lifespan could reach 70 and 150 years of age respectively, but the mechanism underlying the evolution of lifespan differences remain indefinable.

Short-lived species are considered essential for experimental studies, and central pathways that regulate aging - especially the IGF and mTOR pathways - have been discovered using short lived models, such as yeast, worms, and flies (Kaeberlein and Kennedy, 2011)(Kapahi et al., 2010) (Valenzano et al., 2015).

On the other end of the lifespan range, long-lived species have recently been used in comparative genomic studies to identify genes that are uniquely changed in these organisms (Keane et al., 2015; Seim et al., 2013).

Aging is strictly connected with metabolism, interestingly several genes involved in aging and metabolic pathways are conserved across species to modulate aging. Thus, short and long-lived species can be useful for investigate genes important for lifespan and can also provide new insight for the evolutionary lifespan strategies in nature.

Despite the advances of knowledge, much remains to be learned about the genes that drive natural differences in lifespan and their evolutionary selection into the wild.

A common molecular mechanism of growth and aging: Insulin-like growth factor 1 (IGF-1) and mTOR pathway

Insulin-like growth factor 1 pathway is a conserved pathway that have a broader role in promoting somatic growth, development and survival. Recently it has been showed that this pathway is involved in longevity (Clancy, 2001; Rincon et al., 2004; Roth et al., 2003). The insulin/IGF-I signaling cascade includes insulin, IGF-I, IGF-II, insulin receptor, IGF-I receptor, insulin-like growth factor binding protein (IGFBP) and insulin receptor substrates (IRSs). The insulin/IGF-I signaling is present in vertebrate and has homologous pathways in invertebrates. These receptors regulate various signaling pathways such as PI3K, mTOR and FOXO pathways, through different expression level in organs as well as phosphorylation of different substrates.

The insulin receptor and the IGF-1 receptor share some similarities in structure and in the cascade of events that follow their activation, but their ultimate effect is different: insulin mostly mediates metabolism, while

IGF is essential for growth, development (Dupont and LeRoith, 2001; Receptors et al., 2014) and longevity and there are numerous overlapping functions of both pathways (Kim and Accili, 2002). Furthermore, the IGF family also consists of IGF binding proteins which exert their effects on cell function and growth (Rajah, 1997; Valentinis et al., 1995).

Because of the critical role of these signals in regulating cell growth and metabolism in all life stages, IGFs are excellent candidates to regulate not only the programmed aspects of organismal growth, but also aging.

Reduced insulin/IGF-1-like signaling related to dietary restriction increases longevity in nematodes, fruit flies and mice (Fontana et al., 2010)

Insulin like growth factor 1 pathway is closely linked to Target of Rapamycin (TOR) nutrient-sensitive network and play critical roles in the regulation of growth factors, energy metabolism and longevity (Jia, 2004).

In response to the stimulation of high levels of glucose, amino acids and growth factors, IGF 1 induces the activation of TOR signaling through the phosphoinositide 3-kinase (PI3K)/AKT pathway, resulting in an increase in protein synthesis that in turn promotes cellular mass growth (Hands et al., 2009).

Opposite, during starvation, the lack of nutrients reduced insulin/ IGF-1 signaling and activates AMP protein kinase (AMPK) and a NAD(+)-dependent deacetylases called sirtuins, that suppress the mTOR pathway associated with longevity (Van Heemst et al., 2005).

In cells that lose their proliferative competence when the cell cycle is blocked and growth is inhibited, IGF-1-like signaling leads to cellular aging through de-activation of PI-3K/ mTOR pathway driving cellular senescence (Blagosklonny and Hall, 2009).

In conclusion, growth and aging could appear like a biological paradox: growth is energy-driven synthesis of macromolecules and aging is a physiological decline with loss of energy (Blagosklonny and Hall, 2009), but events that lead to a slowdown in growth also decrease aging and prolong life span.

The molecular pathway that drives both growth and aging may be linked to the same evolutionary conserved Insulin/IGF-1 signaling and TOR pathway.

Growth, aging and longevity

Although species with larger size typically live longer than smaller species, the relationship of body size to longevity does not always correlate with prolonged existence.

Faster growth is often associated with shorter lifespan.

The mechanisms that influence growth and body size with a possible impact on aging and lifespan are not yet fully understood. Available data suggests that normal growth involves some intrinsic "costs" that predispose the organism to aging (Bartke, 2017).

Mechanisms linking somatic growth, body size, aging, and lifespan are also influenced by a variety of hormonal, metabolic and nutritional signals, and could influence growth with a secondary impact on aging and lifespan via different signaling pathways.

The reason why larger animals seemed to live longer than others, was suggest by the physiologist Max Rubner in 1908, who postulates the "Rate-of-living theory" demonstrating in smaller size animals that a faster organism's metabolism conducts to a shorter lifespan.

Moreover, aging and DNA repair rate have been related to body size (MacRae et al., 2015; Promislow, 1994; Petralia et al., 2015). The DNA repair capacity apparently is more efficient in longer-living mammals supporting the correlation between DNA repair and longevity in bigger animals. Therefore, body size is a factor that comparative studies of aging should take into consideration (de Magalhes, 2006).

Teleost fishes as model for aging studies

In the past century, progress in knowledge of aging has been largely linked to the animal models such as the most common *Mus musculus* (mouse), *Caenorhabditis elegans* (worm) and *Drosophila melanogaster* (fly). Both invertebrates have a short life span, but a great evolutionary distance from mammals, lacking of specific organs and systems (e.g. blood, immune system and bones). Although the mouse has historically been the aging model par excellence, mammals in general also give birth to relatively few offspring at a time, they have an internal fertilization and it is impossible to observe the embryonic development, hampering the monitoring throughout their life cycle.

Fish are considered excellent models for comparative studies of aging, since several studies demonstrated age-dependent degeneration markers of cellular senescence in different fish tissues and the same age-related pathological process described as in mammals and higher vertebrates (Terzibasi et al., 2007). Moreover, the phylogenetic distance between vertebrate and human is close and fish constitute the largest group of vertebrates and within this group there are a wide species that differ in terms of lifespan (Lucas-Sánchez et al., 2014). Finally, the longevity of different fish species could be easily manipulated by water temperature, dietary restriction. Moreover, space available in the environment and reproductive opportunities are also traits to be consider.

Reproductive aging studies

The evolutionary phenomena of reproductive aging are part of the normal program of reproduction in all organism since survival of a population requires a balance between mortality and reproductive rates that maintains the survival of a species.

Aging in reproductive functions is a natural characteristic present in all organism that could differ in mechanisms and effects in male and female. In both males and females, aging could affect physical, behavioral and physiological changes that can lead to a decrease in reproductive fitness.

Some males, in contrast to females, remain reproductively competent during their whole lifespan and females show substantial differences in timing and events associated with the age-related loss of reproductive senescence.

The advantages of fish models in reproductive senescence studies consists in (1)the characteristic external fertilization, (2)the production of a large number of offspring and (3)the easily visualized embryonic development that cannot be addressed in mammals for example, in humans.

Moreover, fish represents an excellent animal model in reproduction investigation by the possibility to explore gametogenesis studying oocytes at different stages.

The ability of an oocyte to develop into a viable embryo depends on the accumulation of specific maternal information and molecules. Oocyte competence is characterized by accumulation of specific maternal RNAs, proteins (including growth and transcription factors), lipids, vitamins and hormones.

In long-lived fish, fecundity increases with continued growth with no indication of reproductive senescence, instead little is known about reproductive senescence in fish which lifespan is less of 5 years (vom Saal et al., 1994). Deeper studies are needed to better understand the biochemical, physiological and molecular mechanism on reproductive aging using short lifespan fish as model and in the present thesis, focus was addressed to *Nothobranchius furzeri* reproduction.

Nothobranchius furzeri: the shortest-lived vertebrates

In 2003 Cellerino and Valdesalici suggested the killifish from the genus *Nothobranchius* as a potential fish model for aging studies (Valdesalici and Cellerino, 2003).

The African turquoise killifish *Nothobranchius furzeri* is a naturally short-lived vertebrate that inhabits seasonal freshwater ponds in the southeast of Africa from regions characterized by an alternate arid and rainy season where water is produced by brief seasonal rains.

Several laboratory strains exist, captured at different geographic locations and lifespan ranging from the shorter life expectancy of about 13 weeks (GRZ strain from semi-arid habitat) to the longest life expectancy of about 24 weeks (MZM strain from humid region) (Terzibasi et al., 2008; Tozzini et al., 2013).

Reproductive strategies in *Nothobranchius furzeri*

N. furzeri is a gonochoristic teleost (testes and ovaries are in separate individuals) with both ovaries asynchronous in females. Sex is genetically determined (Valenzano et al., 2009) and sexual dimorphism was evident after reaching sexual maturity at about 6 weeks post hatching (Genade et al., 2005).

Females are normally smaller than males and present a grey color while males are colorful with a yellow or red fin, depending on specific strain.

Mating system is promiscuous, males potentially fertilize the eggs of several females but each female is fertilized by only one male.

Due to temporary habitat in which they live, these fish are adapted an unusual reproductive strategies to survival before their seasonal habitat disappears (arid season), by developing embryos that are resistant to desiccation.

During the rainy season, when the water pools are formed, the adult males stimulate the mature females to lay eggs and the fertilized eggs are then buried in the muddy bottom. Once the puddle dries up, during the arid season, the embryos survive encased in the dry mud and they enter into a state of diapause. Hatching happens when the new rainy season begins and ponds are formed once again: a new cycle starts (Genade et al., 2005).

As a result of the adaptation to the ephemeral nature of the habitat, *Nothobranchius furzeri* is characterized by rapid growth, early sexual maturation and an exceptional short lifespan that allow its survival (Blažek et al., 2013.; Cellerino et al., 2016; Genade et al., 2005).

Embryonic development and diapause

In annual fish, embryogenesis could be characterized by “diapause” that affects the length of embryonic development. Diapause is defined as a temporary developmental arrest with a dramatic reduction in metabolic rate which can occur at two/three stages:, diapause I and diapause III, diapause II optional (Cellerino et al., 2016). Diapause I occurs during epiboly, the optional diapause II could occur during the segmentation period and diapause III happens at pre-hatching stage in embryos ready to hatch (Arezo et al., 2005). Embryos that bypass diapause II are defined “escape embryos”, while embryos that enter into diapause II are defined “diapausing embryo” (Podrabsky et al., 2010) and follow different developmental pathways to the timing of

an embryos trajectory. These different developmental trajectories are a special embryos adaptation to face unpredictable environmental during arid season and allow them to survive during the desiccation of their habitat.

Applications for aging studies

This peculiar short lifespan of both GRZ and MZM strains, makes these fish especially attractive for aging studies showing the typical age-dependent phenotypes (e.g. loss of color and body mass, curvature of the dorsal spine and deterioration of caudal fin) accompanied by aging-related diseases throughout organismal lifespan (Genade et al., 2005). These characteristics, combined with the fact that they are small vertebrates and can be bred easily in the laboratory, make this fish an attractive model organism to study vertebrate aging (Di Cicco et al., 2011).

Although only few laboratory are currently analyzing aging in *Nothobranchius furzeri,* the recent results obtained in this species are creating the prerequisites for considering *N. furzeri* a very attractive model for future aging studies.

Long-lived organisms: growth and age of Bluefin tuna fish *Thunnus thynnus*

Among vertebrates, marine fish are considered one of the longest-lived species including sharks that can live over 400 years. Among the largest and highly-valued members of the marine fish we found the Atlantic Bluefin tuna (*Thunnus thynnus*) and 40 years old the maximum age registered. The largest Atlantic Bluefin tuna (ABFT) caught off was 679 kg of weight and among the several tuna species (Scombridae, Thunnini) found worldwide, bluefin tunas is one of the largest (Collette et al. 2001).

Then, given the peculiar body size, their lifespan biological data and growth rate are needed. Moreover, information on age and growth for commercial fish species are very important for the stock assessment. Despite the importance of these evidence, the bluefin tuna population has suffered of a lack of information until relatively recent times. Mainly, the age and growth of ABFT could be estimated by direct measurements of fish length and/or weight over time or using hard structures such as caudal vertebrae, otoliths or dorsal fin spines (Ruiz and Landa, 2002). Otoliths are the most widely used hard structure to determine age of teleost fish since their composition can provide information about the growth rate of the full life history. This technique is based on counting periodic growth marks (annuli) from all size and age classes of tuna specimens and it is also potentially applicable to very old and large fish (Campana, 2001). Results from tuna have shown

a maximum ABFT age exceeding over 40 years (Secor et al., 2008). In most *Thunnus* species, studies on gender-specify growth rate found a relevant number of males reaching larger sizes than females. This could be due to an higher cost of reproduction energy request in females than in male leading to slower growth rates after maturity (Gunn et al., 2008). Many studies on growth rate have improved estimates of growth and size of Atlantic Bluefin tuna, but further research is needed to improve the knowledge on all life traits and the evolutionary process of lifespan among *Thunnus* species.

ICCAT

Tunas are highly migratory species and an international cooperation for a suitable tunas control were required in the past.

The International Commission for the Conservation of Atlantic Tunas (ICCAT) is the fisheries organization for the protection and management of several tunas species, since 1969.

The Commission undertakes studies and research on biometry, ecology and oceanography with a special focus on the effects of fishing on stock abundance.

Thanks to financial support by Ministry of Agriculture, Food and Forestry Policies (MIPAAF), we was able to conduct studies on tunas current stock conditions (2015-2016) related to this PhD project.

References

Arezo, M.J., Pereiro, L., Berois, N., 2005. Early development in the annual fish Cynolebias viarius. J. Fish Biol. 66, 1357–1370.

Bartke, A., 2017. Somatic growth, aging, and longevity. Aging Mech. Dis. 3, 14.

Blagosklonny, M. V., Hall, M.N., 2009. Growth and aging: a common molecular mechanism. Aging (Albany. NY). 1, 357–362.

Blažek, R., Polačik, M., Reichard, M., 2013. Rapid growth, early maturation and short generation time in African annual fishes. *EvoDevo,* 4-24.

Campana, S.E., 2001. Accuracy, precision and quality control in age determination, including a review of the use and abuse of age validation methods. J. Fish Biol. 59, 197–242.

Cellerino, A., Valenzano, D.R., Reichard, M., 2016. From the bush to the bench : the annual Nothobranchius fishes as a new model system in biology 91, 511–533.

Clancy, D.J., 2001. Extension of Life-Span by Loss of CHICO, a Drosophila Insulin Receptor Substrate Protein. Science. 292, 104–106.

De Magalhães J.P. 2006. Species Selection in Comparative Studies of Aging and Antiaging Research. Handb. Model. Hum. Aging 9–20. doi:10.1016/B978-012369391-4/50003-5

Di Cicco, E., Tozzini, E.T., Rossi, G., Cellerino, A., 2011. The short-lived annual fish Nothobranchius furzeri shows a typical teleost aging process reinforced by high incidence of age-dependent neoplasias. Exp. Gerontol.

Dupont, J., LeRoith, D., 2001. Insulin and Insulin-Like Growth Factor I Receptors: Similarities and Differences in Signal Transduction. Horm. Res. Paediatr. 55(suppl 2), 22–26.

Fontana, L., Partridge, L., Longo, V.D., 2010. Extending Healthy Life Span--From Yeast to Humans. Science (80-.). 328, 321–326.

Genade, T., Benedetti, M., Terzibasi, E., Roncaglia, P., Valenzano, D.R., Cattaneo, A., Cellerino, A., 2005. Annual fishes of the genus Nothobranchius as a model system for aging research. Aging Cell 4(5), 223-233

Gunn, J.S., Clear, N.P., Carter, T.I., Rees, A.J., Stanley, C.A., Farley, J.H., Kalish, J.M., 2008. Age and growth in southern bluefin tuna , Thunnus maccoyii (Castelnau): Direct estimation from otoliths , scales and vertebrae 92, 207–220.

Hands, S.L., Proud, C.G., Wyttenbach, A., 2009. mTOR's role in ageing: protein synthesis or autophagy? Aging (Albany. NY). 1, 586–597.

Jia, K., 2004. The TOR pathway interacts with the insulin signaling pathway to regulate C. elegans larval development, metabolism and life span. Development 131, 3897–3906.

Kaeberlein, M., Kennedy, B.K., 2011. Hot topics in aging research: Protein translation and TOR signaling, 2010. Aging Cell 10, 185–190.

Kapahi, P., Chen, D., Rogers, A.N., Katewa, S.D., Li, P.W.L., Thomas, E.L., Kockel, L., 2010. With TOR, less is more: A key role for the conserved nutrient-sensing TOR pathway in aging. Cell Metab. 11, 453–465.

Keane, M., Semeiks, J., Webb, A.E., Li, Y.I., Quesada, V., Craig, T., Madsen, L.B., van Dam, S., Brawand,

D., Marques, P.I., Michalak, P., Kang, L., Bhak, J., Yim, H.S., Grishin, N. V., Nielsen, N.H., Heide-Jørgensen, M.P., Oziolor, E.M., Matson, C.W., Church, G.M., Stuart, G.W., Patton, J.C., George, J.C., Suydam, R., Larsen, K., López-Otín, C., O'Connell, M.J., Bickham, J.W., Thomsen, B., deMagalhães, J.P., 2015. Insights into the evolution of longevity from the bowhead whale genome. Cell Rep. 10, 112–122.

Kim, J.J., Accili, D., 2002. Signalling through IGF-I and insulin receptors: where is the specificity? Growth Horm. IGF Res. 12, 84–90.

Lucas-Sánchez, A., Almaida-Pagán, P.F., Mendiola, P., de Costa, J., 2014. Nothobranchius as a model for aging studies. A review. Aging Dis. 5, 281–91.

MacRae, S.L., Croken, M.M.K., Calder, R.B., Aliper, A., Milholland, B., White, R.R., Zhavoronkov, A., Gladyshev, V.N., Seluanov, A., Gorbunova, V., Zhang, Z.D., Vijg, J., 2015. DNA repair in species with extreme lifespan differences. Aging (Albany. NY). 7, 1171–1184.

Podrabsky, J.E., Garrett, I.D.F., Kohl, Z.F., 2010. Alternative developmental pathways associated with diapause regulated by temperature and maternal influences in embryos of the annual killifish Austrofundulus limnaeus. J. Exp. Biol. 213, 3280–8.

Promislow, D.E., 1994. DNA repair and the evolution of longevity: a critical analysis. J. Theor. Biol. 170, 291-300.

Rajah, R., 1997. Insulin-like Growth Factor (IGF)-binding Protein-3 Induces Apoptosis and Mediates the Effects of Transforming Growth Factor-beta 1 on Programmed Cell Death through a p53- and IGF-independent Mechanism. J. Biol. Chem. 272, 12181–12188.

Receptors, I., Nakae, J.U.N., Kido, Y., Accili, D., Berrie, N., Physicians, C., Columbia, S., 2014. Distinct and Overlapping Functions of Insulin and IGF-1 Receptor. Endocr Rev. 22, 818–835.

Rincon, M., Muzumdar, R., Atzmon, G., Barzilai, N., 2004. The paradox of the insulin/IGF-1 signaling pathway in longevity. Mech. Ageing Dev. 125, 397–403.

Ronald S. Petralia, Mark P. Mattson, and P.J.Yoo, 2015. Ageing and longevity in the simplest animals and the quest for immortality. Ageing Res Rev 66–82.

Roth, G.S., Ingram, D.K., Lane, M.A., Acad, A.N.Y., Tatar, M., Bartke, A., Antebi, A., 2003. The Endocrine Regulation of Aging by Insulin-like Signals 299, 1346–1352.

Ruiz, P.M., Landa, J., 2014. Protocol for sampling of hard parts for bluefin tuna (Thunnus thynnus) growth studies Collect. Vol. Sci. Pap. ICCAT, 70, 380-393.

Secor, D.H., Wingate, R.L., Neilson, J.D., Rooker, J.R., Campana, S.E., 2008. Growth of Atlantic bluefin tuna: direct age estimates. Iccat, Scrs/2008/084 64, 1–14.

Seim, I., Fang, X., Xiong, Z., Lobanov, A. V., Huang, Z., Ma, S., Feng, Y., Turanov, A.A., Zhu, Y., Lenz, T.L., Gerashchenko, M. V., Fan, D., Hee Yim, S., Yao, X., Jordan, D., Xiong, Y., Ma, Y., Lyapunov, A.N., Chen, G., Kulakova, O.I., Sun, Y., Lee, S.-G., Bronson, R.T., Moskalev, A.A., Sunyaev, S.R., Zhang, G., Krogh, A., Wang, J., Gladyshev, V.N., 2013. Genome analysis reveals insights into physiology and longevity of the Brandt's bat Myotis brandtii. Nat. Commun. 4, 1–8.

Terzibasi, E., Valenzano, D.R., Benedetti, M., Roncaglia, P., Domenici, L., Cellerino, A., 2008. Large Differences in Aging Phenotype between Strains of the Short-Lived Annual Fish Nothobranchius furzeri. PLOSone, 12, 1-13.

Terzibasi, E., Valenzano, D.R., Cellerino, A., 2007. The short-lived fish Nothobranchius furzeri as a new model system for aging studies. Exp. Gerontol. 42, 81–9.

Tozzini, E.T., Dorn, A., Ng, E., Pola, M., Bla, R., Reichwald, K., Petzold, A., Watters, B., Reichard, M., Cellerino, A., 2013. Parallel evolution of senescence in annual fishes in response to extrinsic mortality. BMC Evo Biol, 13-77.

Valdesalici, S., Cellerino, A., 2003. Extremely short lifespan in the annual fish Nothobranchius furzeri. Proceedings. Biol. Sci. 270 Suppl 2, S189-91.

Valentinis, B., Bhala, A., DeAngelis, T., Baserga, R., Cohen, P., 1995. The human insulin-like growth factor (IGF) binding protein-3 inhibits the growth of fibroblasts with a targeted disruption of the IGF-I receptor gene. Mol. Endocrinol. 9, 361–367.

Valenzano, D.R., Kirschner, J., Kamber, R.A., Zhang, E., Weber, D., Cellerino, A., Englert, C., Platzer, M., Reichwald, K., Brunet, A., 2009. Mapping Loci Associated With Tail Color and Sex Determination in the Short-Lived Fish Nothobranchius furzeri. Genetics, 183,1385-95.

Valenzano, D.R., Singh, P.P., Beyer, A., Johnson, E. a, Brunet, A., 2015. The African Turquoise Killifish Genome Provides Insights into Evolution and Genetic Architecture of Resource The African Turquoise Killifish Genome Provides Insights into Evolution and Genetic Architecture of Lifespan . Cell, 6, 1539-54.

Van Heemst, D., Beekman, M., Mooijaart, S.P., Heijmans, B.T., Brandt, B.W., Zwaan, B.J., Slagboom, P.E., Westendorp, R.G.J., 2005. Reduced insulin/IGF-1 signalling and human longevity. Aging Cell 4, 79–85.

vom Saal, F.S., Finch, C.E., Nelson, J.F., 1994. Natural History and Mechanisms of Reproductive Aging in Humans, Laboratory Rodents, and Other Selected Vertebrates. Physiol. Reprod.

Aim of the study

The general aim of my PhD project is to improve the knowledge on aging effects on growth and reproduction in adult and offspring focusing on liver and gonads. We used as experimental models the African killifish *Nothobranchius furzeri*, an extraordinary teleost with the shortest lifespan between vertebrates and adults at different age of Atlantic Bluefin tuna (*Thunnus thynnus),* one of the most fascinating species with high commercial value around the world between the large pelagic fish living in the Atlantic Ocean and Mediterranean Sea.

Objectives:

Task 1.Using annual killifish, *Nothobranchius furzeri* as model, to identify the effects of parental aging, the following objectives were considered:

- Determine the parental aging effects on fecundity and embryos development;
- Determine the parental aging trans generational effects on metabolism and reproduction of F1 adult;
- Determine the female aging effects on oocytes quality.

Task 2.Using Atlantic bluefin tuna, *Thunnus thynnus* as model, growth at different age was studied, the following objectives were considered:

- Determine tuna age and identify the correlation between growth-at-age in bluefin tuna;
- Obtain partial gene sequences from tuna transcriptome using genomics tool;
- Evaluate the expression of the IGF system and mTOR genes to gain information on growth process at different age ;
- Update on the length/weight relationship of ABFT caught by longlines in Mediterranean sea for stock assessment analysis.

To achieve these objectives, this PhD thesis is organized in 5 main chapters; the Chapter 1, 2 and 3 are related to aging effects using the killifish *Nothobranchius furzeri* as model, the last two chapter, Chapter 4 and 5, involve Atlantic Bluefin tuna *Thunnus thynnus* studies.

In *Chapter 1* was characterized the effects of parental aging on embryonic development and adult traits using *Nothobranchius furzeri* as model.

In *Chapter 2* was examined the effects of mating breeders at different age focusing on reproductive fitness and offspring gametogenesis in females using *Nothobranchius furzeri* as model.

In *Chapter 3* was determined the female aging effects on oocytes quality by Raman microspectroscopy in *Nothobranchius furzeri.*

In *Chapter 4* was evaluated the differences in terms of growth rate at different age in *Thunnus thynnus.*

In *Chapter 5* was provided a validate length-weight equation to be used for the next stock assessment of the Mediterranean Bluefin tuna, *Thunnus thynnus*. The equation we elaborated and presented at the Standing Committee on Research and Statistics (SCRS) in 2016 were included in the final equation adopted by ICCAT.

Chapter 1

Published in ZEBRAFISH Journal: **doi.org/10.1089/zeb.2017.1494**

Effects of parental aging during embryo development and adult life: the case of *Nothobranchius furzeri*

Martina Api [1], Piera Biondi [1], Ike Olivotto [1], Eva Terzibasi Tozzini [2], Alessandro Cellerino [2] and Oliana Carnevali [1]

[1] Department of Life and Environmental Science, Università Politecnica delle Marche, Via Brecce Bianche, 60131 Ancona, Italy.
[2] Scuola Normale Superiore, Pisa, Italy.

Corresponding Author: Prof. Oliana Carnevali, Dipartimento di Scienze della Vita e dell'Ambiente, Università Politecnica delle Marche, Via Brecce Bianche, 60131 Ancona, Italy
e-mail: o.carnevali@univpm.it tel +390712204990, fax +390712204650

Key words: IGF system, transgenerational effects, killifish, embryo development plasticity, diapause

Abstract

Studies on parental aging are a very attractive field although it is poorly understood how parental age affects embryonic development and adult traits of the offspring.

In this study, we used the turquoise killifish *Nothobranchius furzeri,* as is the vertebrate with shortest captive lifespan and an interesting model.

The embryos of *N. furzeri* can follow two distinct developmental pathways either entering diapause or proceeding through direct development. Thus, this embryonic plasticity allows this model to be used to study different factors that could affect their embryonic development including parental age.

The first goal of the present study was to investigate whether parental aging could affect the embryo development. To do this, we collected F1 embryos from two breeder groups (old parents and young parents). We monitored the duration of embryonic development and analyzed genes involved in dorsalization process. The second goal was to investigate if embryonic developmental plasticity could be modulated by an epigenetic process. To this end, the expression of *DNMTs* genes was examined. Our data support the hypothesis that diapause, occurring more frequently in embryos from old parents, is associated with increased expression of *DNMT3A* and *DNMT3B* suggesting an epigenetic control.

Finally, we analyzed whether parental age could affect metabolism and growth during adult life. Morphometric results and qPCR analysis of genes from IGF system showed a slower growth in adults from old breeders. Moreover, a gender-specificity effect on growth emerged.

In conclusion, these results may contribute to the better understand the complex mechanism of aging.

INTRODUCTION

For years, researches have tried to uncover the underlying biological processes responsible for aging wondering whether aging is the primary result of an evolutionary process that confers some benefit [1] or it is the result of the age-dependent decline in the force of selection and of antagonistic pleiotropism between developmental and repair processes, as stated by the classical theories of aging [2–5]. It has recently been argued that the progression of the aging process is influenced by developmental events [6]. Indeed, the theory of antagonist pleiotropism postulates that the same alleles that confer an advantage during development and maturation are deleterious late in life. These constraints most likely represent the major determinants of the aging process as a progressive decline of physiological functions, an intrinsic age-related process of loss of viability and increase in vulnerability. Also perturbations of developmental processes can influence aging. For examples, prenatal stress predisposes to negative late-life events [7,8].

Parental age effects are now known to have an impact on offspring longevity [9] and have indeed long been in the list of explanations related to the large set of causations for aging [10].

Reduction in offspring longevity due to maternal age is widely known as the ‘‘Lansing effect’’ [11]. This author viewed aging as the consequences of a “factor” that is transmitted from parent to offspring through the egg, concluding that the older the parent, the more the aging factor is transmitted to the next generation [12].

Although parental effects are known to have an important role in the development of offspring, we know little about the mechanisms responsible for parental effects on offspring adult traits especially in vertebrates while in the invertebrate models *C. elegans*, transgenerational epigenetic influence on aging is well described [13].

In this paper, we examine the transmitted effect of parental age on offspring adult traits using the turquoise killifish *Nothobranchius furzeri*. African annual killifish from the genus Nothobranchius are the vertebrate species with the shortest lifespan recorded in captivity [14–16]. Here, we study *Nothobranchius furzeri* MZM 0410 strain whose median lifespan is in the order of 6-7 months. This makes this species particularly suited for investigating the effects of experimental manipulations on biological and molecular variables across the whole life cycle, from embryos to adult life, and through multiple generations in a short time. Annual killifish embryos are capable of undergoing diapause, that is a developmental arrest associated with lower metabolic activity [17,18]. This could occurs at three specific stages - termed diapause I, II, and III related to environmental conditions (dry and wet season) and temperature [3,19–21]

The embryos from *N. furzeri*, and other annual killifish, are able to avoid developmental arrest in diapause I, II and III giving rise to different developmental pathways [17,18,21] . Thus, this model can be conveniently used to study factors that could affect embryonic development, such as parental age. Notably, it was previously

reported that parental age influences developmental speed in annual fishes [17,22] but the transgenerational consequences of parental age were never investigated before.

The aims of the present study were to test whether parental age (of both mother and father) affects the speed of embryonic development. To this end, we collected embryos from parents at different ages and studied the embryo dorsalization process together with developmental plasticity associated with expression of epigenetic modulators, such as DNA methyltransferases (*DNMT*s) genes.

Finally, we focused our attention on metabolism and growth in adult life by quantifying expression of genes related to the IGF pathways in the offspring from young and old parents. The age at which we chose to sampling F1 adult fish was 6 weeks post hatching (wph) when individuals reach sexual maturity [23] .
In conclusion, this study provides a better understanding of the complex mechanisms of aging, focusing on the effects of parental aging on offspring growth.

MATERIALS and METHODS

Ethics

All the procedures involving animals were conducted according to Italian law on experimental animals and were approved by the Health Ministry's Department of Veterinary Public Health and by the Ethics Committee of Università Politecnica delle Marche (Authorization No. 852/2016-PR).

Optimal rearing conditions were applied throughout the study and all efforts were made to minimize animal suffering by using an excess of anesthetic (MS222, Sigma Aldrich, Milano, Italy).

Fish maintenance and breeder groups formation

Nothobranchius furzeri, strain MZM 0410, were cultured according to the manual for caring *N. furzeri* [24].
A total of 48 female/male adults from *N. furzeri* were placed in twelve aquaria of 20-L (4 fish/tank) with oxygenated water under controlled conditions (26 ± 0.5 °C) with a daily water changes of 10% and maintained on a 12/12 h light/dark cycle. They were fed twice times a day with *Chironomus chironominae* larvae and *Artemia salina* nauplii.
After 6 weeks post hatching (wph), when adult fishes reached sexual dimorphism and maturity, breeding groups were formed, crossing 1 male and 3 females, in each tank.
Three different groups were formed with 8 wph, 14 wph and 20 wph age.
The group with male and females at 14 wph age, were used to generate embryo developmental table.

The 8 wph breeder group were used as young breeders while the group of 20 wph age as old breeders.
All the experiments were conducted in quadruplicate.

Embryo collection

Embryos were maintained at same environmental conditions as adults (26 ± 0.5 °C fresh water) and were daily visually inspected under a stereo microscope to check and discard death embryos.
Embryos from 14 wph parents were sampled at 0, 3, 4, 5, 24 hours post fertilization (hpf), 2, 5, 6, 7, 9, 11, 13, 14, 24 days post fertilization (dpf) and hatching to describe the developmental process.
Additional embryos from 8 and 20 wph parents were sampled to compare the development in these two groups at 8 and 12 days post fertilization.
Embryos from young and old parents were also collected at 4, 5 and 6 dpf for q-PCR analyses.

Morphological analysis

To ensure developmental synchronization, embryos at 3 hpf presenting the formed blastodisc were selected from 8 wph and 20 wph parents age, incubated at 26 ± 0.5 °C fresh water and sampled at 8 and 12 dpf. All the embryos (about 200 for group) were observed under a stereo microscope (Optika SZM-2), photographs were taken with a Optikam B5 digital camera by its associated image acquisition software (Optika Vision Lite 2.13).

Morphometrical analysis

The total length of F1 adults were measured using a 200 mm length calipers (Mini Vernier Calipers 1 mm/mini Ruler Micrometer) from the upper lip to the end of the caudal fin and wet weight was determined using a precision balance (RADWAG PSC/C2, Poland).

RNA extraction and cDNA synthesis

RNA were extracted from total body embryo derived 8 and 20 wph parent age at 4, 5 and 6 dpf as well as from F1 adult's (6 wph) liver using RNAzol solution (Sigma-Aldrich) according to the manufacturer's instructions. RNA was eluted in 10 µl of RNAse-free water. Final RNA concentrations was determined using the Nanophotometer TM P-Class (Implem GmbH, Mönich, Germany) while its integrity was verified by GelRed staining of 28S and 18S ribosomal RNA bands on 1% agarose gel. RNA was stored at -80 °C until use. A total amount of 1 µg of RNA was used for cDNA synthesis with iScript cDNA Synthesis Kit (Bio-Rad, Milano, Italy), and then kept at -20 °C until use.

Real-Time PCR

Relative quantification of gene expression was performed with the SYBR Green method in an iQ5 iCycler thermal cycler (Bio-Rad laboratories).

All samples were analyzed in triplicates and the final volume of each reaction was 20 µl. Reactions contained 1 µl cDNA diluted 1/10, 5µl 2X SYBR Green PCR Master Mix (Bio Rad) containing SYBR Green as a fluorescent intercalating agent, 0.1 µM of forward and reverse primers and 3.8 µl of milliQ water. The reactions were set following Miccoli [25].

Real-time PCR conditions were optimized after various trials at different times and temperatures. The internal reference, chosen with the aim of standardizing the results by eliminating variations in mRNA and cDNA quantity and quality, was the 18S rRNA. The data obtained were analyzed using the iQ5 optical system software version 2.0 (Bio-Rad laboratories). The species-specific primers sequences for *chordin, goosecoid, dnmt3a, dnmt3b, igf1, igf1-ra, ir, igfbp2* and *igfbp3* were designed using Primer3 (210 v. 0.4.0). Primer sequences are reported in Table 1.

Histology and lipid content

Six samples of whole liver from 8 and 20 wph parental age experimental group were sampled and fixed by immersion in 4% paraformaldehyde and stored overnight at 4°C. Samples were then washed in PBS 0.1 M, dehydrated by subsequent washing in a graded series of alcohol concentrations and embedded in liquid paraffin (Bio-Optica, Milano, Italy).

From each sample, slides of 5 µm sections was obtained using microtome (Leitz 1512) and stained with Mayer's hematoxylin and eosin Y (Sigma-Aldrich). Sections were examined using Zeiss Axioskop optical microscope connected with a camera Canon EOS 6D.

Hepatocytes vacuolization was measured to estimate lipid content in the liver, as described by Papadakis [26]. Microphotographs were used from different areas of the liver (n = 3) of each specimen (n = 6) from the two groups. The area covered with lipid vacuoles (ACLV %) in each microphotograph was calculated automatically by Image J ver. 1.49.

Statistical analysis

Results obtained by q-PCR analysis between two experimental groups have been processed with a grouped analyses Two-Way ANOVA with two data sets. Values were compared regardless of experimental group and developmental stages. Multiple comparisons were corrected with the Tukey test and the confidence interval was set at 95% ($p < 0.05$).

Concerning the outputs of the duration of embryonic development in aqueous-phase analyses, the statistical difference was tested by the Student's t-test. Groups were considered significantly different if $p < 0.05$.
All statistical analyses were performed using Prism 6 (GraphPad Software, San Diego, CA, USA).

RESULTS

Stages of embryonic development in *Nothobranchius furzeri*

We characterized the developmental stages of *Nothobranchius furzeri* embryo obtained from 14 weeks-old parents.
Embryogenesis was staged according to the morphological criteria used in both zebrafish and killifish [27,28]. Embryonic development was divided into seven stages: zygote, cleavage, blastula, gastrula, segmentation, pharyngula and hatching (Table 2).

Effect of parental age on embryo developmental timing

The development timing in aqueous medium was defined as the number of days from fertilization to final organogenesis, "golden eye" embryos [see Tab. 2 (O)] occurring at 14 days post hatching. Fully-developed embryos exhibit developed eyes ringed by a gold iris and can be considered ready to hatch [24]. The embryos from old breeders (20 wph) took more time to reach the "golden eye" stage with respect to young (8 wph) breeders (average 29.67 ± 2.73 days vs. average 16.67 ± 1.2 days) suggesting differences in diapause duration.

Fig. 1A showed different embryonic developmental duration in clutch from different parents, the maximum duration of developmental time in embryos from young parents was 22 days including 8 days diapause, while in embryos from old parents it was 35 days including 21 days diapause. Moreover, the rate of diapausing embryos observed were significantly higher in old than in young parents (average 83.33 % vs. average 30.36%) and the mean rate of escape embryos from old parents was 16.67% while in young parents was 69.64 % (Fig. 1B). The delay in embryonic development could be attributed to the occurring of diapause II according to Furness [18] who evidenced the persistent presence of diapause I and III in all embryos while the diapause II may be skipped in escaped embryos.

Phenotype comparative analysis

All embryos from young and old breeders were analysed at 8 and 12 dpf to evaluate the morphological differences by stereo microscope. Embryos from old breeders (20 wph) showed slower development than

embryos from young parents (8 wph) (Figure 2A and 2B) suggesting that old parents embryos may enter in a short diapause II while embryos from young parents escape it.

However, not all embryos from young parents were direct developing (escape embryos). Within a single clutch, a well-defined intraspecific variation was observed; however, most embryos from young parents bypassed diapause.

Molecular analysis of the genes related to dorsalization process in F1 embryo

Both *chordin* and *goosecoid* genes are involved in dorsalization process regulating signaling of the dorsoventral axis [29] during early embryogenesis in vertebrates. We assessed expression of these genes at 4, 5 and 6 dpf.

In embryos from young parents, we found *goosecoid* and *chordin* gene expression increased between 4 and 5 dpf and stable between 5 and 6 dpf.

In embryos from old parents, the levels of these genes remained constant between 4, 5 and 6 dpf evidencing a delay in the developmental process (Fig.3).

Molecular analysis of the chromatin-remodeling genes in F1 embryo

The influence of parental aging on *DNMT3a* and *DNMT3b* expression was investigated (Fig.4). The expression of mRNA coding for *DNMT3a* showed the largest age-dependent modulation in embryos from young parents. It showed a high level at 4 dpf but was undetectable at 5 and 6 dpf. In embryos from old parents at 4 dpf the levels were significantly lower respect to embryos from young parents, similar the level of expression at 5 dpf becoming undetectable at 6 dpf. *DNMT3b* expression was similar, being highest in embryos from young parents at 4dpf where it dropped dramatically at 5 dpf and 6 dpf , these latter levels are comparable to that found in embryos from old parents during all the period analyzed.

Morphometric analysis in F1 adults

Morphometric measures were performed to examine growth differences between F1 adult males and females in the two different groups both at 6 wph when the specimens reach the final size.

A significant difference ($p < 0.05$) in length and body weight among the two groups was observed, with adults from young parent groups showing larger size with respect to adults from old parent groups. Specifically, male total length (T.L) showed a significant difference between the offspring from young (4.50 ± 0.07 cm) and old (3.57 ± 0.09 cm) parents (Fig 5 A).

The same result was observed for total length (T.L) in females, showing a significant difference between F1 from young (3.65 ± 0.08 cm) and old (2.62 ± 0.11 cm) parents (Fig 5 B).

In addition, results obtained by measuring wet weight evidenced a significant increase in F1 males from young (1.22 ± 0.11 g) with respect to old (0.51 ± 0.05 g) parents (Fig.6 C). Similarly, the same trend was obtained in F1 female from young (0.69 ± 0.04 g) and old (0.29 ± 0.01 g) parents (Fig. 6 D).

These results showed a remarkably different rate of growth between F1 females than in the males from young parents.

Histology and lipid content in livers of F1 adults

Accumulation of lipids in the liver (steatosis) is a common finding in captive *N. furzeri* [30]. To verify if the larger size of F1 adults from young parents was associated to an increased steatosis, we analyzed histological sections from the liver of all individuals and quantified the area occupied by vacuoles. The amount of steatosis was not different between the experimental groups (Fig. 6) and quantification of the area covered by lipid vacuoles (ACLV) was very similar in the livers from the four different groups (Fig. 7).

Molecular analysis of the genes related to IGF system in F1 adults

In order to investigate the consequences of different timing in embryonic development on growth-related genes, we analyzed genes in F1 adult livers of males and females at 6 wph. The selected components of the IGF signaling pathways were *IGF1, IGF1-Ra, IR, IGFBP2* and *IGFBP3.*

Comparison between female adults from the two breeder groups revealed a significant higher expression of IGF1 and IR gene. All other comparisons were not significant (Fig. 8). The livers of adult males did not show any significant difference in expression (Fig. 9).

DISCUSSION

Parental aging effects on offspring have been reported in both invertebrates [9,31,32] and vertebrates [33] but very little is known about the molecular mechanisms.
In this paper, we describe the effects of parental aging in *Nothobranchius furzeri* showing that phenotypic plasticity, present in most of the embryos that enter diapause, is influenced by parental aging. The two developmental trajectories from escaping and diapausing embryos appear to diverge, based on morphological and physiological data related to parental aging. To test the hypothesis that embryos from old parents undergo diapause II, leading to metabolic and developmental arrest, we analyzed *chordin* and *goosecoid* gene expression.

Molecular data on *chordin* and *goosecoid* signals, previously associated to specific morphogenetic process in zebrafish[25] confirmed our hypothesis that diapause II occurs in most embryos from old parents retarding their development and suggest that in *N. furzeri* the timing of the dorsalization process is influenced by parental aging. Our results are in accordance with Podrabsky et al. [17] that in *Austrofundulus limnaeus* observed that the proportion of embryos that escape diapause II decreases as the age of the fish increases. According with Furness [34] which postulates that diapause II stage occurs in embryos after the formation of the body axis, we chose 4, 5 and 6 dpf as timing to verify differences during the dorsalization process. Thus, in order to study the beginning of the body axes formation process in embryos from young and old breeders we used *chordin* and *goosecoid* as gene markers to verify changes at molecular level.
Based on the fact that each stage is regulated by specific signals, and that the same stage is characterized by the same molecular markers at the same levels, here we wanted study the dynamics of embryonic development related with parental age, considering the days after fertilization (d.p.f.) and not the developmental stages.
Our data on *chordin* and *goosecoid* signals, confirmed the hypothesis that diapause II occurs in most embryos from old parents slowing their development.

Moreover, results regarding the duration of embryonic development showed that diapause stage, when occurs, has a variable duration depending to parental age: diapause occurring in embryos from young parents evidenced a shorter period than in embryos from old parents, suggesting that diapause II duration can be regulated by parental age.

Regarding the epigenetic control by parental aging, DNA methylation reprogramming after fertilization is a dynamic mechanism that is essential for vertebrate development. In order to study the relationship between embryo development and methylation process, we analyzed two members of the DNA methyl-transferase gene family, the *DNMT3a* and *DNMT3b* genes. Both of these are functionally related genes essential for the de novo [35] of methylation which plays an essential role in normal development of organisms [36] controlling early

development and having a long-term effect on growth in some teleost species. The increase of *DNMT3a* and *b* suggests changes in the DNA methylation process by age factors produced by parents. Future deeper study are requested to elucidate the epigenetic effects of parental age on the F1 generation. The remarkable phenotypic differences evidenced in the present study in the development of embryo from different age-breeders could be related to methylation changes. Cytosine methylation by DNA (cytosine-5)-methyltransferases (*DNMTs*) is the most common covalent modification of DNA in eukaryotes, the inactivation of *DNMT3a* and *DNMT3b* causes a complete failure in the genome-wide methylation.

The differences in timing expression of both these genes let us hypothesize that changes in embryonic development could be under methylation control. However, our results underline that the developmental plasticity, believed to be restricted during early development, could affects the growth process and size also during adult life as confirmed by our morphometric results in F1 generation. There are many pathways associated with growth, such as IGFs signaling [37]. IGF proteins and their associated signaling pathways are highly conserved across vertebrates [38] from humans [39,40] chickens , *Xenopus* [41] to zebrafish [42]. This signaling consists of multiple ligands, receptors and IGF-binding proteins. IGF1 binds with high affinity to IGF1-R, which starts the physiological response to its ligand. The IGF1 could also be bound by insulin receptor (IR) which has a close homology with IGF1-R [43]. Moreover, some IGFBPs display IGF-dependent action. The most important IGF-1 binding protein is IGFBP-3 which has growth-promoting effects and the role of IGFBP-3 appears to control the IGF1 concentrations. In liver, IGF1 synthesis is concomitant with IGFBP-3 gene expression. The second most abundant form of IGFBP is IGFBP-2 and has a growth-inhibiting action being inversely related to the GH level. So, the IGFBP-2 concentration is inversely related to the IGF-1 level in liver [44]. This hypothesis is provided by several studies that suggest that IGF1 might be a useful growth index [45,46] . Because of the critical role of these signals in regulating cell growth and metabolism in all life stages, IGFs are excellent candidates for regulating not only the programmed aspects of organismal growth but also aging. The results here obtained evidenced female from old parents present statistically significant lower levels of the IGF signals associated with lower growth, suggesting a postponed aging in this group. To note, in this paper we focused on the comparative quantification of gene expression levels without considering protein levels that are not always consistent with transcript levels results.
In addition, our data suggest that parental aging, affects the gene expression of IGF system in F1 generation in a gender-specific manner with a more pronounced growth in females than males, the former reaching the sexual maturity faster and stopping their reproduction earlier than male.

Due to the ecological strategy of the genus *Nothobranchius*, inhabiting the temporary African water bodies subject to annual desiccation, they have adopted a unique biology that allows them to survive across multiple generations. Specifically, considering the annual cycle, characterized by a raining followed by a dry season , the advancement of the sexual maturity in both male and female from young parents represent an important

ecological advantage that allowed them to reach multiple generations within the same raining season. On the contrary the specimens from old parents adopt a different strategy that includes diapause II stage, to survive during the dry season suggesting that parental aging may affect reproductive fitness and thus off spring number.

However, further studies are needed to define whether the differences on development timing and growth of the offspring may affect lifespan in this specie. Moreover, future studies on the effects of parental aging on offspring reproduction are requested to clarify whether different rates of growth of the offspring has an evolutionary and ecological significance in *N. furzeri* life cycle.

Acknowledgement

The authors wish to thank Dr. Chiara Carla Piccinetti for the technical support at the fish facilities. The study was supported by Fondo di Ateneo 2016 to OC.

REFERENCES

1. Mitteldorf J, Martins ACR. Programmed Life Span in the Context of Evolvability. Am Nat. 2014;184(3):289-302.
2. Liu Y, Zhi M, Li X. Parental age and characteristics of the offspring. Ageing Res Biol 2011;10:115-123.
3. Tozzini ET, Dorn A, Ng E, et al. Parallel evolution of senescence in annual fishes in response to extrinsic mortality. BMC Evol Biol 2013; 13:77.
4. Lematre J-F, Berger V, Bonenfant C, et al. Early-late life trade-offs and the evolution of ageing in the wild. Proc. R. Soc. B 2015; 282: 1-10.
5. Blažek R, Polačik M, Kačer P et al. Repeated intraspecific divergence in life span and aging of African annual fishes along an aridity gradient. Evolution 2016; 71:386-402.
6. de Magalhães JP. Programmatic features of aging originating in development: aging mechanisms beyond molecular damage? FASEB J 2012; 26(12):4821-4826.
7. Ekamper P, Van Poppel F, Stein AD, Bijwaard GE, Lumey LH. Prenatal Famine Exposure and Adult Mortality From Cancer, Cardiovascular Disease, and Other Causes Through Age 63 Years. Am J Epidemiol 2015;181(4): 271-279.
8. Tobi EW, Goeman JJ, Monajemi R, et al. Corrigendum: DNA methylation signatures link prenatal famine exposure to growth and metabolism. Nat Commun. 2015; 6:7740.
9. Priest NK, Mackowiak B, Promislow DEL, Evolution S, May N. The Role of Parental Age Effects on the Evolution of Aging 2014; 56(5):927-935.
10. Permissions F. Age-Specific Changes in Epistatic Effects on Mortality Rate in Drosophila melanogaster. J heredity 2005; 96(5):513-521.
11. Lints FA, Hoste C. The Lansing effect revisited—I. Life-span. Exp Gerontol 1974; 9(2):51-69.
12. Lints FA, Hoste C. The Lansing Effect Revisited. II.-Cumulative and Spontaneously Reversible Parental Age Effects on Fecundity in Drosophila melanogaster. Evolution 1977; 31(2):387.
13. Greer EL, Maures TJ, Ucar D, et al. Transgenerational Epigenetic Inheritance of Longevity in C. elegans. Nature 2011; 17; 479(7373): 365–371.
14. Terzibasi E, Valenzano DR, Cellerino A. The short-lived fish Nothobranchius furzeri as a new model system for aging studies. Exp Gerontol 2007; 42(1-2):81-89.
15. Di E, Terzibasi E, Rossi G, Cellerino A. The short-lived annual fish Nothobranchius furzeri shows a typical teleost aging process reinforced by high incidence of age-dependent neoplasias. EXG. 2011;46(4):249-256.

16. Cellerino A, Valenzano DR, Reichard M. From the bush to the bench : the annual Nothobranchius fishes as a new model system in biology. 2016; 91:511-533.

17. Podrabsky JE, Garrett IDF, Kohl ZF. Alternative developmental pathways associated with diapause regulated by temperature and maternal influences in embryos of the annual killifish Austrofundulus limnaeus. J Exp Biol 2010; 213(Pt 19): 3280-3288.

18. Furness AI, Lee K, Reznick DN. Adaptation in a variable environment: phenotypic plasticity and bet-hedging during egg diapause and hatching in an annual killifish. Evolution 2015;69(6):1461-1475.

19. Genade T, Benedetti M, Terzibasi E, et al. Annual fishes of the genus Nothobranchius as a model system for aging research. Aging Cell 2005;4(5):223-233.

20. Valenzano DR, Terzibasi E, Cattaneo A, Domenici L, Cellerino A. Temperature affects longevity and age-related locomotor and cognitive decay in the short-lived fish Nothobranchius furzeri. Aging Cell 2006: 5(3): 275-278.

21. Polačik M, Blažek R, Řežucha R, Vrtílek M, Terzibasi Tozzini E, Reichard M. Alternative intrapopulation life-history strategies and their trade-offs in an African annual fish. J Evol Biol 2014; 27(5):854-865.

22. Polačik M, Smith C, Reichard M. Maternal source of variability in the embryo development of an annual killifish. J Evol Biol 2017; 30(4):738-749.

23. Blažek R, Polačik M, Reichard M. Rapid growth, early maturation and short generation time in African annual fishes. EvoDevo 2013; 4:24.

24. Genade T. LABORATORY MANUAL FOR CULTURING N. furzeri. http://www.nothobranchius.info/pdfs/lab_protocols_1.pdf.

25. Miccoli A, Dalla Valle L, Carnevali O. The maternal control in the embryonic development of zebrafish. Gen Comp Endocrinol 2017; 245:55-68.

26. Papadakis IE, Kentouri M, Divanach P, Mylonas CC. Ontogeny of the digestive system of meagre Argyrosomus regius reared in a mesocosm and quantitative changes of lipids in the liver from hatching to juvenile. Aquaculture 2013; 388-391:76-88.

27. Kimmel CB, Ballard WW, Kimmel SR, Ullmann B, Schilling TF. Stages of embryonic development of the zebrafish. Dev Dyn an Off public 1995; 203(3):253-310.

28. Hartmann N, Englert C. A microinjection protocol for the generation of transgenic killifish (Species: Nothobranchius furzeri). Dev Dyn 2012;241(6):1133-1141.

29. Branam AM, Hoffman GG, Pelegri F, Greenspan DS. Zebrafish chordin-like and chordin are functionally redundant in regulating patterning of the dorsoventral axis. Dev Biol 2010; 341(2): 444-458.

30. Di Cicco E, Tozzini ET, Rossi G, Cellerino A. The short-lived annual fish Nothobranchius furzeri shows a

typical teleost aging process reinforced by high incidence of age-dependent neoplasias. Exp Gerontol 2011; 46(4):249-256.

31. Hercus MJ, Hoffmann AA. Maternal and grandmaternal age influence offspring fitness in Drosophila. Proc R Soc London B Biol Sci 2000; 267(1457).

32. Mishra N, Shakarad MN. Effects of Parental Age and Substrate Quality on Pre-Adult Fitness of Progeny. Imp J Interdiscip Res 2016; 2(8):2454-1362.

33. Torres R, Drummond H, Velando A, Leonard ML. Parental Age and Lifespan Influence Offspring Recruitment: A Long-Term Study in a Seabird. Plos One 2011; 6(11): 1-7.

34. Furness AI. The evolution of an annual life cycle in killifish: adaptation to ephemeral aquatic environments through embryonic diapause. Biol Rev 2016; 91(3):796-812.

35. Li J-Y, Pu M-T, Hirasawa R, et al. Synergistic function of DNA methyltransferases Dnmt3a and Dnmt3b in the methylation of Oct4 and Nanog. Mol Cell Biol 2007; 27(24):8748-8759.

36. Mhanni R A McGowan AA. Global changes in genomic methylation levels during early development of the zebrafish embryo. Dev Genes Evol 2004; 214:412-417.

37. Gabillard J-C, Weil C, Rescan P-Y, Navarro I, Gutierrez J, Le Bail P-Y. Does the GH/IGF system mediate the effect of water temperature on fish growth? A review. Cybium 2005; 29(2):107-117.

38. Lin K, Hsin H, Libina N, Kenyon C. Regulation of the Caenorhabditis elegans longevity protein DAF-16 by insulin/IGF-1 and germline signaling. Nature Genet 2001; 28:139-145.

39. Werner H, LeRoith D. The Role of the Insulin-like Growth Factor System in Human Cancer. Adv Cancer Res 1996; 68:183-223.

40. Caro JF, Poulos J, Ittoop O, Pories WJ, Flickinger EG, Sinha MK. Insulin-like Growth Factor I Binding in Hepatocytes from Human Liver, Human Hepatoma, and Normal, Regenerating, and Fetal Rat Liver. J Clin Invest 1988; 81(4):976-981.

41. Clairmont KB, Czech MP. Chicken and Xenopus Mannose 6-Phosphate Receptors Fail to Bind Insulin-like Growth Factor II . J Biol Chem 1989; 264(28):16390-16392.

42. Nelson SN, Van G, Kraak D. Characterization and regulation of the insulin-like growth factor (IGF) system in the zebrafish (Danio rerio) ovary. Gen Comp Endocrinol 2010;168:111-120.

43. Annunziata M, Granata R, Ghigo E. The IGF system. Acta Diabetol 2011; 48:1-9.

44. Clemmons DR. Insulin-like growth factor binding proteins and their role in controlling IGF actions. Cytokine Growth Factor Rev. 1997; 8(1):45-62.

45. Beckman BR. General and Comparative Endocrinology Perspectives on concordant and discordant relations

between insulin-like growth factor 1 (IGF1) and growth in fishes. Gen Comp Endocrinol 2011;170(2):233-252.

46. Picha ME, Turano MJ, Beckman BR, Borski RJ. Endocrine Biomarkers of Growth and Applications to Aquaculture: A Minireview of Growth Hormone, Insulin-Like Growth Factor (IGF)-I, and IGF-Binding Proteins as Potential Growth Indicators in Fish. N Am J Aquac 2008; 70(2):196-211.

Tables

Table 1. List of primers used to amplify selected genes through q-PCRs

Gene	Forward 5'-3'	Reverse 5'-3'	Acc. number
chordin	GCTGTCCCGTCTGTGATGAA	GGAGGAACAAAGGGATGCCA	HADY01001320
goosecoid	ACCGAACCATCTTCACCGAC	CCACATCCGGGTACTTGGTC	HADY01023130
dnmt3a	ATTTCTTCGCCAACAACCAC	GCCCACAGTGATGGAATCTT	XM015947606
dnmt3b	CATGAGAAGGGTGGAGTGGT	AGCTGCCAACTCGATGATCT	HAEJ01018161
igf1	GGCAAATCTCCACGATCTCTAC	CGGTTTCTCTTGTCTCTCTCAG	KC306958
igf1-ra	AGCAGTACCGTCAGCACAAA	AGGTGGCGAAACGTAGAAGG	HADY01009044
ir	CTGTTTATGGCCGTTGTGGG	GCCTTCGTAGACCATCCCAA	EF464718
igfbp2	AGGCCCACTAAAGAAACCATGT	TTGGGCCGAGTAGGTCTCA	KC306953
igfbp3	ACAAACTGCTCCAGAAGGCA	CACGGCCCATACTCTGTCTC	KC306954

Table 2. Developmental process of *Nothobranchius furzeri* embryo from 14 weeks old parents

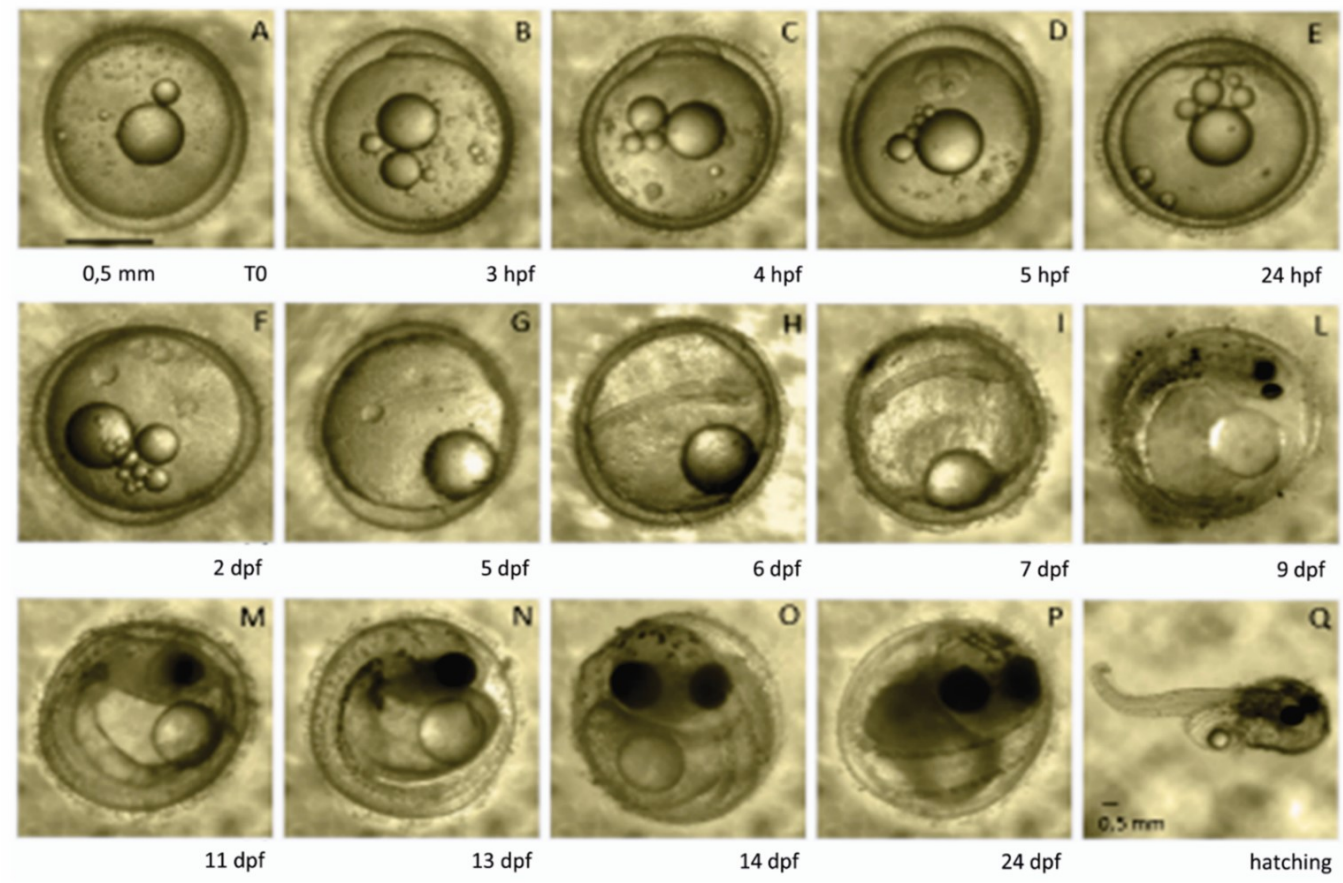

Embryos collect from killifish was incubated at 26 ± 0.5 °C in fresh water and careful daily observation of the embryonic development was performed by stereomicroscope. (A) The newly fertilized egg is in the zygote period until the first cleavage occurs. (B) After 3 hours post fertilization the blastodisc was formed. (C) Cleavage stages at 4 hpf (2 cell stage). (D) 5 hpf (4 cell stage). (E) 24 hpf (blastula stage). (F) Completion of epiboly and diapause I was occurring. (G) Neural keel. (H) Beginning of gastrula stage. (I) Early somite embryo and segmentation period diapause II may occur at this stage corresponding to late somite stage. (L) Beginning of pharyngula stage with early pigmentation in retina and skin, this stage is past diapause II. (M,N,O) Organogenesis is nearly completed. (P) Pre-hatching after 10 days on peat moss and (Q) hatching. Scale bar 0,5 mm.

Figures

Figure 1 Parental age effects on offspring embryo development.

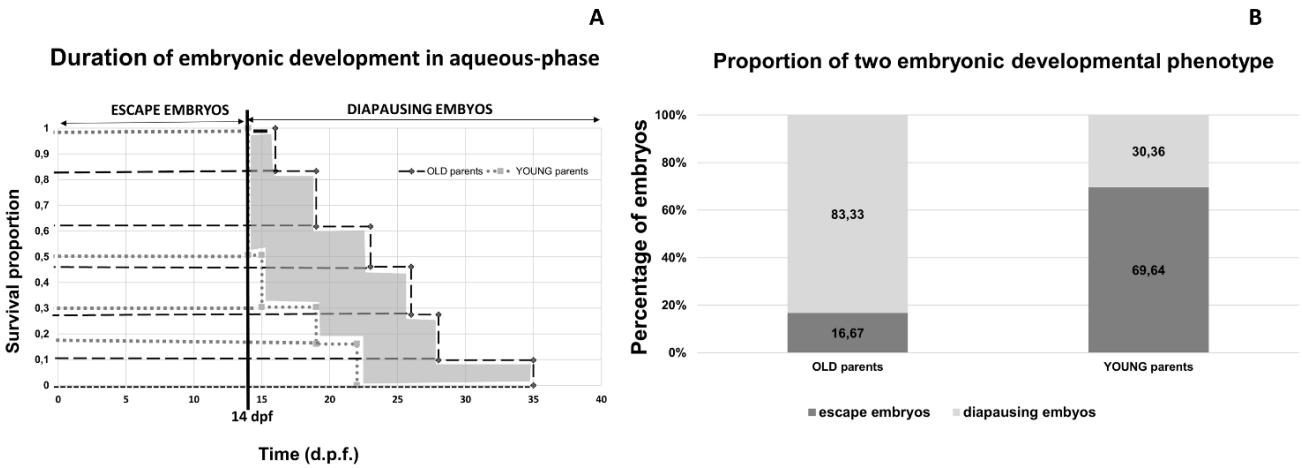

Survivorship at "golden eye" stage before hatching of embryos from young and old parents as estimated by Kaplan-Meyer analysis. In dark, embryos from old parents and in grey embryos from young parents. The time of embryonic development were significantly different (Unpaired *t*-test, $p < 0.10$) in embryo from young parents compared with embryo from old parents. The time differences to reach the "golden eye" in the two groups were evidenced in grey (Fig1A). The mean proportion of escape and diapausing embryo from old and young parents were shown. Dark grey bars represent escape embryos while light grey bars represent diapausing embryos. Numbers inside the bars are relate to mean rate of embryo collected from each experimental group. There is a significant difference in the proportion of escape embryos produced by young parents (Unpaired *t*-test, $p < 0.0001$;Fig 1B).

Fig. 2 Embryos from young and old parents at 8 dpf (pharyngula stage) (A) and embryos from young and old parents at 12 dpf (prehatching stage) (B) in three different views observed by stereo microscope. Scale bar 0,5 mm

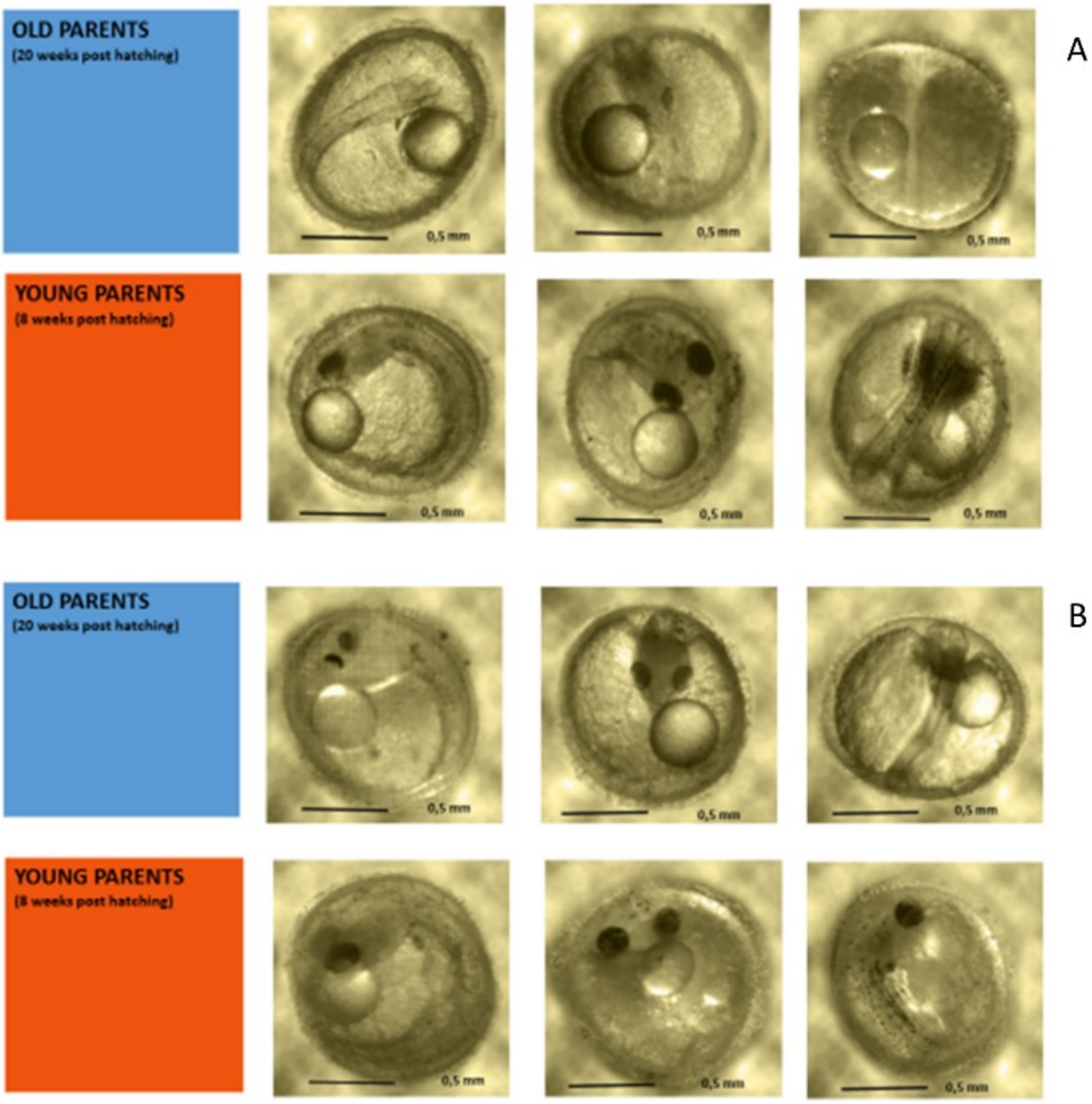

Fig. 3 Expression profiles of *goosecoid* and *chordin* at 4, 5 and 6 dpf. Transcript levels were determined by qPCR and normalized within each developmental stage, using 18s as reference gene. Error bars indicate mean ± S.D. Letters symbolize the statistical difference within the same experimental group at different developmental stages and among the two groups. Confidence interval set at 95% ($p < 0.05$).

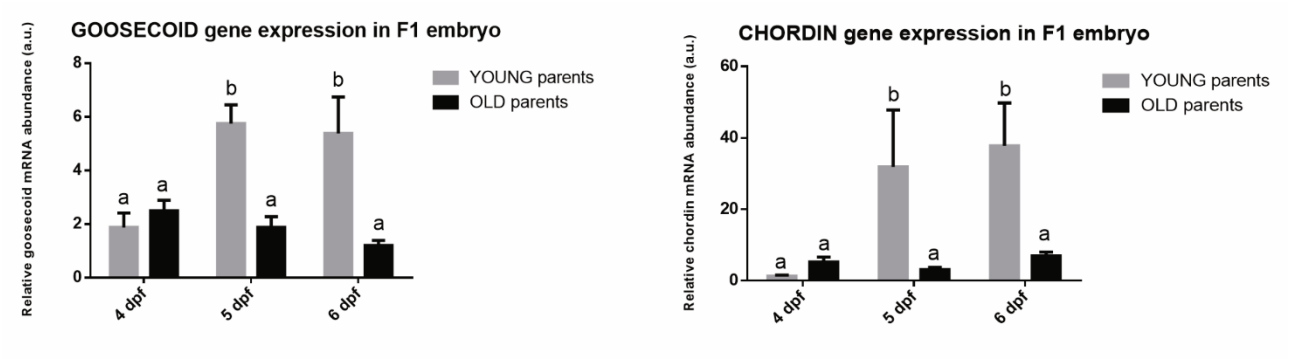

Fig. 4 Temporal expression profiles of *dnmt3a* and *dnmt3b* at 4, 5 and 6 dpf.

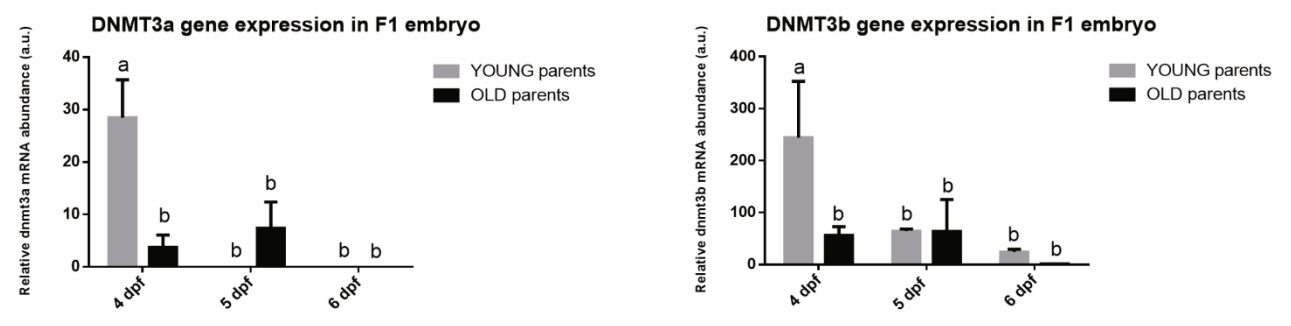

Fig. 5 Total length of killifish adults in male (A) and female (B) from young and old parents groups . Data are the mean ± S.D. **Total wet weight of killifish adults in male (C) and female (D) from young and old parents groups .** Data are the mean ± S.D and whiskers represent 95% confidence intervals.

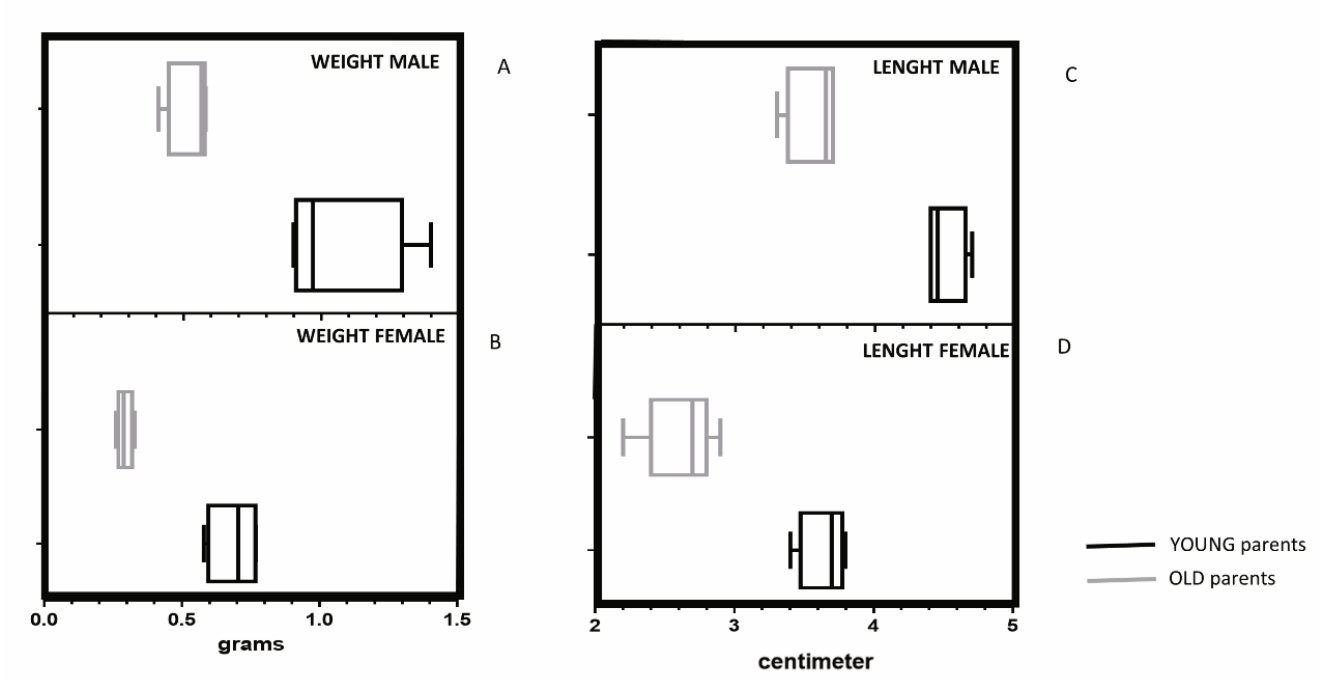

Fig. 6 Histological sections of liver in the different experimental groups: (A) F1 female from old parents; (B) F1 female from young parents; (C) F1 male from old parents; (D) F1 male from young parents. Lipid vacuolization is visible in all groups.

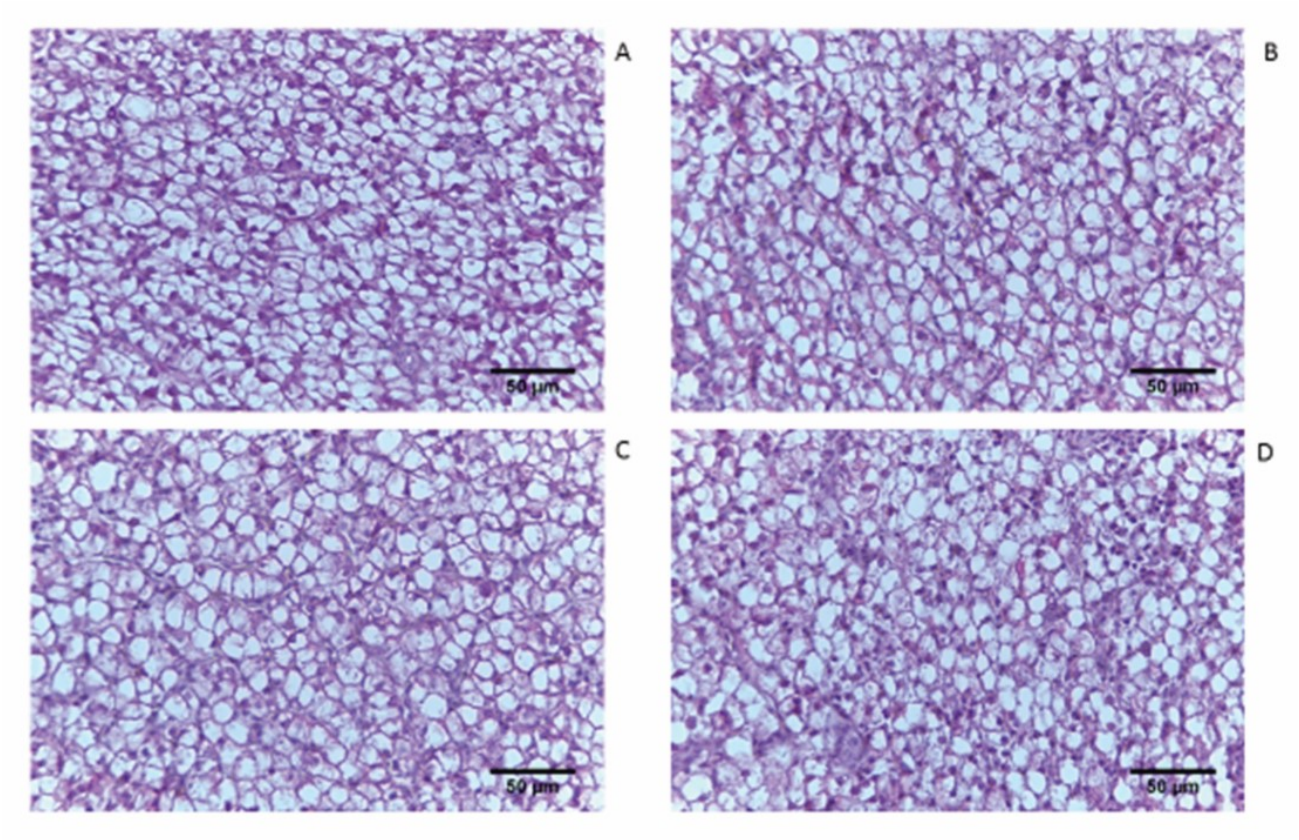

Fig. 7 Lipid content. Percentage of area covered with lipid vacuoles (ACLV %), in *N. furzeri* liver. (A) F1 female adults liver from young and old parents, (B) F1 male adults liver from young and old parents. Values represent the means ± S.D.

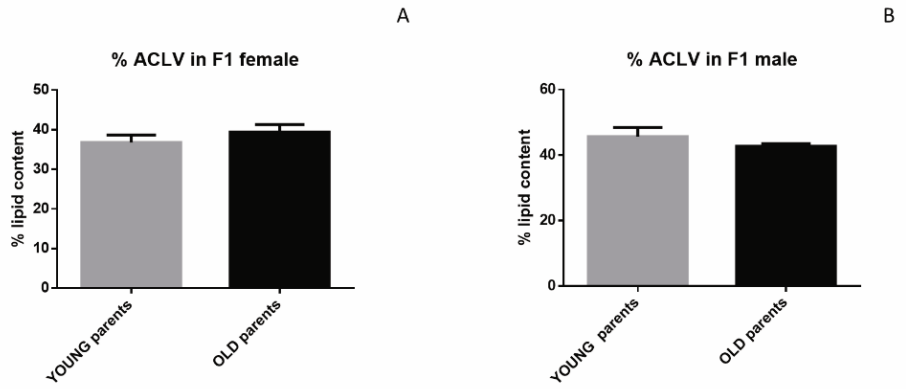

Fig. 8 Gene expression quantification in the liver of female from young and old parents of: *igf1* (A), *ir* (B), *igf1ra* (C), *igfbp-3* (D) and *igfbp*-2 (E) . Values with asterisk are significantly different ($P < 0.05$).

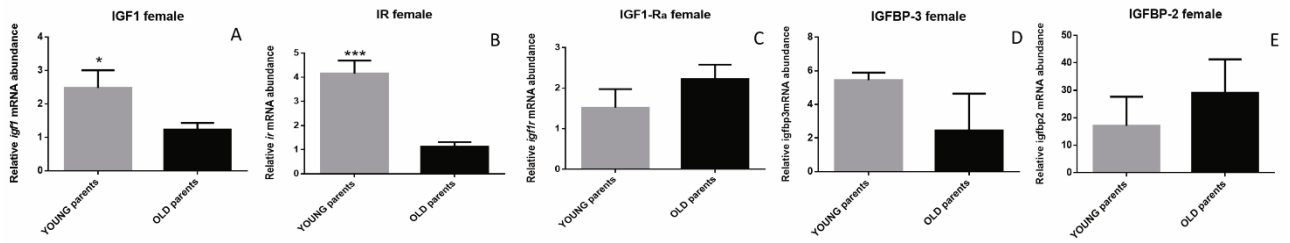

Fig. 9 Gene expression quantification in the liver of male from young and old parents of: *igf1* (A), *ir* (B), *igf1ra* (C), *igfbp-3* (D) and *igfbp-2* (E).

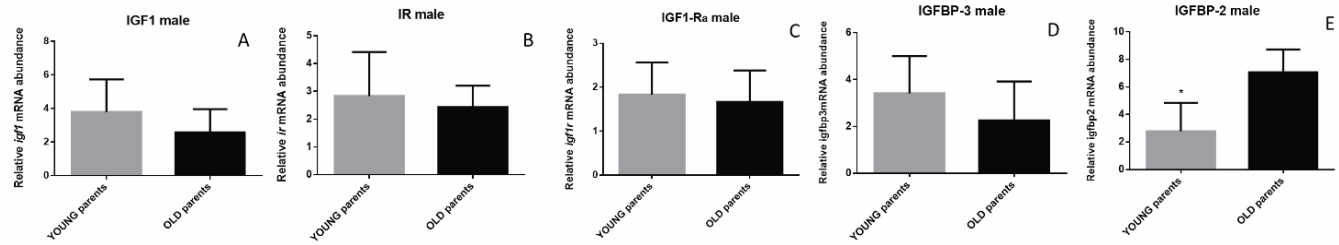

Chapter 2

Submitted to Aging Cell Journal: **ID ACE-18-0036**

Breeders age affects reproductive success in *Nothobranchius furzeri*

Abstract

The present study was conducted to examine the effects of mating breeders at different age on reproductive fitness and females offspring gametogenesis using *Nothobranchius furzeri* as model.

In *N. furzeri*, the increase of maternal and paternal age are often predictable indicators of the future deterioration on their natural habitat, as ephemeral puddles, during dry seasons in African regions. We previously revealed that elderly parents respond to their physiological decline state by decelerating developmental and growth rate in F1 offspring. Here, we focused on the effects of different age-parents at the onset of offspring's sexual maturity since interaction between growth and reproduction traits occurs generally in vertebrates and could represent a life strategy. In this paper, the consequences of breeders aging in reproductive performance were emphaticized.

For this purpose, four different age breeder groups (OLD BREEDERS, OLD FEMALE/young male, YOUNG FEMALE/old male and YOUNG BREEDERS groups) have been set up. The age-specific breeder differences in reproductive performance were examined by analyzing:

(i) the number of spawned eggs and the rate of their fertilization, together to the F1 embryonic survival and hatching;

(ii) the gametogenesis process in F1 female by histological approach;

(iii) the F1 oocytes quality both analyzing the gene expression of age molecular markers like *sirt1* and *foxo3a* and by biochemical composition of vitellogenic oocytes using spectroscopic approach.

Results suggest that mostly advanced maternal but also paternal age affect reproductive performance and could influence the onset of sexual maturity in offspring.

INTRODUCTION

The success of a life strategy of an organism depends on the evolutionary plasticity in life traits and it is defined by trade-offs among development, growth, reproduction and survival.

Factors affecting early development such as environmental factors as well as maternal effects, can therefore have an important influence both on the optimization of life history as reproductive fitness and survival, in many vertebrate species.

In fact, detrimental effects for the offspring is giving by parental influences since the developing embryo is also dependent on the resources present in the eggs [2,3].

It is known in literature that eggs formation incur costs in terms of time, energy and nutrients, and can influence the fitness of both parents and offspring [4].

Most of explanations for age-specific effects on reproduction is provided by studies on birds, such as egg production, incubation or chick rearing [5–7] . Nowadays, it remain unclear whether and how the eggs are influenced by elderly parents and what are the potential consequences for their offspring in adult life [8]. The understanding of these evolutionary consequences have been documented only recently [9,10].

In this paper we focused on the effects of parental age (female, male and both) on reproductive success in terms of number of spawned eggs, embryonic survival and hatching, since different authors postulated that puberty is influenced by many factors [11–13], including prenatal factors.

We also took into consideration the effects on the onset of sexual maturity in F1 generation observed across different age-related breeder groups considering previous results evidencing different growth rate in F1 generation from different age-breeders.

For this study on reproductive success between different-age breeder groups, we used as an aging fish model, the killifish, *Nothobranchius furzeri* which short lifespan is accompanied by a rapid growth and sexual maturity. This killifish reach sexual maturity at about 4-6 weeks post hatching [14] and after that, females spawn dozen eggs several times each day that can be fertilized by different males. Moreover, similarly to zebrafish, embryos are transparent and it is possible to visualize if fertilization was occurred. For these characteristics, *N. furzeri* results a suitable model for reproductive aging studies.

MATERIALS AND METHODS

Ethics

All the procedures involving animals were conducted according to Italian law on experimental animals and were approved by the Health Ministry's Department of Veterinary Public Health and by the Ethics Committee of Università Politecnica delle Marche (Authorization No. 852/2016-PR).

Optimal rearing conditions were applied throughout the study and all efforts were made to minimize animal suffering by using an excess of anesthetic (MS222, Sigma Aldrich, Milano, Italy).

Experimental design

Nothobranchius furzeri, strain MZM 0410, were cultured according to the manual for caring *N. furzeri* [15].
A total of 64 female/male adults from *N. furzeri* were placed in sixteen aquaria of 20-L (4 fish/tank) with oxygenated water under controlled conditions (26 ± 0,5 °C) with a daily water changes of 10% and maintained on a 12/12 h light/dark cycle. They were fed twice times a day with *Chironomus chironominae* larvae and *Artemia salina* nauplii.
Four different-age breeder groups were formed crossing 1 male and 3 females adults in each tank.
The groups defined "YOUNG BREEDER" were formed with males and females at 8 weeks post hatching (wph) while the groups defined "OLD BREEDER" were composed of males and females at 20 wph. The breeder groups which females were 8 wph age and males 20 wph were defined "YOUNG FEMALE/old male" breeder groups while the breeders which females were 20 wph age and males 8 wph age were called "OLD FEMALE/young male" breeder groups.
All the experiments were conducted in quadruplicate and F1 generations were obtained from the four different breeder groups and analyzed.
After 6 weeks post hatching (wph), when all offspring females have developed sex-specific coloration, were sacrificed by using an overdose of anesthetic (MS222, Sigma Aldrich, Italy) and wet weight of both ovaries were determined using a precision balance (RADWAG PSC/C2, Poland).
During the experiment, each breeder group was kept separately and each group had 4 replicates for a total of sixteen tanks containing each a spawning dish with sand to facilitate the regular oviposition by females with subsequent fertilization by the male. *Nothobranchius furzeri* females after reaching sexual maturity spawn daily allowing regular collection of eggs. A spawning dish was put in each tank every morning at 9:00 a.m. and then removed at 5:00 p.m. to check daily egg production and to record the reproductive fitness by visualizing fertilized eggs under stereomicroscope. This daily check was repeated for 10 days.

Histological study of gametogenesis

Whole gonads from F1 females at 6 wph were sampled and prepared for histological examination. Samples were fixed by immersion in 4% paraformaldehyde, washed in PBS 0.1 M, dehydrated in alcohol and embedded in liquid paraffin (Bio-Optica, Italy). Slides of 5µm sections was obtained using microtome (Leitz 1512) and stained with Mayer's hematoxylin and eosin Y (Sigma-Aldrich). Finally, the sections were examined using Zeiss Axioskop optical microscope connected with a camera Canon EOS 6D.

Morphological study on germ cell distribution in F1 gonads

The *N.furzery* ovary is asynchronous containing pre-vitellogenic, vitellogenic and late-vitellogenic oocytes according to their diameter size (< 300, 700 to < 900 and ≥1000 μm respectively). The diameter of each oocyte was measured with a micrometer (Image J software) on a screen of five sections of each F1 ovary from the four groups. The micrometer was calibrated with a 4x objective and the diameter measured was the mean of two values made perpendicular to each other.

The germ cell distribution from each specimens was expressed as mean number (n) of each class of oocytes and the rate (%) was calculated according to the following formula: n*100/ovary weight (mg).

Fourier Transform Infrared Microspectroscopy (FTIRM)

The ovaries (n=3/experimental group) were mounted with OCT (optimal cutting temperature) and cryosectioned.

FTIRM was used in the present study to explore the effects of parental age on biochemical composition of vitellogenic oocytes. FTIRM measurements were carried out by using a Bruker VERTEX 70 interferometer coupled with the Hyperion 3000 Vis-IR micro-scope and equipped with a liquid nitrogen cooled bidimensional focal plane array (FPA) detector (area size 64 × 64 pixels). For each sample, images were acquired in transmission mode using a 15× condenser/objective, therefore achieving a pixel resolution of about 2.65 μm. Each section was examined under the microscope, in order to detect the regions containing the vitellogenic oocytes, on the basis of their dimension and characteristics, as explained by Carnevali and colleagues[16]. On each selected region, IR images were taken acquiring simultaneously groups of 4096 spectra, averaging 256 scans for each detector pixel with a spectral resolution of 4 cm^{-1}. Background single channel images were acquired on clean regions of the CaF_2 windows. Bigger images were done by defining a grid of images, until a maximum of 36,864 microspectra. By using OPUS 7.2 software (Bruker), chemical maps were generated for each sample, integrating under the Lipids stretching region (3100–2800 cm^{-1}), the amide I and II modes, representative of Proteins (1720–1480 cm^{-1}), and Phosphate groups stretching region (1100-1065 cm^{-1}). 50 spectra were extracted from IR images of each sample (OPUS 7.2, Bruker), selecting the oocytes cytoplasmic zone, specifically on visible cytoplasmic vesicles, and 50 spectra were extracted from the oocyte membrane. All the extracted spectra were two-point baseline linear fitted in the spectral range of 4000–900 cm^{-1}, compensated from the atmospheric contributions of aqueous vapour and CO_2, and vector normalized. Spectra were analysed in the following spectral regions: 3030-2800 cm^{-1} (representative of Lipids and =CH groups); 3027-2995 cm^{-1} (ν=CH, stretching mode of =CH groups in lipid chains); 1780-1715 cm^{-1} (νCOO, stretching mode of lipids ester moieties); 1715-1481 cm^{-1} (Amide I and II bands, representative of all cellular proteins); 1177-1130 cm^{-1} (ν C-OH, stretching vibrations of hydrogen-bonding C-OH, mostly related to carbohydrates);

1140–1030 cm^{-1} (ν_{sym} PO_2-, symmetric stretching mode of phosphates, Phosphates). The sum of the area integral of lipids and the region 1775−1065 cm^{-1} is considered as representative of the overall cellular bimolecular content (*Cell*). On all the spectra collected from oocytes of each experimental group an integration of the bands was performed. In order to normalize all the peculiar characteristics of each spectrum in terms of intensity and absorbance, integrals were reported as band ratios.

Quantitative RT-PCR

Real time PCR was performed with the SYBR Green method in an iQ5 iCycler thermal cycler (Bio-Rad laboratories) with 1μg of total RNA from each class of F1 oocytes samples from different experimental groups was used in the RT reactions, as previously described by Maradonna et al. [17]

All primer sets were designed to span a terminal intron and produce an amplicon in the size range of 100-200 bp. Each PCR product was also verified by gel electrophoresis for each primer pair. Primer sequences are reported in Table 1.

Statistical analysis

Results obtained by q-PCR analysis, comparisons of traits and germ cell distribution between four experimental groups have been processed with a grouped analyses one-way ANOVA. Values were compared regardless of two data set. Multiple comparisons were corrected with the Tukey test and the confidence interval was set at 95% ($p < 0.05$).

All infrared FT-IR results were analysed using one-way ANOVA, followed by Dunnett's post-hoc test, in order to compare the differences between the four experimental groups. Significance between groups was set at $p < 0.05$. Results are presented as mean ± standard deviation.

All statistical procedures were run using GraphPad Prism 6.

RESULTS

The effects of mating different age groups

Reproductive performance was measured in terms of spawned eggs, fertilized eggs, embryonic survival and hatching.

The highest number of spawned eggs were produced by YOUNG BREEDERS (daily mean value or d.m.v. 160,4 ± 64,98), followed by YOUNG FEMALE/old male (d.m.v. 120,2 ± 23,57), OLD BREEDERS (d.m.v.

76,7 ± 26,92) and finally OLD FEMALE/young male breeder groups (d.m.v. 60,5 ± 28,56). YOUNG BREEDERS and YOUNG FEMALE/old male breeder groups, spent more energy for the production of eggs laying resulting in an highest number of spawned eggs than the other two breeder groups , the differences were statistically significant ($F_{3, 36} = 12,83$, $P < 0,0001$). We considered fertilized eggs all those starting the cleavage process, in this study there were no significant differences in the fertilized rate between groups ($P = 0,0541$).

Embryonic survival rate evidenced the best performance in YOUNG FEMALE/old male group followed by YOUNG BREEDERS, OLD BREEDERS and OLD FEMALE/young male breeder groups ($F_{3, 8} = 55,86$; $P < 0,0001$).

F1 hatching was significantly greater in YOUNG BREEDERS group than all other groups ($F_{3, 7} = 1152$; $P < 0,0001$) with the lowest hatching rate observed in OLD BREEDERS groups (Tab.2).

Histological analysis and oocytes frequency in F1 ovary from different breeder groups at 6 weeks post hatching

In order to investigate differences in gametogenesis in *N. furzeri* offspring gonads from different age-breeder groups, histological sections of ovaries in all specimens were analyzed (Fig.1).

Results from F1 ovaries showed in YOUNG BREEDER groups the lowest number of pre-vitellogenic oocytes (n=45,88) with significant differences (P=0,0311; F=4,964) with respect to OLD FEMALE/young male breeders (n=51,07), YOUNG FEMALE/ old male breeder (n=53,67) and OLD BREEDER groups (n=87,53). Vitellogenic oocytes from OLD BREEDER groups (n= 36,8) showed lower rate (P <0,0001; F=33,17) compared with OLD FEMALE/young male breeder groups (n=39,37) YOUNG FEMALE/old male breeder (n=68,66) and YOUNG BREEDER groups (n=85,42). The number of oocytes that reached late-vitellogenic stage is higher in F1 ovaries from YOUNG BREEDER groups (n=21,05) and YOUNG FEMALE/old male breeder (n =19,29) with significant differences (P= 0,0029; F=11,39) compared to OLD FEMALE/young male (n=5,67) and OLD BREEDER groups (n=7).

With respect to distribution of each class of oocytes on ovary weight for each experimental group, the percentage of pre-vitellogenic oocytes from F1ovaries of OLD BREEDERS groups was 58,31% followed by OLD FEMALE/young male breeders, YOUNG FEMALE/ old male and YOUNG BREEDER groups (53,34, 37,84 and 30,15%, respectively).

In contrast, 37,74% of .vitellogenic oocytes were present from F1 ovaries of .OLD BREEDERS groups, 40,51% of vitellogenic oocytes were observed from OLD FEMALE/young male breeders, 48,54% of vitellogenic oocytes in YOUNG FEMALE/old male breeder and finally 55,83% of vitellogenic oocytes in YOUNG BREEDER groups.

The post-vitellogenic stage was higher in F1 ovary from YOUNG BREEDER groups (14,03%) followed by YOUNG FEMALE/old male breeder (13,62%), OLD FEMALE/young male breeder (6,15 %) and OLD BREEDER groups (3,95%) (Fig.2)(Tab 3).

Biochemical analysis in vitellogenic oocytes in offspring from different breeder groups

For all ovary sections, specific areas containing vitellogenic class oocytes were selected, and photomicrographs and corresponding chemical maps were acquired. Chemical maps obtained by integration under the regions corresponding to lipids, proteins and phosphate groups (Fig. 3), visually show, with assigned colour scale, the presence and the localization of the aforementioned biomolecules and chemical groups.

Specific band area ratios were calculated by using the area integrals described in the Experimental section, in order to highlight the differences among the F1 ovaries of the four experimental groups, in terms of presence and characteristics of vitellogenin-derived proteins inside the oocytes, and in terms of molecular features of the oocyte membrane.

Regarding **membranes**, the analysis of their numerical variation among the experimental groups lead to the following considerations: (i) the total amount of cellular lipids (**Lipids**), calculated as ratio between the integrated area in the 3030-2800 cm^{-1} spectral region (corresponding to CH_2 and CH_3 symmetric and asymmetric stretching modes) and *Cell* value, showed a significant decrease in both F1 OLD BREEDER and F1 OLD FEMALE/young male groups, while there is no significant difference between F1 YOUNG BREEDER and F1 YOUNG FEMALE/old male groups; (ii) the value **Phosphates**, calculated as the integrated area of the band at ~1080 cm^{-1} to *Cell* value is significantly lower in F1 OLD BREEDER and F1 OLD FEMALE/young male groups respect to F1 YOUNG BREEDER and F1 YOUNG FEMALE/old male ones; (iii) the unsaturation level in lipid chains (**Unsaturation**), calculated as a ratio between the integrated area of the band at 3010 cm^{-1} and the Lipid spectral region, is significantly lower in both F1 OLD BREEDER and F1 OLD FEMALE/young male groups, while there is no significant difference between F1 YOUNG BREEDER and F1 YOUNG FEMALE/old male groups; (iv) the total amount of cellular proteins (**Proteins**), calculated as ratio between the integrated area of the 1715-1481cm^{-1} spectral region (corresponding to Amide I and II bands) and *Cell* value, is significantly higher in both F1 OLD BREEDER and F1 OLD FEMALE/young male groups. Results are summarized in Figure 4.

Regarding **cytoplasm**, the most significant variations reported among the experimental groups are the following: (i) the total amount of cellular lipids (**Lipids**), calculated as ratio between the integrated area in the 3030-2800 cm^{-1} spectral region (corresponding to CH_2 and CH_3 symmetric and asymmetric stretching modes) and *Cell* value, showed a significant increase in both F1 OLD BREEDER and F1 OLD FEMALE/young male groups, while there is no significant difference between F1 YOUNG BREEDER and F1 YOUNG FEMALE/old male groups; (ii) the total amount of cellular proteins (**Proteins**), calculated as ratio between the

integrated area of the 1715-1481cm^{-1} spectral region (corresponding to Amide I and II bands) and *Cell* value, is significantly lower in both F1 OLD BREEDER and F1 OLD FEMALE/young male groups; (iii) the value **Phosphates**, calculated as ratio between the integrated area of the band at ~1080 cm^{-1} and *Cell* value is significantly lower in F1 OLD BREEDER and F1 OLD FEMALE/young male groups respect to F1 YOUNG BREEDER and F1 YOUNG FEMALE/old male ones; (iv) the value **Sugars C-OH**, calculated dividing the integrated area of the band centred at 1157 cm^{-1} and the one centred at 1080 cm^{-1}, is significantly higher in both F1 OLD BREEDER and F1 OLD FEMALE/young male groups; (v) both the values indicative of lipid oxidation (**Lipid oxidation =CH** and **Lipids oxidation COO**), respectively obtained dividing the integrated area of the band at 3010 cm^{-1} and the one centred at 1740 cm^{-1} by the Lipid spectral region, share the same trend, showing a significant increase in F1 OLD BREEDER and F1 OLD FEMALE/young male groups respect to F1 YOUNG BREEDER and F1 YOUNG FEMALE/old male ones. Results are summarized in Figure 5.

Molecular analysis of *sirt1* and *foxo3a* genes in F1 offspring

Both *sirt1* and *foxo3a* genes are involve in the cell adaptive response to oxidative stress and aging. We assessed expression of both these genes in F1 oocytes at different developmental stage.

SIRT1 gene expression in oocytes from F1 ovaries from all groups, did not show differences in pre-vitellogenic oocytes, while there was an increase in F1 female vitellogenic oocytes from YOUNG BREEDER group respect to all other experimental groups. In late vitellogenic oocytes YOUNG BREEDER group together with F1 YOUNG FEMALE/old male breeder group showed the highest expression levels of SIRT1 (ANOVA, $P < 0,05$).

Opposite trend was observed for FOXO3a gene expression in oocytes at different stage of maturation obtained from F1 female from YOUNG BREEDERS and YOUNG FEMALE/old male breeder groups which showed lower gene levels than the other breeder groups (ANOVA, $P < 0,05$) (Fig. 6).

DISCUSSION

This study was set up to address three questions: could male and/or female breeder age affect reproductive performance? Is there a consequence of maternal and paternal aging on onset of offspring sexual maturity in female? Do parental age influence females offspring's gametes in terms of quality?
The answer to these questions was provided by statistical, molecular, histological and spectroscopic approaches.

Age-specific breeder differences in reproductive performance

Fecundity of females from different-age breeder groups was studied as well as the batch fecundity. The number of released eggs per spawning were influenced by maternal age but not the fertilization rate .The age-specific nature of these maternal effects could reflect the degree of energetic resources allocated: younger mothers contributes most of the mRNA, lipid, carbohydrate and protein molecules than the older, facilitating the eggs production as previously evidenced also by Mousseau and Fox [18] and Priest et al.[19]

Maternal contribution was relevant also in terms of embryos quality, resulting in best success of embryonic survival and hatching rate from young females. As mothers age for reproductive effort, also paternal age may play a role in the survival of the offspring affecting the reproductive capacity underlying that gamete quality, related fertilization and hatching success change with breeders aging. Gagliano and Mc Cormick postulated that manipulating maternal condition by altering food availability could affect the maternal energy allocation to offspring and influence early life-history traits and survivorship in the coral reef fish *Pomacentrus amboinensis* [20]. Maternal energy allocation promote an higher fecundity in annual killifish from unpredictable environments, such as temporary pools on African savannah, that generates selective pressure on reproductive traits due to high mortality risk [21].

Here, we showed that not only environmental conditions and food availability [22] but also parental age could be a key factor for reproductive fitness in *N. furzeri* and this could be caused mostly to maternal physiological decline due to aging that affect energy allocation in reproduction.

Maternal age as a factor that affects biochemical compositions in F1 vitellogenic oocytes

The calculated band area ratios for vitellogenin oocyte membranes suggest a deep modification in the molecular composition of the membrane, related to breeders' age: all the main components of the membrane, such as lipids, proteins and phosphate groups, are affected by parental age. In particular, we report a decrease of the unsaturation level of the phospholipid chains, which suggests a decrease of membrane fluidity in F1 OLD BREEDER and F1 OLD FEMALE/young male groups. The vibrational analysis performed on cytoplasmic vesicles revealed that vitellogenin-derived proteins are greatly altered in relation to parental age. The amount of proteins and phosphates is lower in F1 OLD BREEDER and F1 OLD FEMALE/young male groups, while carbohydrate groups and lipids are more abundant in these experimental groups. Particularly, it is interesting to highlight that =CH and COO groups, typical of lipids that have undergone a lipid peroxidation, share the same trend, with higher values in F1 OLD BREEDER and F1 OLD FEMALE/young male groups suggesting a deeper oxidative stress status.

An important result, which is common to all the band area ratios analysed (with exception of the unsaturation level in oocyte membranes) is that maternal age seems to be the factor that mostly affects the molecular composition of membrane and vitellogenin-derived proteins in the offspring ovary: in fact, there is no significant difference between F1 OLD BREEDER and F1 OLD FEMALE/young male groups, or between F1 YOUNG BREEDER and F1 YOUNG FEMALE/old male groups.

These remarks along with the finding of an higher lipid oxidation which could affect the membrane fluidity, let us suppose a poor quality and quantity in terms of macromolecules of vitellogenic oocytes in F1 ovary from OLD BREEDERS and OLD FEMALE/young male breeder groups suggesting a trans generationa maternal control of these components.

SIRT1 as a regulator of the oxidative stress in oocytes

Sirtuins are key molecule responsible for the regulation of oxidative stress acting as a sensor of the energy status in different cells, including oocytes, since variation in NAD+/NADH ratio controls their activity [23,24]. Sirt1, a member of the Sirtuin gene family, can upregulate key antioxidant enzymes such as catalase, through forkhead box O- (FoxO-) dependent activity [25,26].

The SIRT1-FOXO3A axis might be one of the signaling pathways with a main role in the regulation of oxidative stress. Through deacetylation of the FOXO3a transcription factor, SIRT1 stimulates the expression of catalase and manganese superoxide dismutase, playing a role in damage surveillance and oxidative stress responses.[27,28]

Moreover, several studies based on the observation of increased ROS levels and disturbed spindle organization under SIRT1 inhibition, a role as a guardian of meiosis and also on oocyte maturation, might be suggested [6,7]. Results from real-time PCR revealed higher levels of *Sirt1* mRNA in F1 oocytes from YOUNG BREEDERS (vitellogenic and late vitellogenic oocytes) and YOUNG FEMALE/old male (late vitellogenic oocytes) respect to the other experimental groups suggesting an higher protection against oocytes damage in offspring from younger parents. Moreover, in accordance with a role of *Foxo3a* in the antioxidant response, this gene decreased with the opposite trend as *Sirt1,* indicating a regulatory relationship between both genes and suggesting that *Foxo3a* acts downstream to *Sirt1* activity.

This data, together with finding from biochemical results, suggest that F1 female oocytes from old mother and old parents were more vulnerable to the effects of endogenous oxidative stress.

Parental age influences gametogenesis in offspring

A study conducted by Polačik et al. showed as in *N. furzeri*, high energetic reserves in embryos and small hatching length are traits characteristic for a "fast phenotype" reaching sexual maturity earlier than the "slow" fish that hatched with smaller reserves [29].

It is well known that energy substrates, as vitellogenin, is allocated into the gonad prior to the females breeding in [30], so we tested whether maternal and paternal age could affected not only the reproductive fitness related with the embryo numbers, but also with the allocation of energy into developmental gonad resulting on onset of sexual maturity in female offspring.

In the same conditions of food availability and environment, females from old mother reached sexual maturity later than females from young mother probably due to different maternal energy allocation into reproductive tissue.

Our hypothesis is that resources allocated for reproductive process seems to be intrinsically regulated via germ cell by maternal contribution: mothers' age seem to influence the physiological reproductive capacity of deriving offspring suggesting an energy-driven selective mechanisms operating to determine the timing of onset of sexual maturity in female offspring.

We demonstrated that female from annual killifish displayed marked plasticity in sexual maturity traits, triggered by parental age and we suppose that a rapid sexual maturity can be a reproductive strategies for *N.furzeri* living in ephemeral habitats and permit offspring survival, but further work is required to clarify this interesting result.

CONCLUSION

This is one of the very few studies related to the effects of maternal and paternal age on reproductive fitness using *Nothobranchius furzeri* as experimental model.

All our findings suggest that both advanced maternal and paternal age affect reproductive performance and could influence on the initial investment of energy allocation in offspring reproduction prior to mating.

The energy allocation age-related to gametogenesis is part of life history traits and delay in sexual maturity is a central aspect of theories that explain the biology of evolution.

Due to the ecological peculiar strategy of the genus *Nothobranchius*, inhabiting the temporary African water bodies subject to annual desiccation, the advancement of the sexual maturity in both male and female from young parents represent an important ecological advantage that allow to reach several generation quickly within the same raining season and may improve the offspring's chance of survival.

Results suggest that both parental age can lead to phenotypic variation directly via germ cell to offspring and this could be related to adaptive respond for natural selection [31] to environmental cue.

Taking all this together, future works are necessary to investigate molecular and epigenetic mechanisms related to parental age for better understand the factors transmitted via germ cell to progeny and improve the knowledge on the complex mechanism of aging.

REFERENCES

1. Lindstrom J. Early development and fitness in birds and mammals. *TREE* 1999; 14(9): 343-47.
2. Cunningham EJA, Russell AF. Egg investment is influenced by male attractiveness in the mallard. *Nature*. 2000;404:74-77.
3. Kunz T. and Orell K.S. Energy cost of reproduction. *Encyclop. Energy* 2004; 5: 423-442.
4. Monaghan P, Nager RG. Why don't birds lay more eggs? *Trends Ecol Evol*. 1997;12(7):270-274.
5. McCleery R., Perrins C., Sheldon B., Charmantier A. Age-specific reproduction in a long-lived species: the combined effects of senescence and individual quality. *Proc R Soc B Biol Sci*. 2008;275(1637):963-970.
6. Forslund P, Pärt T. Age and reproduction in birds - hypotheses and tests. *Trends Ecol Evol*. 1995;10(9):374-378.
7. Angelier F, Moe B, Weimerskirch H, Chastel O. Age-specific reproductive success in a long-lived bird: Do older parents resist stress better? *J Anim Ecol*. 2007;76(6):1181-1191.
8. Hipfner JM, Gaston AJ, Herzberg GR, Brosnan JT, Storey AE. Egg composition in relation to female age and relaying: constraints on egg production in thick-billed murres (uria lomvia). *Auk*. 2003;120(3):645.
9. Priest NK, Mackowiak B, Promislow DEL. The role of parental age effects on the evolution of aging. *Evolution (N Y)*. 2002;56(5):927.
10. Fox CW, Bush ML, Wallin WG. Maternal age affects offspring lifespan of the seed beetle , Callosobruchus maculatus. 2003;(Klass 1977):811-820.
11. Gluckman PD, Hanson MA. Evolution , development and timing of puberty. *Trends in Endocr Metab* 2006;17(1).
12. Louis GMB, Gray LE, Marcus M, et al. Environmental Factors and Puberty Timing : Expert Panel Research Needs. *Pediatrics* 2008.S192-207
13. Rhind SM, Rae MT, Brooks AN. Review Effects of nutrition and environmental factors on the fetal programming of the reproductive axis . *Reproduction* 2001; 20:205-214.
14. Blažek R, Polačik M, Reichard M. Rapid growth, early maturation and short generation time in African annual fishes. *EvoDevo,* 2013, 4:24.
15. Genade T. LABORATORY MANUAL FOR CULTURING N. furzeri.
16. Carnevali O, Conti C, Ferraris P, et al. FT-IR Microspectroscopy on molecular building of Zebrafish oocytes. *J Mol Struct*. 2009;938(1-3):207-213.

17. Maradonna F, Gioacchini G, Falcinelli S, et al. Probiotic supplementation promotes calcification in Danio rerio larvae: a molecular study. *PLoS One*. 2013;8(12).

18. Mousseau and Fox..Evolution of maternal effects:past and present *Adapt significance Matern Eff*. 1998;13(10).

19. Priest NK, Mackowiak B, Promislow DEL, Evolution S, May N. The Role of Parental Age Effects on the Evolution of Aging *Evolution* 2014;56(5):927-935.

20. Gagliano M, McCormick MI. Maternal condition influences phenotypic selection on offspring. *J Anim Ecol*. 2007;76(1):174-182.

21. Vrt M, Reichard M. Female fecundity traits in wild populations of African annual fish : the role of the aridity gradient. *Ecol Evo* 2016; 6(18):5921-31.

22. Vrtílek M, Reichard M. Highly plastic resource allocation to growth and reproduction in females of an African annual fish. *Ecol Freshw Fish*. 2015;24(4):616-628.

23. Emidio G Di, Falone S, Vitti M, et al. SIRT1 signalling protects mouse oocytes against oxidative stress and is deregulated during aging. *Hum Reprod* 2017;29(9):2006-2017.

24. Tatone C, Emidio G Di, Vitti M, et al. Sirtuin Functions in Female Fertility : Possible Role in Oxidative Stress and Aging. *Ox Med Cell Long* 2015; (2015): 1-13.

25. Furukawa-hibi Y, Chen C, Horio Y. SIRTl is critical regulator of FOXO-mediated transcription in response to oxidative stress. *Int J Mol Med* 2005, 16(2):237-243.

26. Motta MC, Divecha N, Lemieux M, et al. Mammalian SIRT1 Represses Forkhead Transcription Factors. *Cell* 2004;116:551-563.

27. Luo J, Nikolaev AY, Imai S, et al. Negative Control of p53 by Sir2 Promotes Cell Survival under Stress. *Cell* 2001;107:137-148.

28. Caito S, Rajendrasozhan S, Cook S, et al. SIRT1 is a redox-sensitive deacetylase that is post-translationally modified by oxidants and carbonyl stress. *FASEB, 24(9)*:3145-3159.

29. Polačik M, Blažek R, Řežucha R, Vrtílek M, Terzibasi Tozzini E, Reichard M. Alternative intrapopulation life-history strategies and their trade-offs in an African annual fish. *J Evol Biol*. 2014;27(5):854-865.

30. Mcbride RS, Somarakis S, Fitzhugh GR, et al. Energy acquisition and allocation to egg production in relation to fish reproductive strategies. *Fish Fish*. 2015;16(1):23-57.

31. Mousseau TA, Fox CW. The adaptive significance of maternal effects. *Trends Ecol Evol* 1998;13(10):403-407.

Tables

Table 1 List of primers used to amplify selected genes through q-PCRs

Gene	Forward 5'-3'	Reverse 5'-3'	Acc. number
sirt1	TCAGACGGGACCCTAGACC	GCGTAGCAGCTTCTCTTGCT	EU271679
foxo3a	AGGCGACAGCAACAGCTCA	GGAGCTTTGCCTCCTTTACC	EF464717

Tab. 2 Comparisons of traits between different-age breeder groups. Letters representing statistically significant differences in each trait ($p > 0,05$).

Trait	OLD BREEDERS	OLD FEMALE/young male breeder	YOUNG FEMALE/old male breeder	YOUNG BREEDERS
Number of spawned eggs	767 [a]	605 [a]	1202 [b]	1604 [b]
Rate of eggs fertilized	58,54%	52,84%	64,96%	62,68%
Rate of F1 embryonic survival	11,36% [a]	8,16% [b]	18,32% [c]	14,2% [d]
Rate of F1 hatching	41,18% [a]	50% [b]	62,5% [c]	77% [d]

Tab. 3 Summary of the mean number and rate of each F1 germ cell class between experimental groups. Values with different letters indicate different significant differences in each class of germ cell ($p > 0,05$).

	F1 OLD BREEDER groups		F1 OLD FEMALE/young male groups		F1 YOUNG FEMALE/old male groups		F1 YOUNG BREEDER groups	
	Cell counts	Distribution	Cell counts	Distribution	Cell counts	Distribution	Cell counts	Distribution
Class of germ cells:	n	%	n	%	n	%	n	%
PRE-VITELLOGENIC OOCYTES	87,53 (± 8,16) [a]	58,31 (± 35,41)	51,07 (± 4,03) [a]	53,34 (± 15,99)	53,67 (± 3,53) [a]	37,84 (± 6,73)	45,88 (± 0,99) [b]	30,15 (± 10,93)
VITELLOGENIC OOCYTES	36,8 (± 2,64) [a]	37,74 (± 4,47)	39,37 (± 0,96) [a]	40,51 (± 3,29)	68,66 (± 1,39) [b]	48,54 (± 3,17)	85,42 (± 2,19) [b]	55,83 (± 19,38)
POST-VITELLOGENIC OOCYTES	7 (± 0,35) [a]	3,95 (± 0,60)	5,67(± 2,01) [a]	6,15 (± 6,25)	19,29 (± 1,56) [b]	13,62 (± 3,59)	21,05 (± 0,99) [b]	14,03 (± 6,10)

n = total mean number of germ cells % = rate of germ cell distribution on gonadal weight in each ovary section observed with x 10 objective

Figures

Fig. 1 Comparisons of histological sections of ovary in different experimental groups at 4X magnification : (A) F1 ovary from YOUNG FEMALE/ old male presents an higher number of vitellogenic oocytes, (B) F1 ovary from YOUNG BREEDERS presents an higher content of late vitellogenic oocytes , (C) F1 ovary from OLD FEMALE/young male prevalently shows pre-vitellogenic and vitellogenic oocytes, (D) F1 ovary from OLD BREEDERS shows an higher number of pre-vitellogenic oocytes. Scale bar 500 µm. Symbols indicate**:** ■ pre-vitellogenic oocytes, ● vitellogenic oocytes, ▲ late-vitellogenic oocytes.

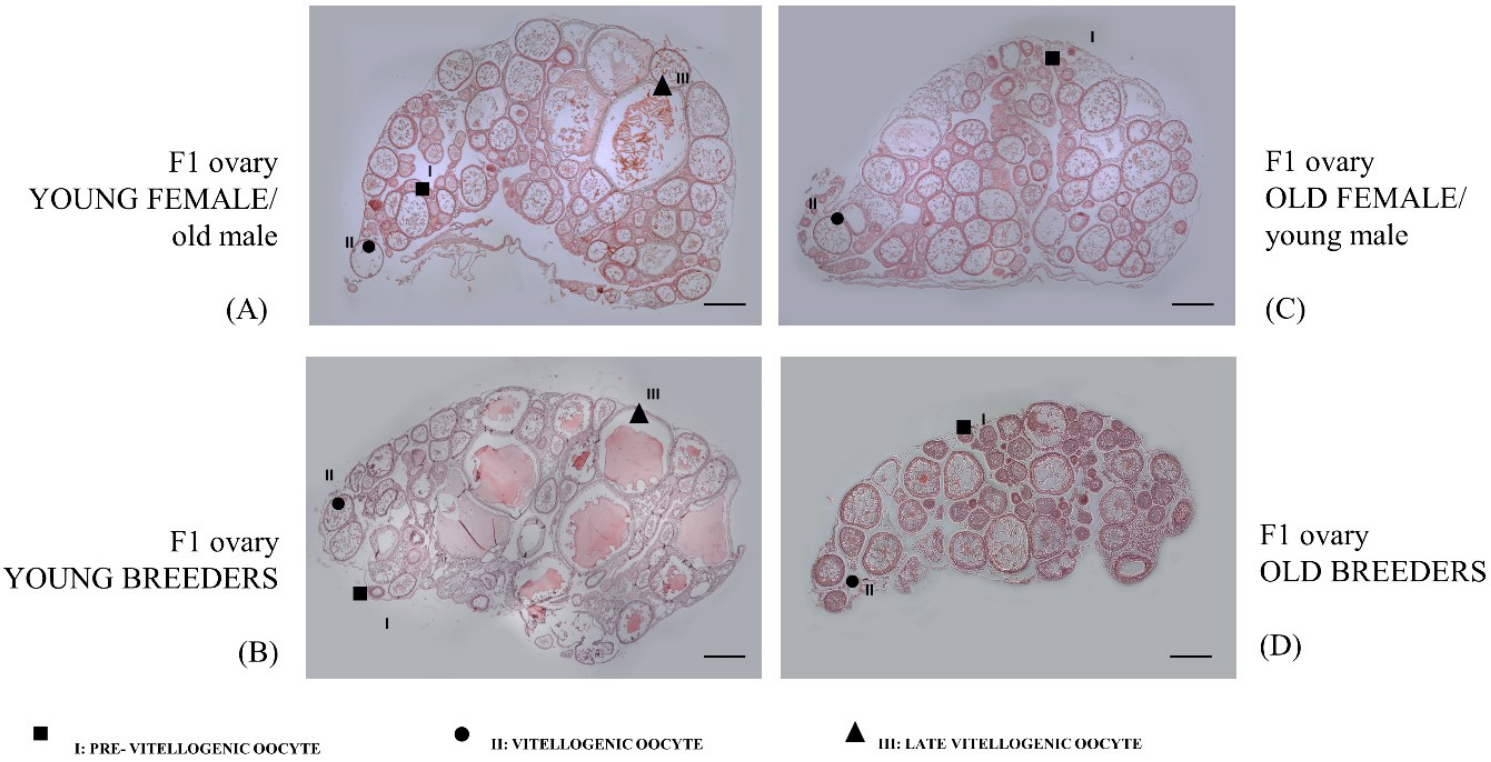

Fig. 2 Rate of oocytes for each class (pre-vitellogenic, vitellogenic and late-vitellogenic oocytes) in F1 ovaries from different breeder groups. In dark grey pre-vitellogenic oocytes rate , in grey vitellogenic oocytes rate and in light grey late-vitellogenic oocytes rate were presented for each experimental group.

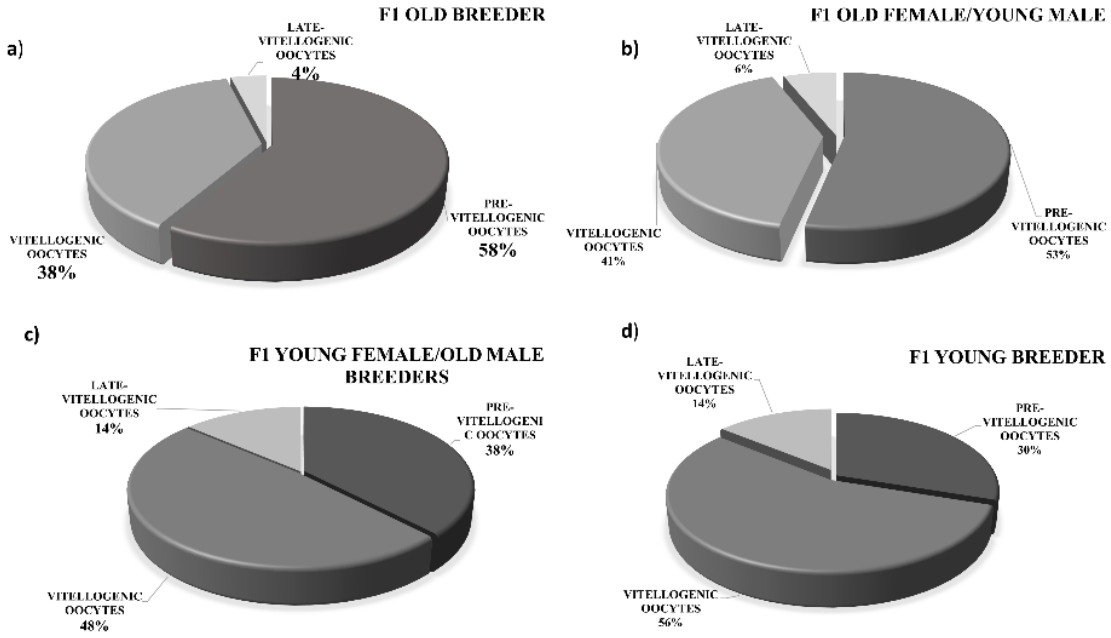

Fig 3 Total absorbance cartogram of vitellogenic oocyte (A column); chemical maps of the integrated areas under the Lipid region (3030-2800 **cm^{-1}) (B column), the Amide I and II bands under the protein region (**1715-1481**cm^{-1}) (C column) and the phosphate and carbohydrate zones (**1140–1030 **cm^{-1}) (D column).**

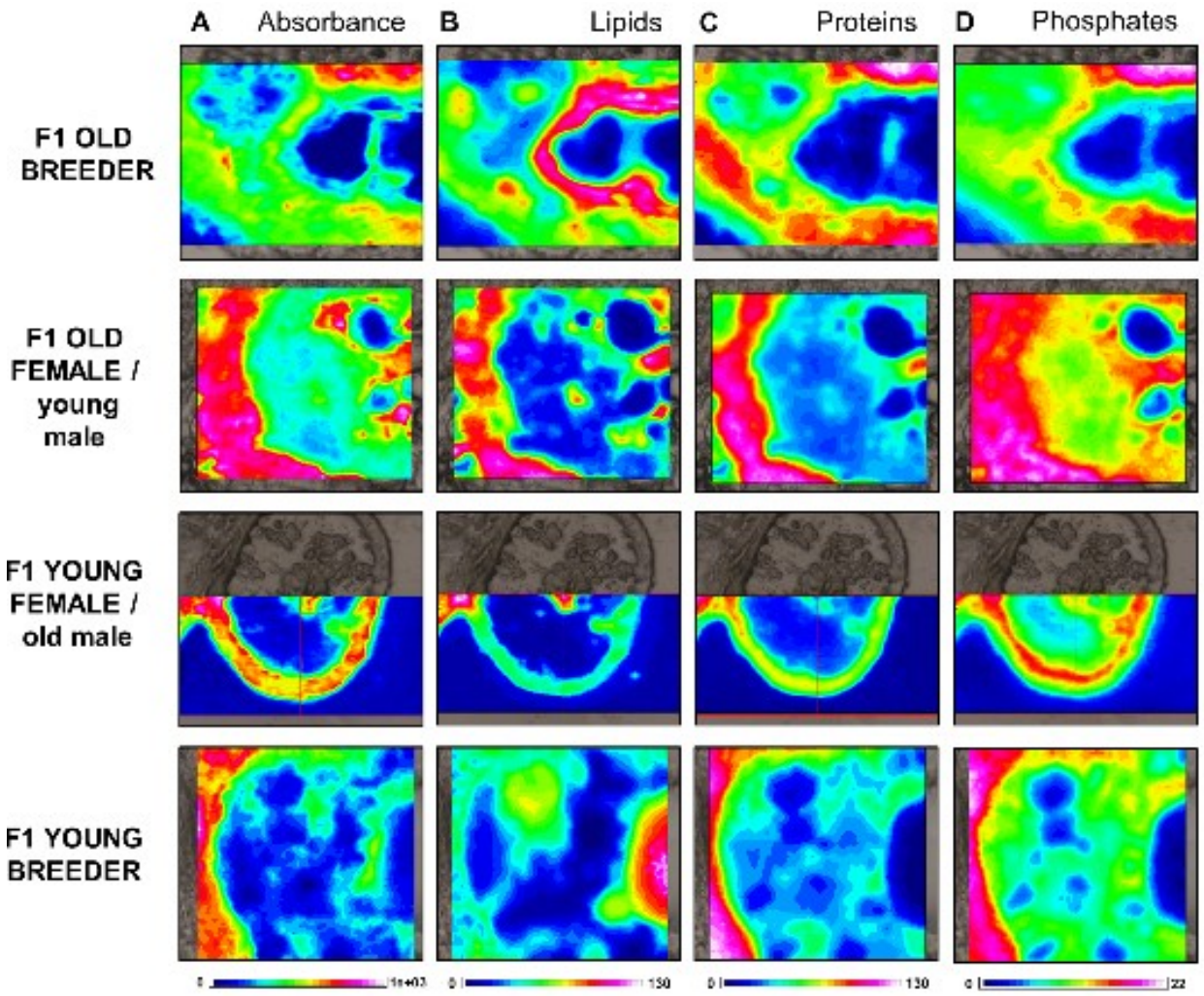

Fig 4 . Results of ANOVA performed on band area ratios in membrane. Histograms showing means and standard deviations of the selected biomarkers for the experimental groups. Statistical significance was set at $p < 0.05$.

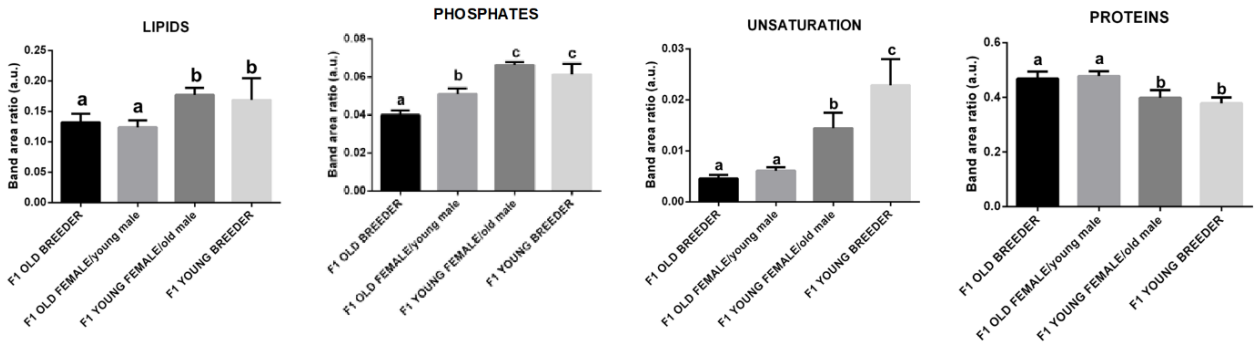

Fig 5.Results of ANOVA performed on band area ratios in cytoplasm. Histograms showing means and standard deviations of the selected biomarkers for the experimental groups. Statistical significance was set at $p < 0.05$

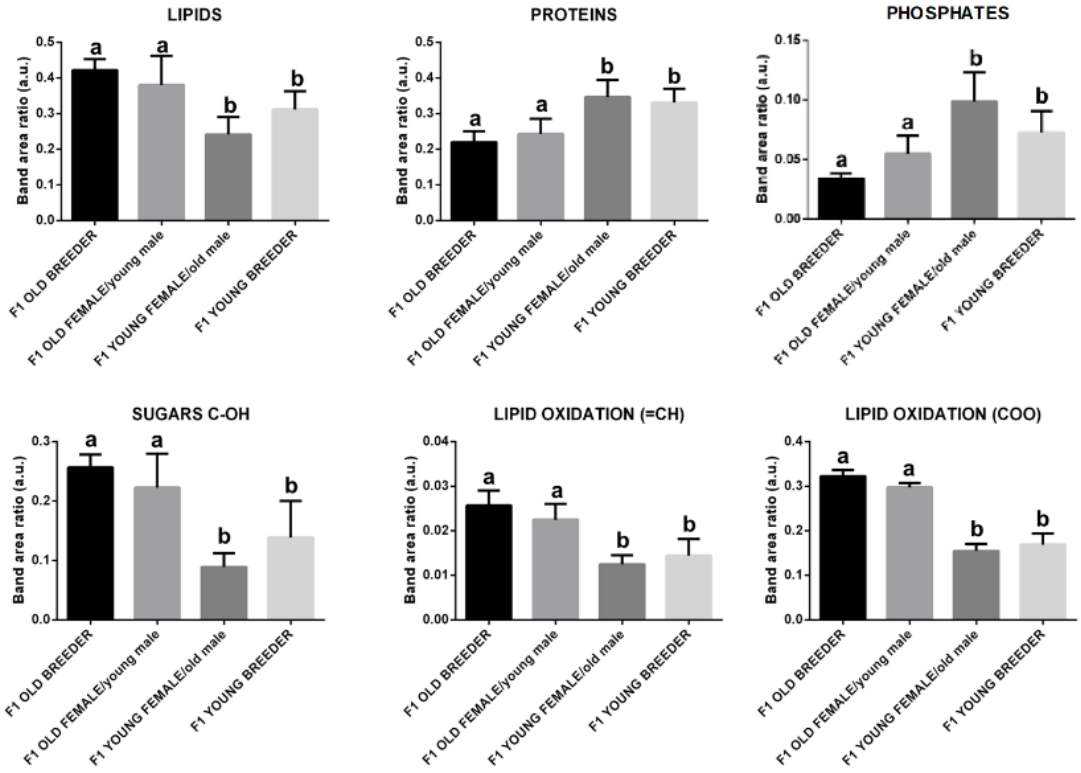

Fig. 6 Gene expression quantification of *sirt1* and *foxo3a* in the three oocytes classes (pre- vitellogenic, vitellogenic and late vitellogenic) of female from the four experimental groups. Transcript levels were determined by qPCR and normalized using *arp* as reference gene. Error bars indicate mean ± S.D. Letters symbolize the statistical difference. Confidence interval set at 95% (p< 0,05).

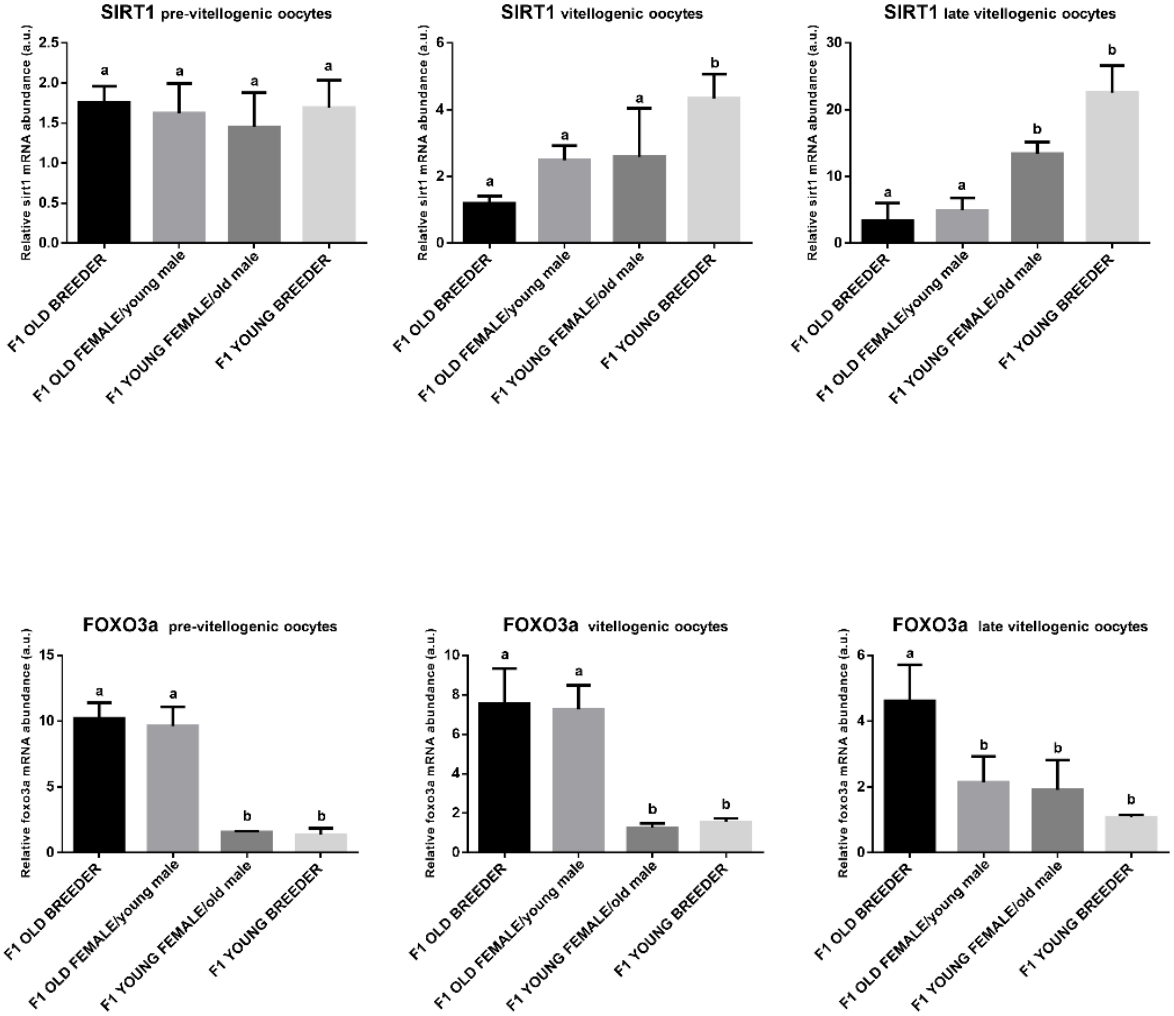

Chapter 3

Molecular differences in *Nothobranchius furzeri* oocytes: influence of maternal age

Abstract

A new fish model, considered the shortest-lived vertebrate, is emerging as new experimental model for aging studies. The killifish *Nothobranchius furzeri,* which life expectancy is less of one year, is becoming attractive for aging research in different field, such as genetic, biology, pharmacology and neurobiology.

In this study, we focused on the effects of maternal aging on oocyte macromolecular structure since the oocytes quality decline is one of the major cause of reproductive problem in vertebrate.

In this study, the use of Raman microspectroscopy (RMS) provided new insights on the effects of maternal age on *Nothobranchius furzeri* oocytes.

In this preliminary study, we investigated the molecular differences comparing oocytes laid (but not fertilized) from young females (14 weeks post hatching) and old females (28 weeks post hatching) of *N.furzeri*, exploiting for the first time, RMS.

Single RMS spectra obtained from maps acquired along the Z axis of oocytes, were divided in six regions according to their distance from the surface, and checked for similar features.

Results showed a deep age-related alteration of spectral features related to amino acid and lipid class composition and content. These classes of biomolecules are essential for a proper oocyte maturation, and further embryo development hence suggesting that maternal aging impairs the accumulation of maternal factors crucial for a proper early embryo development.

INTRODUCTION

Aging is one of the most complex biological processes and can be defined as a progressive functional decline of physiological function with age, including a decrease in fecundity.

In females, oocytes ageing cause morphological and cellular alterations associate with decline in homeostatic capacities resulting in degenerative changes[1].

Most of our understanding about the effects of aging has been obtained thanks to studies on the yeast *Saccharomyces cerevisiae*, the nematode worm *Caenorhabditis elegans*, the fruit fly *Drosophila melanogaster*, and the house mouse *Mus musculus* but in the last decade a new vertebrate emerged as model for aging studies the annual killifish *Nothobranchius furzeri*.

In this study the *Nothobranchius furzeri*, which lifespan is about 6 months accompanied by faster growth and rapid sexual maturity exhibiting early age-related biomarkers was used as experimental model. The peculiar life cycle of killifish is relatively unique because they are adapted to inhabits temporal ponds in regions characterized by dry and rainy season alternation from South Africa[2].

Considering the habitat in which killifish lives, studies on the effects of aging on oocytes and egg envelope, particularly important for embryonic survival buried in the mud, are very fascinating.

Light and TEM micrographs of egg envelope in developing oocytes showed hair-like structures projecting toward and among the follicular cells providing to mechanical resistance, allowing gas exchange, and helping to keep the eggs associated to the substrate[3].

Raman microspectroscopy (RMS) is a powerful, rapid and well-assessed spectroscopic technique to study the composition of cells. RMS spectra contain information about chemical, biological and physical changes of cellular biomolecules, giving a molecular fingerprint of the studied sample[4,5]. RMS can be performed on cells under physiological conditions, due to the weak contribution of water, with no need of staining[6]. In literature, the use of RMS on female gametes is described in only few studies, focused on describing the molecular architecture of oocytes from several species[7–9], following the changes occurring during maturation[10], on investigating age-induced effects on mouse oocytes[11], and on analyzing the structure of the zona pellucida of ovine oocytes after vitrification[12].

Due to the growing interest and importance of *Nothobranchius furzeri* in the field of reproductive aging, in this study we aimed to investigate the molecular architecture of oocytes of this fish, comparing the spectral features between oocytes retrieved from young females (14 weeks post hatching) and old females (28 weeks post hatching), in order to shed new light on the characteristics of female gametes of a species characterized

by rapid sexual maturity of any reported vertebrate species that in *N. furzeri* is attained at 4-6 weeks post hatching[13].

EXPERIMENTAL SECTION

Ethics

All the procedures involving animals were conducted according to Italian law on experimental animals and were approved by the Health Ministry's Department of Veterinary Public Health and by the Ethics Committee of Università Politecnica delle Marche (Authorization No. 852/2016-PR). Optimal rearing conditions were applied throughout the study.

Animals

Nothobranchius furzeri, strain MZM 0410, were cultured according to the manual for caring *N. furzeri* [14].

A total of 32 female/male adults from *N. furzeri* were placed in eight aquaria of 20-L (4 fish/tank) with oxygenated water under controlled conditions (26 ± 0.5 °C) and maintained on a 12/12 h light/dark cycle. They were fed twice a day with *Chironomus chironominae* larvae and *Artemia salina* nauplii.

Two breeder experimental groups, differing for female age, were formed crossing 1 male and 3 female adults. The Old-Female group was composed of males at 16 weeks post hatching (wph) and females at 28 wph; the Young-Female group was composed of males at 16 wph and females at 14 wph. During the experiment, both breeder groups, each one with 4 replicates, were kept separately and a spawning dish with sand was put to facilitate the regular oviposition by females. *Nothobranchius furzeri* females after reaching sexual maturity at about 4-8 wph, depending of environmental conditions, temperature and food availability, spawn daily allowing regular collection of eggs.

For each experimental group, 5 oocytes were collected and then named **Young** and **Old**, according to female age.

To prepare samples for Raman characterization, oocytes not fertilized collected from both experimental groups were fixed by immersion in 4% paraformaldehyde (PFA) for 15 minutes and then washed in PBS 0.1 M three times to remove residual PFA from oocytes. After these steps, each single oocyte was put in a single vial and stored at -20°C.

RMS measurements and data analysis

A Horiba Jobin-Yvon LabRAM HR800 spectrometer, equipped with a 532-nm diode laser as source was used. All measurements were acquired by using a x100 long working distance objective (Olympus, N.A. 1). The spectrometer was calibrated to the 520.7 cm^{-1} line of silicon prior to spectral acquisition. A 600 lines per mm grating was chosen. A 200 μm confocal pinhole was used for all measurements. The spectra were dispersed onto a 16-bit dynamic range Peltier cooled CCD detector. Oocytes were deposed onto glass slides, and 1D-depth profiling was performed on 5 oocytes for each experimental group: these maps (5/oocyte), acquired along the Z axis, were obtained after focusing the laser on the surface of the oocyte and then acquiring a spectrum every 11 μm, from a starting point of -5 μm, to an ending point of 200 μm. The spectral range from 400 to 1800 cm^{-1}, the so-called fingerprint region, was chosen and spectra were acquired for 2x40 seconds at each spot.

Single RMS spectra were extracted from the Z-maps, divided according to their distance from the surface, and checked for similar features, in order to convert the physical regions into a lower number of spectral regions. RMS spectra were first submitted to multivariate analysis. PCA is a multivariate technique widely performed to highlight spectral variability among different groups or to recognize outliers. It allows the discrimination of different spectral groups of similar variability, using Principal Components (PCs) and scores plots; moreover, the usefulness of PCA in spectroscopy studies resides in the loadings, in which the variations among groups are highlighted according to wavenumbers [15]. PCA was carried out by using an in-house developed algorithm with R Studio (RStudio: Integrated Development for R. RStudio, Inc., Boston, MA), to compare spectra from **Young** and **Old** experimental groups in each identified region. Prior to quantitative analysis of band areas, spectra were smoothed using 7 smoothing points and baseline-corrected with the polynomial method (2 iterations) (OPUS 7.1 software).

The most representative bands composing the RMS spectrum were selected and submitted to an integration procedure, in order to measure peak intensities (relative to the local baseline, Integration mode K, OPUS software): 616–632 cm^{-1} (C-C twisting mode of phenylalanine, ‘622’); 634–653 cm^{-1} (C-C twisting mode of phenylalanine and tyrosine, ‘644’); 752–771 cm^{-1} (ring breathing of tryptophan, ‘759’); 822–841 cm^{-1} (asymmetric O-P-O stretching of tyrosine, ‘831’); 842–867 cm^{-1} (amino acid sidechain νC–C of proline, ‘853’); 870–889 cm^{-1} (ring breathing of tryptophan, ‘881’); 908–949 cm^{-1} (skeletal C-C vibration mode, α-helix, ‘930’); 994–1016 cm^{-1} (symmetric ring breathing mode of phenylalanine, ‘1003’); 1024–1040 cm^{-1} (CH_2/CH_3 bending modes of phospholipids, ‘1032’); 1117–1139 cm^{-1} (νC-C skeletal of acyl backbone in lipids, ‘1125’); 1144–1166 cm^{-1} (C=C stretching mode of carotenoids, ‘1160’); 1194–1219 cm^{-1} (ν(C-C_6H_5) of tryptophan and phenylalanine, ‘1208’); 1224–1253 cm^{-1} (Amide III, ‘1247’); 1259–1281 cm^{-1} (Amide III of proteins in the α-helix conformation, ‘1266’); 1293–1308 cm^{-1} (CH_2 deformation of lipids, ‘1305’); 1308–

1325 cm^{-1} (CH_3/CH_2 twisting mode of lipids, '1313'); 1330–1350 cm^{-1} (nucleic acid vibrational mode, '1340'); 1420–1491 cm^{-1} (δCH_2, '1450'); 1502–1536 cm^{-1} (-C=C- of carotenoid, '1525'); 1600–1628 cm^{-1} (tyrosine and tryptophan νC=C, '1615'); 1629–1716 cm^{-1} (amidic νC=O, '1661'); 1730–1769 cm^{-1} (C=O of lipids, '1750'). Band assignment is given on the basis of the review of Movasaghi and colleagues [16].

Statistical analysis

Normally distributed data deriving from integration of RMS spectra were presented with box charts, highlighting percentiles, median and outliers of data from each experimental group. Significant differences between experimental groups were determined by Student's *t*-test), using the statistical software package Prism6 (Graphpad Software, Inc. USA). Statistical significance was set at $p < 0.01$.

RESULTS

Killifish oocytes collected from **Young** (females at 14 wph) and **Old** (females at 28 wph) were deposed onto glass slides and analysed using RMS.

Single RMS spectra were extracted from the Z-maps, divided according to their distance from the surface, and checked for similar features: six regions (Regions I-II-III-IV-V-VI) were found to be characterized by the same type of spectra (Figure 1 and Figure 2). Region I corresponds to the surface; Region II corresponds to the region at ~10 μm under the surface; Region III corresponds to the region at ~30 μm under the surface; Region IV corresponds to the region at ~50 μm under the surface; Region V corresponds to the region at ~110 μm under the surface; Region VI corresponds to the region at ~155 μm under the surface

PCA was carried out to highlight spectral variability among different groups, and to discriminate different spectral groups of similar variability, using Principal Components (PCs) and scores plots.

Figure 3A shows the representative RMS spectra of Region I from oocytes of **Young** and **Old** groups, with the most visible discriminant features highlighted by dashed rectangles. Results of PCA are reported in Figures 2B and 2C: the score plot (Fig. 3B) shows a clear segregation of **Young** and **Old** groups along the PC2 axis (19.65% of the explained variance), and the corresponding loading (Fig. 2C) confirms the spectral features discriminating the two experimental groups as the band centered at 1003 cm^{-1}, the 1200–1400 cm^{-1} region, the band at 1525 cm^{-1}, and the 1600–1800 cm^{-1} region.

In Figure 4, the results of the comparison of Region II in **Young** and **Old** groups are reported: Figure 4A shows the representative RMS spectra of Region II from oocytes of **Young** and **Old** groups, with the most visible

discriminant features highlighted by dashed rectangles. Figure 4B reports the score plot of PCA, which shows a clear segregation of **Young** and **Old** groups along the PC1 axis (68.15% of the explained variance); in Figure 4C, the loading corresponding to PC1 confirms the spectral features discriminating the two experimental groups as and the band centered at 1003 cm^{-1}, the 1200–1400 cm^{-1} region, the band at 1450 cm^{-1}, the band at 1525 cm^{-1}, and the 1600–1800 cm^{-1} region.

Figure 5 reports the results of the comparison of Region III in **Young** and **Old** groups: Figure 5A shows the representative RMS spectra of Region III from oocytes of **Young** and **Old** groups, with the most visible discriminant features highlighted by dashed rectangles. Figure 5B reports the score plot of PCA, which shows a clear segregation of **Young** and **Old** groups along the PC1 axis (68.15% of the explained variance); in Figure 5C, the loading corresponding to PC1 confirms the spectral features discriminating the two experimental groups as the band centered at 1003 cm^{-1}, the 1150–1300 cm^{-1} region, the band at 1525 cm^{-1}, and the 1600–1800 cm^{-1} region.

In Figure 6, the results of the comparison of Region IV in **Young** and **Old** groups are reported: Figure 6A shows the representative RMS spectra of Region IV from oocytes of **Young** and **Old** groups, with the most visible discriminant features highlighted by dashed rectangles. Figure 6B reports the score plot of PCA, which shows a clear segregation of **Young** and **Old** groups along the PC1 axis (66.94% of the explained variance); in Figure 6C, the loading corresponding to PC1 confirms the spectral features discriminating the two experimental groups as the band centered at 1003 cm^{-1}, the 1200–1300 cm^{-1} region, the band at 1450 cm^{-1}, the band at 1525 cm^{-1}, and the 1600–1800 cm^{-1} region.

Figure 7 reports the results of the comparison of Region V in **Young** and **Old** groups: Figure 7A shows the representative RMS spectra of Region V from oocytes of **Young** and **Old** groups, with the most visible discriminant features highlighted by dashed rectangles. Figure 7B reports the score plot of PCA, which shows a segregation of **Young** and **Old** groups along the PC1 axis (65.5% of the explained variance), with only three **Young** spectra e one **Old** spectrum out of the PCA region characterizing the experimental groups; in Figure 7C, the loading corresponding to PC1 confirms the spectral features discriminating the two experimental groups as the band centered at 1003 cm^{-1}, the 1200–1300 cm^{-1} region, the band at 1525 cm^{-1}, and the band at 1660 cm^{-1}.

In Figure 8, the results of the comparison of Region VI in **Young** and **Old** groups are reported: Figure 8A shows the representative RMS spectra of Region VI from oocytes of **Young** and **Old** groups, with the most visible discriminant features highlighted by dashed rectangles. Figure 8B reports the score plot of PCA, which shows a clear segregation of **Young** and **Old** groups along the PC1 axis (71.6% of the explained variance); in Figure 8C, the loading corresponding to PC1 confirms the spectral features discriminating the two

experimental groups as the band centered at 1003 cm^{-1}, the 1200–1400 cm^{-1} region, the band at 1525 cm^{-1}, and the 1600–1800 cm^{-1} region.

The most representative bands composing the RMS spectrum were selected and submitted to an integration procedure, in order to measure peak intensities (see Experimental section), to compare the alterations on oocytes related to the age of killifish. The analysis of the numerical variations of specific band area ratios, particularly related to proteins and protein characteristics, showed a deep alteration of numerous spectral features of the six identified Regions, as an effect of killifish age (Figure 9).

Region I (Figure 9A) is characterized by age-induced alterations affecting amino acid composition, as shown by the changes in the intensity of the bands at 644 cm^{-1} (due to phenylalanine and tyrosine vibrations), 759 and 881 cm^{-1} (due to tryptophan vibrations), 1208 cm^{-1} (due to tryptophan and phenylalanine vibrations), and 1615 cm^{-1} (due to tyrosine and tryptophan vibrations). The decrease in the intensity of the bands at 930 and 1266 cm-1, both assigned to vibrations of α-helix conformations of proteins, indicates a partial loss of properly folded peptide structures. Furthermore, the quantity of protein seems to be affected, as evidenced by the decrease in the intensity of the bands at 1660 cm^{-1} (assigned to the vibration of the amidic C=O) and at 1247 cm^{-1} (reported in literature as Amide III). Lipid content is also affected by age, as shown by the decrease of the bands at 1032 cm^{-1} (assigned to phospholipids), 1305 cm^{-1} (due to lipid CH_2 deformations), and 1750 cm^{-1} (due to vibrations of lipid C=O). Particularly relevant is the significant decrease affecting the bands at 1160 cm^{-1}, and especially at 1525 cm^{-1}, both attributed to vibrations of the C=C group in carotenoid structures.

Region II (Figure 9B) is characterized by age-induced alterations affecting all the spectral features, with exception of the band at 1450 cm^{-1}, assigned to the bending mode vibrations of CH_2 groups, and the one at 1247 cm^{-1} (Amide III). Age determines an alteration in the amino acid composition of **Old** oocytes, as shown by the changes in the intensity of the bands at 622 and 1003 cm^{-1} (due to phenylalanine vibrations), 644 cm^{-1} (due to phenylalanine and tyrosine vibrations), 831 cm^{-1} (due to tyrosine vibrations), 853 cm^{-1} (due to proline vibrations), 759 and 881 cm^{-1} (due to tryptophan vibrations), 1208 cm^{-1} (due to tryptophan and phenylalanine vibrations), and 1615 cm^{-1} (due to tyrosine and tryptophan vibrations). The decrease in the intensity of the bands at 930 and 1266 cm^{-1}, both assigned to vibrations of α-helix conformations of proteins, indicates a partial loss of properly folded peptide structures. The decrease in the intensity of the bands centered at 1660 cm^{-1} (assigned to the vibration of the amidic C=O) is associated with a decrease in protein amount. Lipid amount is also affected by age, as shown by the increase of the bands at 1032 cm^{-1} (assigned to phospholipids), and 1125 cm^{-1} (due to vibrations of lipid acyl backbones), and the decrease of the bands at 1305 cm^{-1} (due to lipid CH_2 deformations), 1750 cm^{-1} (due to vibrations of lipid C=O), and 1313 cm^{-1} (assigned to CH_2/CH_3 groups of

lipids). Also in Region II the bands at 1160 cm^{-1}, and especially at 1525 cm^{-1}, both attributed to vibrations of the C=C group in carotenoid structures, show a decrease in intensity.

Region III (Figure 9C) is characterized by age-induced alterations affecting all the spectral features, with exception of the band at 1450 cm^{-1}, assigned to the bending mode vibrations of CH_2 groups, at 1247 cm^{-1} (Amide III), and at 1032 cm^{-1} (due to phospholipids). **Old** oocytes are characterized by a deep alteration of the amino acid composition, as demonstrated by the increase of the intensity of the bands at 622 and 1003 cm^{-1} (phenylalanine), at 644 cm^{-1} (phenylalanine and tyrosine), at 831 cm^{-1} (tyrosine), at 853 cm^{-1} (proline), at 759 and 881 cm^{-1} (tryptophan), at 1208 cm^{-1} (tryptophan and phenylalanine), and at 1615 cm^{-1} (tyrosine and tryptophan). In Region III, the trend associated with the presence of protein α-helix conformations is not homogeneous: the band at 930 cm^{-1} increases, while the one at 1266 cm^{-1} displays an opposite trend. The increase in the intensity of the band centered at 1660 cm^{-1} (amidic C=O) is associated with an increase in protein amount. Age determines an increase in the lipid amount: the bands at 1125 cm^{-1} (acyl backbones), 1305 cm^{-1} (CH_2 groups), 1313 cm^{-1} (CH_2/CH_3 groups), and 1750 cm^{-1} (lipid C=O) show a significant increase. Region III is characterized by a significant decrease of the bands at 1160 cm^{-1}, and especially at 1525 cm^{-1}, both attributed to vibrations of the C=C group in carotenoid structures.

Region IV (Figure 9D) is characterized by age-induced alterations affecting all the spectral features, with exception of the band at 881 cm^{-1} (tryptophan), 930 cm^{-1} (α-helix), and 1032 cm^{-1} (phospholipids). Hence, also this 50μm-deep region, is characterized by an alteration of the amino acid composition, as shown by the increase of the bands at 622 and 1003 cm^{-1} (phenylalanine), 644 cm^{-1} (phenylalanine and tyrosine), 759 cm^{-1} (tryptophan), 831 cm^{-1} (tyrosine), 853 cm^{-1} (proline), 1208 cm^{-1} (tryptophan and phenylalanine), and 1615 cm^{-1} (tyrosine and tryptophan). A significant decrease of the intensity of the band centered at 1266 cm^{-1}, assigned to vibrations of α-helix conformations of proteins, indicates a partial loss of properly folded peptide structures. Furthermore, a visible discriminant spectral feature of this region is the significant decrease of the band at 1660 cm^{-1} (assigned to the vibration of the amidic C=O), which is associated with a decrease in protein amount. Lipid amount is affected in the same way as the previously described regions, as shown by the increase of the bands at 1125 cm^{-1} (due to vibrations of lipid acyl backbones), and the decrease of the bands at 1305 cm^{-1} (due to lipid CH_2 vibrations), 1750 cm^{-1} (due to vibrations of lipid C=O), and 1313 cm^{-1} (assigned to CH_2/CH_3 groups of lipids). Also in Region IV the bands at 1160 cm^{-1}, and especially at 1525 cm^{-1}, both attributed to vibrations of the C=C group in carotenoid structures, show a decrease in intensity.

Region V (Figure 9E) is characterized by age-induced alterations partly affecting the spectral features associated with the amino acid composition, such as 644 cm^{-1} (phenylalanine and tyrosine), 831 cm^{-1} (tyrosine), 853 cm^{-1} (proline), 759 cm^{-1} (tryptophan), 1003 cm^{-1} (phenylalanine), 1208 cm^{-1} (tryptophan and phenylalanine), and 1615 cm^{-1} (tyrosine and tryptophan). The decrease in the intensity of the bands at 930 and 1266 cm^{-1} (α-helix conformations of proteins) indicates a partial loss of properly folded peptide structures. The decrease in the intensity of the band centered at 1660 cm^{-1} (amidic C=O) is associated with a decrease in protein amount. Age determines an alteration in the lipid amount: the band at 1125 cm^{-1} (acyl backbones) increases, the bands at 1305 cm^{-1} (CH_2 groups), 1313 cm^{-1} (CH_2/CH_3 groups) and 1750 cm^{-1} (lipid C=O) decrease. Region V is characterized by a significant decrease of the bands at 1160 cm^{-1}, and especially at 1525 cm^{-1}, both attributed to vibrations of the C=C group in carotenoid structures.

Also the deepest region analyzed, Region VI, shows spectral alterations induced by female age. The amino acid composition is partly modified, as shown by the changes in intensity of the bands at 644 cm^{-1} (phenylalanine and tyrosine), 831 cm^{-1} (tyrosine), 881 cm^{-1} (tryptophan), 1003 cm^{-1} (phenylalanine), 1208 cm^{-1} (tryptophan and phenylalanine), and 1615 cm^{-1} (tyrosine and tryptophan). The amount of properly folded protein structures is negatively affected by age, as shown by the decrease in the intensity of the bands at 930 and 1266 cm^{-1} (α-helix conformations of proteins). The decrease in the intensity of the band centered at 1660 cm^{-1} (amidic C=O) is associated with a decrease in protein amount. Age determines a decrease in the lipid amount: the bands at 1305 cm^{-1} (CH_2 groups), 1313 cm^{-1} (CH_2/CH_3 groups) and 1750 cm^{-1} (lipid C=O) decrease. Region VI shows a significant decrease of the bands at 1160 cm^{-1}, and especially at 1525 cm^{-1}, both attributed to vibrations of the C=C group in carotenoid structures.

DISCUSSION

In the present study, *Nothobranchius furzeri* oocytes were investigated for the first time by RMS. In particular, the vibrational technique was applied to evaluate the alterations in the molecular architecture of female gametes determined by the maternal age. The results obtained, together with the previous studies reported in literature[7–12], let us suggest that RMS can be used to assess oocyte - macromolecular composition and provisionally their quality in this species as well as in others.

Oocytes were retrieved and classified according to female age into two experimental groups: **Young** (14 wph-females; n.5) and **Old** (28 wph-females; n.5). 1D-depth profiling let obtain RMS spectra, which were classified as belonging to six regions: Regions I-II-II-IV-V-VI.

The results of PCA showed a clear segregation of **Young** and **Old** spectra in each region, and evidenced the most discriminant spectral features in the 1000-1800 cm^{-1} region, as highlighted in the loading of relative PCs. For a better understanding of the changes induced by age in **Old** oocytes, the most representative bands composing the RMS spectrum were selected and submitted to an integration procedure. All the results obtained showed a deep and homogeneous alteration of the molecular architecture of **Old** oocytes. With exception of Region I, which resulted to be less modified by female age, all the other regions showed an almost complete alteration of **Old** spectral features suggesting that the major changes occurs at cytoplasmic level. Age affects the protein component of **Old** oocytes, in terms of amount, secondary structure, and amino acid composition. About protein amount, we found in all the regions (except Region III) a decrease of the intensity of the band at 1660 cm^{-1}, indicating a decrease in protein content: Davidson and colleagues[10] reported a higher protein content in good quality murine oocytes, hence letting us suggest a loss of quality in killifish oocytes collected from old females. Together with the alteration in protein amount, we found an impairment in protein secondary structure, evidenced by the decrease of the intensity of the bands at 930 and 1266 cm^{-1} (except for Region III), which suggests a partial loss of properly folded peptide structures. These findings can be explained by a process of age-related oxidative stress, which impacts the main cellular macromolecules, and in particular, causes changes in protein structure, partly due to oxidative modifications [17,18]. Furthermore, we found an alteration in the amino acid composition of oocytes, as shown by the changes in intensity of the bands associated to phenylalanine, tyrosine, proline, and tryptophan. Why the intensity of these bands oscillate is not clear, but could be explained by amino acid substitutions, which are among the causes of defective folding[17], or by the oxidation of amino acid side chains, leading to alterations of the vibrational signals associated with chemical groups[19]. The amino acid profile in fish oocyte is important since the proteolysis of yolk components will provide free amino acids (FAAs) essential for early embryo development.

Lipid component is crucial for the development of the oocyte: together with other molecules (including RNAs, proteins, vitamins and hormones), lipids are accumulated within the oocyte from plasma very low density lipoproteins (VLDL) and from vitellogenins (VTGs) in order to make possible a proper oocyte growth and maturation[21]. The general decrease in the intensity of the bands centered at 1305, 1313 and 1750 cm^{-1}, respectively due to CH_2 vibration of lipids, CH_3/CH_2 twisting mode of lipids, and C=O of lipids, demonstrate a decrease in the lipid content. Taken into account the crucial role of lipids in oocyte maturation, the age-induced decrease of lipids suggests an impairment of oocyte quality.

Particularly relevant is the decrease in all the selected regions in the content of carotenoids in **Old** oocytes. It is known that fish eggs contain carotenoids, retinals and retinols, used during embryonic development, after fertilization, which are mainly transported from the liver to the developing oocytes by VTG[22].

As fish from the two experimental groups were maintained in the same conditions, and fed in the same way, differences in terms of concentration of these molecules can only be attributed to their transport to the oocyte and/or uptake. This result, associated with the previously described decrease in lipid content, suggests a lack in the uptake of VTG and, hence, of carotenoids by the oocyte: in this sense, the quality of oocytes collected from old females is deeply impaired, as aging impacts the accumulation of maternal factors crucial for a proper early embryo development.

The changes of the major macromolecular classes appear to be homogeneous along all the cytoplasmic selected regions (II-VI) evidencing a typical composition within the two groups supporting the effects of the maternal aging on oocyte biochemical profile.

Concluding, the results obtained in this study using for the first time RMS to study *Nothobranchius furzeri* oocytes evidenced that female aging deeply impacts on the molecular architecture of oocytes, mainly affecting protein composition and lipid content. Moreover, the finding of a decrease in the content of carotenoids in **Old** oocytes let suggest a lack in the proper uptake of these molecules and of VTGs, essential for the proper oocyte growth and maturation and further embryo development.

In the future, this latter aspect will be further analyzed, in order to shed new light on the mechanisms underlying the age-induced decline of oocyte quality.

Figures

Figure 1. On the left, graphic representation of sections of oocyte for the spectrum acquisition. On the right, image from *Nothobtnchius furzeri* oocyte, scale bar 200 µm.

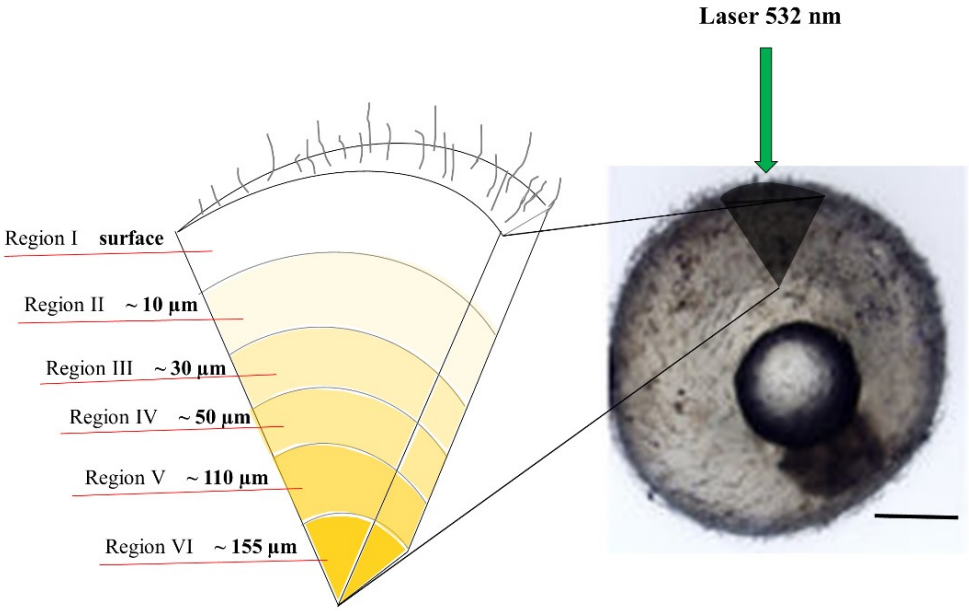

Figure 2. Waterfall plot of spectra representative of Regions I-II-III-IV-V-VI of **Young** (A) and **Old** (B) experimental groups. The X-axis is composed of the Raman shift values (cm^{-1}); the Y-axis represents the intensity, expressed in arbitrary units (a.u.); the Z-axis indicates the six regions from the surface to 155 µm-deep.

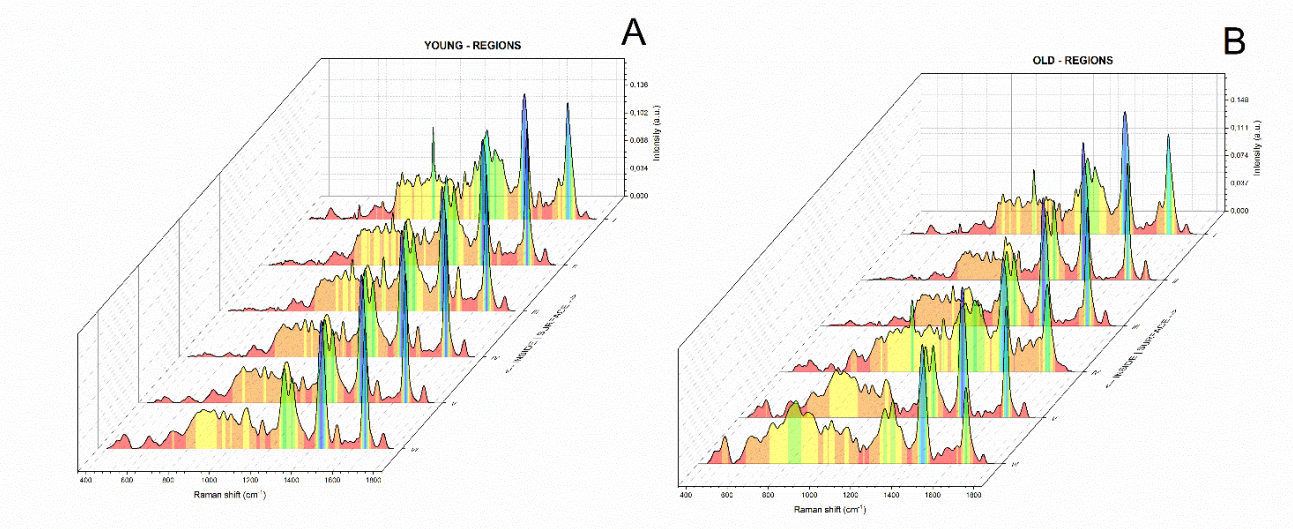

Figure 3. Representative RMS spectra of Region I of **Young** and **Old** experimental groups (A); the most visible discriminant spectral regions are highlighted with dashed rectangles. PCA score plot built using PC1 (59.59% of explained variance) and PC2 (19.65% of explained variance) (B). Loading corresponding to PC2 (C).

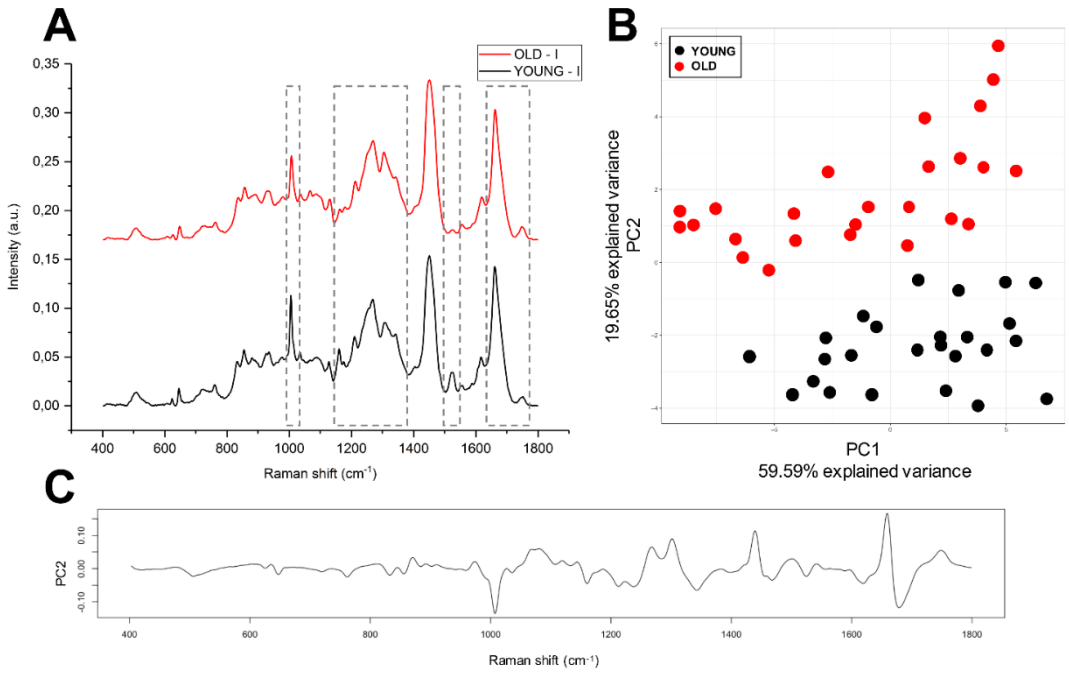

Figure 4. Representative RMS spectra of Region II of **Young** and **Old** experimental groups (A); the most visible discriminant spectral regions are highlighted with dashed rectangles. PCA score plot built using PC1 (68.15% of explained variance) and PC2 (15.79% of explained variance) (B). Loading corresponding to PC2 (C).

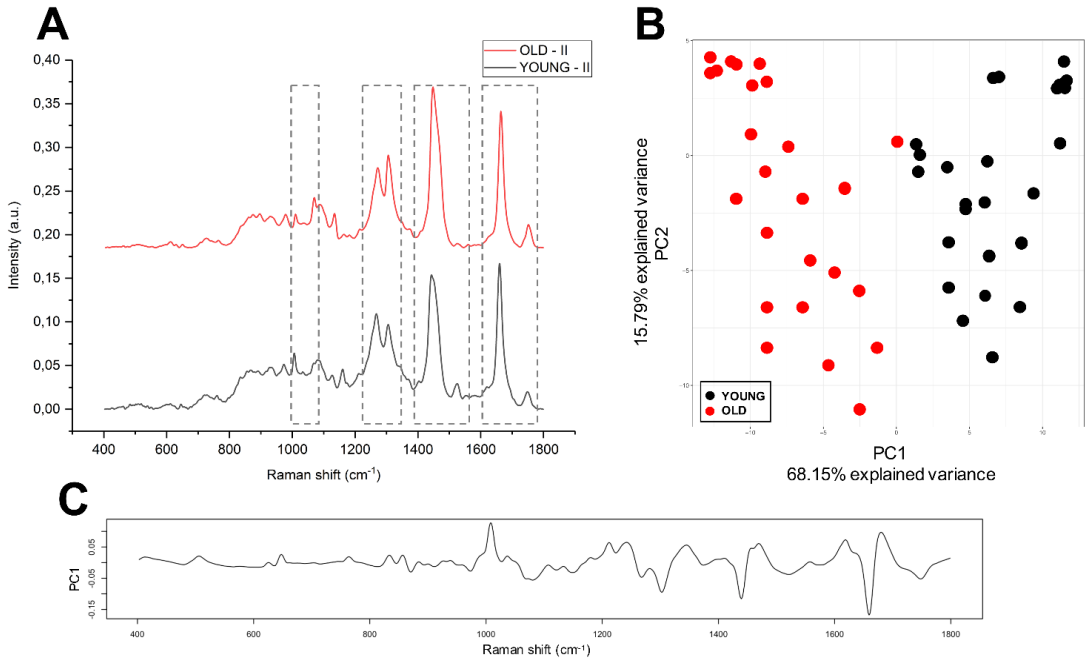

Figure 5. Representative RMS spectra of Region III of **Young** and **Old** experimental groups (A); the most visible discriminant spectral regions are highlighted with dashed rectangles. PCA score plot built using PC1 (65.43% of explained variance) and PC2 (19.74% of explained variance) (B). Loading corresponding to PC2 (C).

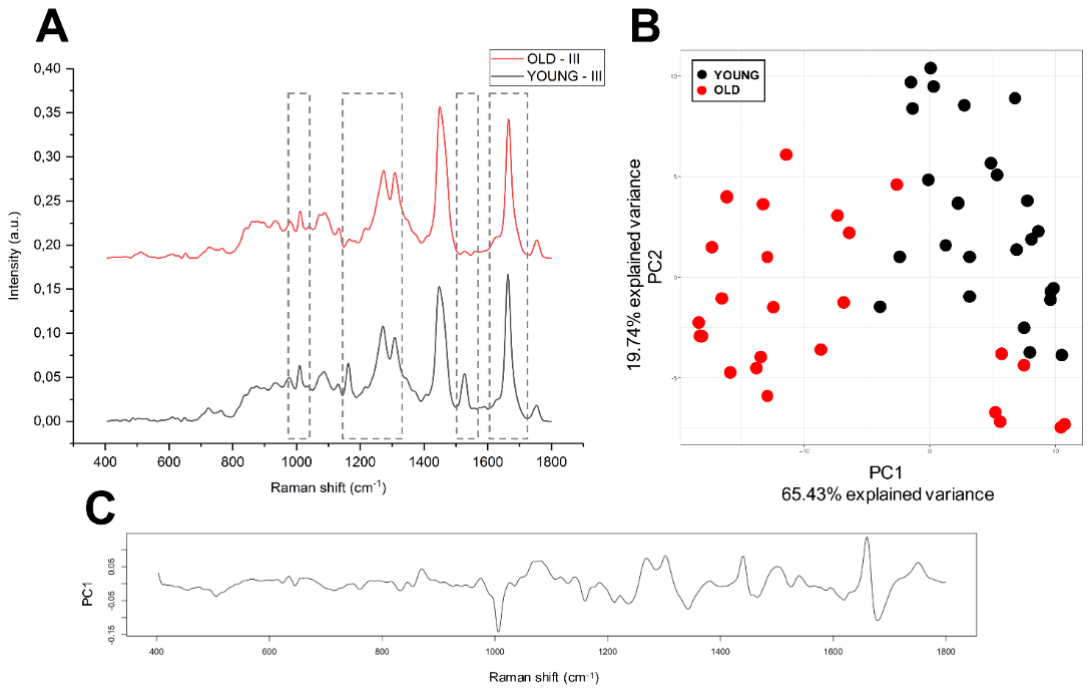

Figure 6. Representative RMS spectra of Region IV of **Young** and **Old** experimental groups (A); the most visible discriminant spectral regions are highlighted with dashed rectangles. PCA score plot built using PC1 (66.94% of explained variance) and PC2 (16.35% of explained variance) (B). Loading corresponding to PC2 (C).

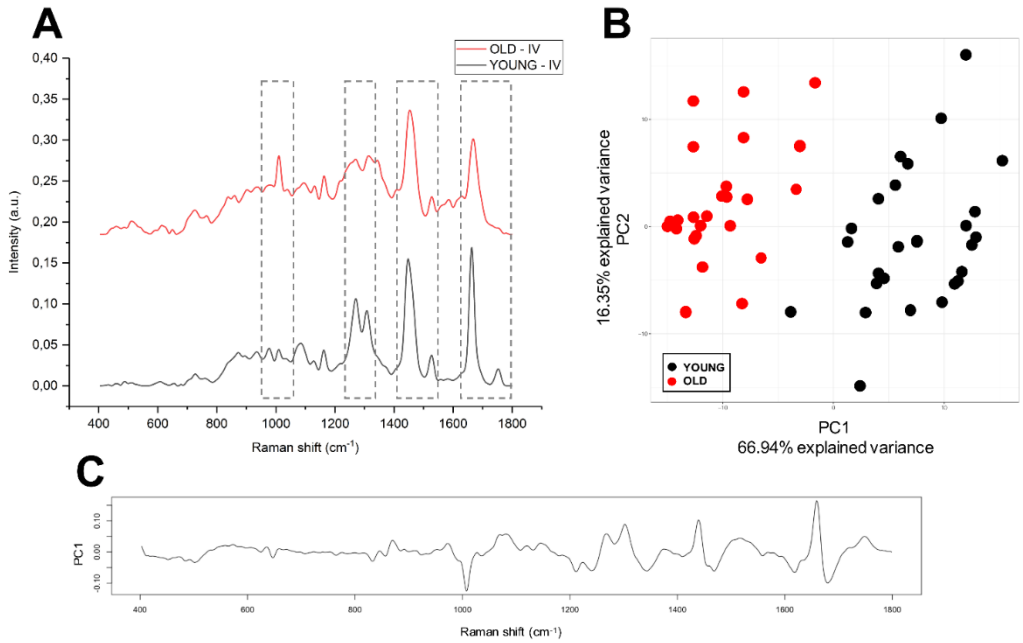

Figure 7. Representative RMS spectra of Region V of **Young** and **Old** experimental groups (A); the most visible discriminant spectral regions are highlighted with dashed rectangles. PCA score plot built using PC1 (65.5% of explained variance) and PC2 (12.32% of explained variance) (B). Loading corresponding to PC2 (C).

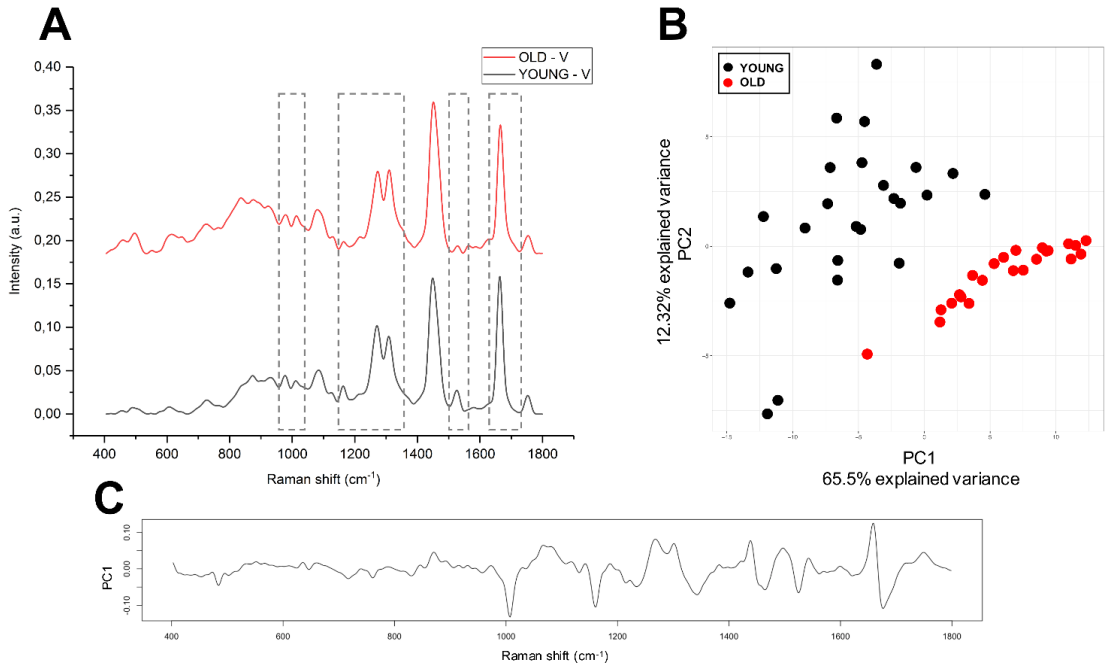

Figure 8. Representative RMS spectra of Region VI of **Young** and **Old** experimental groups (A); the most visible discriminant spectral regions are highlighted with dashed rectangles. PCA score plot built using PC1 (71.6% of explained variance) and PC2 (9.174% of explained variance) (B). Loading corresponding to PC2 (C).

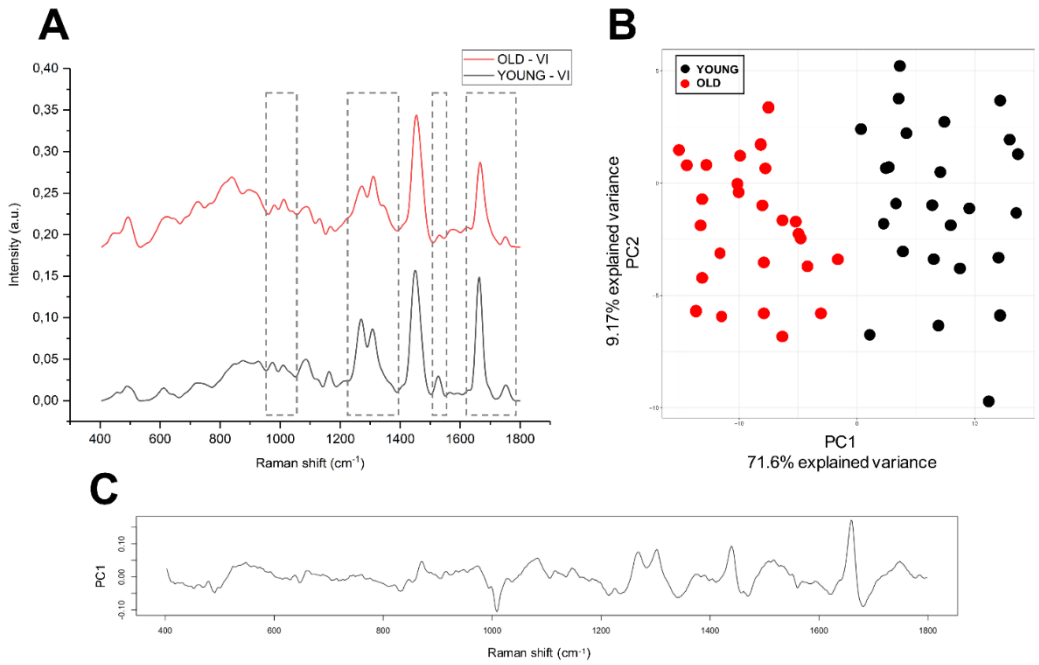

Figure 9. Box charts report the results of the integration procedure on all the bands of interest, in Regions I-II-III-IV-V-VI (respectively, A-B-C-D-E-F). Boxes are plotted along the Raman shift values of the spectrum, and are composed as follows: center line marks the median, edges indicate the 25^{th} and 75^{th} percentile, whiskers indicate the 5^{th} and the 95^{th} percentile, colored diamonds indicate the outliers (if present). Yellow dashed rectangles indicate statistically significant difference among groups. Statistical significance was set at 0.01.

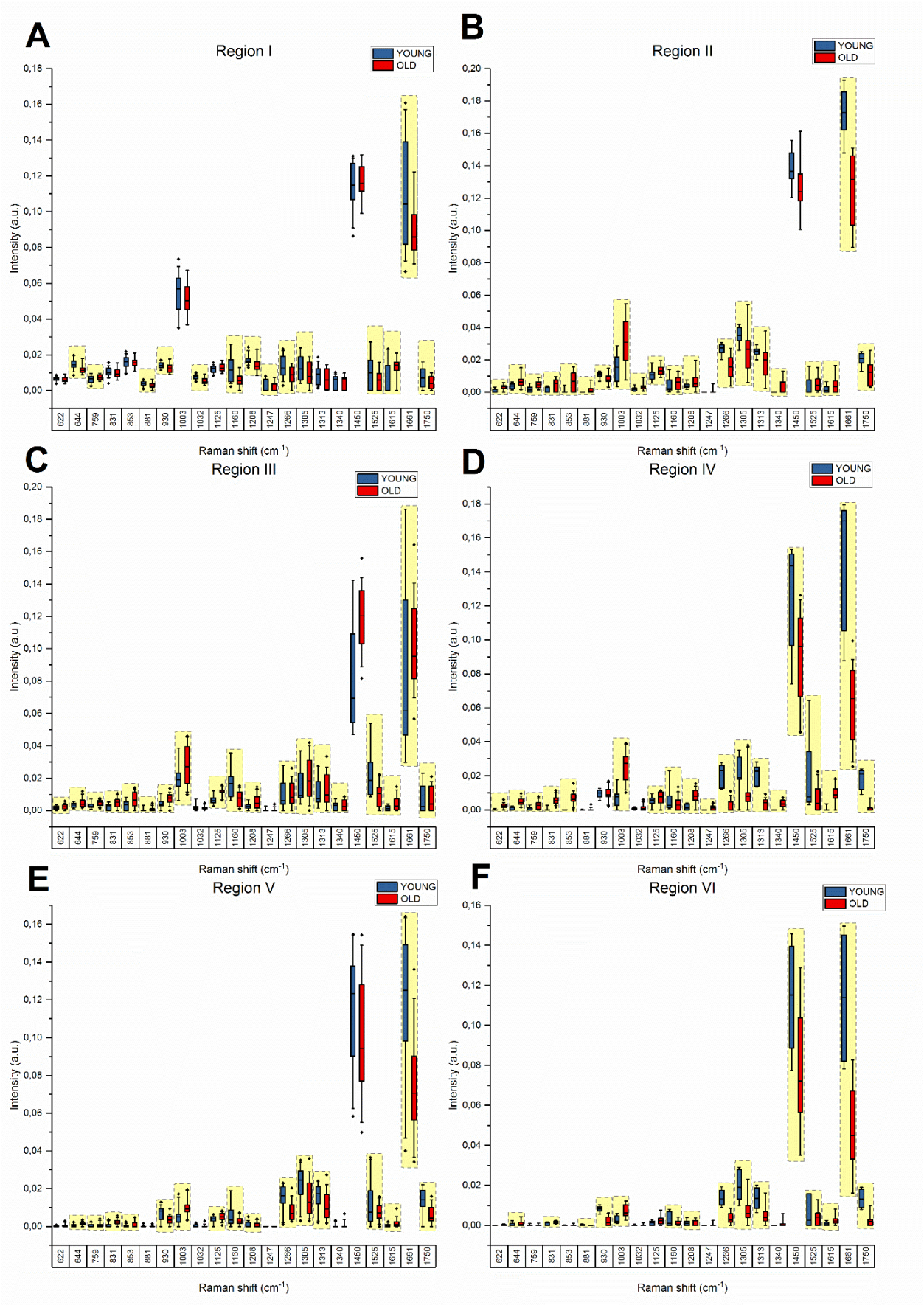
A
Region I
YOUNG
OLD
Intensity (a.u.)
Raman shift (cm-1)
B
Region II
C
Region III
D
Region IV
E
Region V
F
Region VI

REFERENCES

1. Miao, Y. L., Kikuchi, K., Sun, Q. Y. & Schatten, H. Oocyte aging: Cellular and molecular changes, developmental potential and reversal possibility. *Hum. Reprod. Update* **15,** 573–585 (2009).

2. Cellerino, A., Valenzano, D. R. & Reichard, M. From the bush to the bench: The annual Nothobranchius fishes as a new model system in biology. *Biol. Rev.* **91,** 511–533 (2016).

3. Babin, P. J., Cerdà, J. & Lubzens, E. *The fish oocyte : from basic studies to biotechnological applications*. (Springer, 2007).

4. Matthäus, C., Bird, B., Miljković, M., Chernenko, T. & Romeo, M. Infrared and Raman Microscopy in Cell Biology. *Methods Cell Biol.* **89,** 275–308 (2008).

5. Chan, J., Fore, S., Wachsmann-Hogiu, S. & Huser, T. Raman spectroscopy and microscopy of individual cells and cellular components. *Laser Photonics Rev.* **2,** 325–349 (2008).

6. Notingher, I. *et al.* In situ characterisation of living cells by Raman spectroscopy. *Spectroscopy* **16,** 43–51 (2002).

7. Wood, B. R. *et al.* Shedding new light on the molecular architecture of oocytes using a combination of synchrotron fourier transform-infrared and raman spectroscopic mapping. *Anal. Chem.* **80,** 9065–9072 (2008).

8. Rusciano, G. *et al.* Raman spectroscopy of Xenopus laevis oocytes. *Methods* **51,** 27–36 (2010).

9. Heraud, P. *et al.* Label-free in vivo Raman microspectroscopic imaging of the macromolecular architecture of oocytes. *Sci. Rep.* **7,** 8945 (2017).

10. Davidson, B., Murray, A. A., Elfick, A. & Spears, N. Raman Micro-Spectroscopy Can Be Used to Investigate the Developmental Stage of the Mouse Oocyte. *PLoS One* **8,** (2013).

11. Bogliolo, L. *et al.* Raman spectroscopy-based approach to detect aging-related oxidative damage in the mouse oocyte. *J. Assist. Reprod. Genet.* **30,** 877–882 (2013).

12. Bogliolo, L. *et al.* Raman microspectroscopy as a non-invasive tool to assess the vitrification-induced changes of ovine oocyte zona pellucida. *Cryobiology* **64,** 267–272 (2012).

13. Blažek, R., Polačik, M. & Reichard, M. Rapid growth, early maturation and short generation time in African annual fishes. doi:10.1186/2041-9139-4-24

14. Genade, T. L ABORATORY MANUAL FOR CULTURING N. furzeri. *Nat. Hist.* 16 (2007).

15. Bonnier, F. & Byrne, H. J. Understanding the molecular information contained in principal component analysis of vibrational spectra of biological systems. *Analyst* **137,** 322–332 (2012).

16. Movasaghi, Z., Rehman, S. & Rehman, I. U. Raman Spectroscopy of Biological Tissues. *Appl. Spectrosc. Rev.* **42,** 493–541 (2007).

17. Gregersen, N., Bross, P., Vang, S. & Christensen, J. H. Protein Misfolding and Human Disease. *Annu. Rev. Genomics Hum. Genet.* **7,** 103–124 (2006).

18. Haigis, M. C. & Yankner, B. A. The Aging Stress Response. *Mol. Cell* **40,** 333–344 (2010).

19. Berlett, B. S. & Stadtman, E. R. Protein Oxidation in Aging, Disease, and Oxidative Stress. *J. Biol. Chem.* **272,** 20313–20316 (1997).

20. Lubzens, E., Young, G., Bobe, J. & Cerdà, J. Oogenesis in teleosts: How fish eggs are formed. *Gen. Comp. Endocrinol.* **165,** 367–389 (2010).

21. Babin, P. J., Carnevali, O., Lubzens, E. & Schneider, W. J. in *The Fish Oocyte: From Basic Studies to Biotechnological Applications* 1–508 (Springer, 2007). doi:10.1007/978-1-4020-6235-3

22. Lubzens, E., Lissauer, L., Levavi-Sivan, B., Avarre, J. C. & Sammar, M. Carotenoid and retinoid transport to fish oocytes and eggs: What is the role of retinol binding protein? *Mol. Aspects Med.* **24,** 441–457 (2003).

Chapter 4

Published in General and Comparative Endocrinology: **doi.org/10.1016/j.ygcen.2018.01.010**

Effects of age on growth in Atlantic Bluefin tuna *(Thunnus thynnus)*

Martina Api [a], Erica Bonfanti [a], Francesco Lombardo [a], Paolo Pignalosa [b], Gary Hardiman [c] and Oliana Carnevali [a]

[a] Department of Life and Environmental Sciences (DiSVA)-Università Politecnica delle Marche, Via Brecce Bianche, 60131 Ancona, Italy

[b] OCEANIS Srl, Ercolano (NA), Italy

[c] Center for Genomic Medicine, Bioinformatics, Departments of Medicine & Public Health Sciences, Medical University of South Carolina (MUSC), Charleston, SC 29425, USA; Laboratory for Marine Systems Biology, Hollings Marine Laboratory, Charleston, SC 29412, USA

Corresponding Author: Prof. Oliana Carnevali, Dipartimento di Scienze della Vita e dell'Ambiente, Università Politecnica delle Marche, Via Brecce Bianche, 60131 Ancona, Italy email: o.carnevali@univpm.it tel +390712204990, fax +390712204650

Key words: IGF system, Atlantic Bluefin Tuna, growth, age, size

Abstract

Atlantic Bluefin Tuna *Thunnus thynnus* (ABFT) is considered one of the most important socio-economic species but there is a lack of information on the physiological and molecular processes regulating its growth and metabolism. In the present study, we focused on key molecules involved in growth process.

The aim of the present study was to associate molecular markers related to growth with canonical procedures like morphological measurements such as curved fork length (CFL) and round weight (RWT). The ABFT specimens (n=41) were organized into three different groups A, B and C according to their age. The molecular analysis of liver samples revealed that *igf1, igf1r* and *mTOR* genes, involved in growth process, were differentially expressed in relation to the age of the fish.

In addition, during the analyzed period, faster growth was evident from 5 to 8 years of age, after that, the growth rate decreased in terms of length yet increased in terms of adipose tissue storage, as supported by the higher fat content in the liver.

These results are useful in expanding basic knowledge about the metabolic system of ABFT and provide new knowledge for the aquaculture industry.

1. Introduction

The Atlantic bluefin tuna *Thunnus thynnus* (Linnaeus, 1758) is a fascinating species with high commercial value around the world between the large pelagic fish living in the Atlantic Ocean and Mediterranean Sea. Most of our knowledge on the biology of Atlantic bluefin tuna (ABFT) started to emerge in the last decade, however, the biological information available indicates that a substantial amount of uncertainty still exists regarding their rate of growth and information concerning the life cycle is also fragmented. From the Food and Agriculture Organization (FAO) species catalogue it emerged that, between several tuna species (*Scombridae, Thunnini*) found worldwide, Atlantic Bluefin Tuna grows in a manner to be the largest fish ever caught, with a record of an individual of 679 kg caught off Nova Scotia in 1979 (Kitagawa and Shingo, 2015). Therefore, given its relatively large body size, information on the rapidity of ABFT growth requires deeper study. In general, the main objective of age and growth studies in fish is to estimate their mean size at each age class and determine their growth parameters.

In order to provide information on growth differences during the life of ABFT, different methods for aging analysis can be applied, including length frequency analysis, tagging studies and examination of body hard parts (vertebrae, spines and otoliths); however, there are few studies on ABFT growth as a function of length-weight or length-age relationships (Fromentin and Powers, 2005; Mesa et al., 2005; Santamaria et al., 2009; Quelle et al., 2016;). Otoliths are one of the most widely used fish structures for conducting a broad range of studies, including age estimation of teleost. The otolith reading is based on the number of marks, usually called annuli, which are formed each year throughout the life of ABFT (Division and Scotia, 2001). Fisheries-based information on distribution and biometric data of catch-at-size (CAS) and catch-at-age (CAA) has been sufficiently accumulated in the past but scientific researches on growth at a molecular level have been lacking due to the absence of whole genome sequencing for ABFT.

The aim of the present study was to correlate biometric data with the age estimated by otolith reading and with molecular markers belonging to IGF signaling. In addition, lipid accumulation in the liver was also analyzed. In this regard, a total of 41 specimens of ABFT from the Mediterranean Sea were sampled during the month of November when bluefin tuna were reproductively inactive.

Based on otolith readings, we were able to generate three different age groups (delineated as A, B and C), ranging from 5 to 13 years old, to study the length-weight relationship and the size at age between groups, in order to generate bluefin tuna growth curves.

In addition, we used the Atlantic bluefin tuna expressed sequence tags (ESTs) available in public databases (e.g. SRA and the NCBI EST) to develop sensitive RT-qPCR assays to monitor gene expression in this species and uncover novel insights on IGF signaling. This approach allowed us to gain novel information on life cycle of ABFT in Mediterranean Sea.

The insulin-like growth factor (IGF) system is an evolutionarily conserved signalling pathway. Studies in several species suggest that the IGF signalling plays a fundamental role in controlling animal development and growth. Thus, the importance of the present study is to improve the knowledges on ABFT growth following a molecular approach.

These results can improve the knowledges on the biology of this fascinating species that suffer of overfishing and thus today needs more attention than ever for conservation and management purposes.

2. Methods

2.1. Sampling

A total of 41 Atlantic Bluefin tuna (*Thunnus thynnus*) samples were obtained from capture-based tuna farming company, **Fish & Fish Co. Ltd, Malta. ABFTs** were caught by Italian purse seiners during the fishing season 2015 and sampled onboard of a Japanese commercial vessel. The ABFTs were obtained from the same farming cage in order to guarantee the same nutritional conditions for all the specimens sampled.
These fish, originally caught in the wild, were maintained in cages under fattening conditions for 5 months and the sampling activity was performed during November 2015.

The sex of fish was also determined by visual examination of the gonads after dissection. For each specimen, different tissue samples were sampled as liver, gonads and pairs of otoliths.

Otolith sampling was performed following a specific procedure, e.g. by first making a transverse cut in the upper part of the head using a metal saw and then both otoliths were extracted from the semicircular cavities of the inner ear situated at the base of tuna brain.

2.2. Preparation of otoliths for age estimation

2.2.1. Preparation and method overview

All samples were prepared as multiple transverse sections. Sagittal otoliths were embedded in rows of five in blocks of Polyplex Clear Ortho Casting Resin ensuring that the primordium of each otolith was in line. Each otolith was sectioned on the transverse axis. Up to five sections, approximately 300 μm thick, were cut through the otoliths centers with a modified high-speed gem-cutting saw, with a 250 μm thick diamond impregnated blade. Sections from each sample were cleaned, dried and mounted on clear glass microscope slides (50 x 76 mm). The sections were covered with further resin and glass coverslips were placed over the top.

2.2.2. Age reading procedure

Otolith sections were read using a research grade Leica microscope (M125) at 25x magnification. Each section of the otolith was inspected and the section with the clearest zone pattern was chosen for aging. The age of each sample was determined by counting the number of assumed annual opaque zones along a count path from the primordium to the otolith edge on the dorsal or ventral side of the otolith to the sulcus. The same individual read all prepared otoliths twice and then a final "agreed" zone count was produced. To avoid the potential for biasing age estimates, all counts were made without knowledge of fish size.

2.2.3. Data acquisition

A customized version of the image analysis system IC Capture© was used to count and measure manually marked zones on the otoliths and collects an image from each sampled aged.

A CCD digital camera mounted onto the dissecting microscope (Leica MZ80) was used to display the live image on the monitor. Using the image analysis system, the starting point (first apex), the end point of each opaque zone and the otolith edge was marked with a screen cursor along the preferred measurement path. For tuna species, this is along the ventral arm. The numbers of zones marked and the measurements from the primordium to each subsequent mark along the transverse section was automatically exported to a Microsoft database. The otolith image was automatically captured. In addition, the sample was assigned a readability score which rates the otoliths on a sale of 1 to 5 and the marginal edge type was recorded. The edge type is an indicator of the likelihood of zone formation in the next period of deposition. An edge type 1 indicates that an opaque zone is likely to form soon; an edge type 2 indicates that the reader thought that the opaque zone had recently formed and edge type 3 indicates the zone is forming on the edge (Fig.1).

2.3. Morphometrical analysis

Curved fork length (CFL - a line along the contour of the body from the tip of the upper jaw to the fork of caudal fin; cm) and total round body weight (RWT, kg) were measured for all tuna sampled.

Following the harvesting step, for each specimens the CFL was obtained with measuring tape to the nearest centimeter and body weight with electronic balance.

2.4 SEQUENCE ANALYSIS and expression of target genes

2.4.1. Thunnus thynnus cDNA sequences

Sequence similarity searching was carried out using the Basic Local Alignment Search Tool (BLAST) software (Liebert et al., 2000; Camacho et al., 2009). BLAST Software and Databases were downloaded from https: //blast.ncbi.nlm.nih.gov/Blast.cgi?PAGE_TYPE=BlastDocs&DOC_TYPE=Download.

We searched public databases (e.g. SRA and the NCBI EST) for Atlantic Bluefin Tuna (*Thunnus thynnus*) sequences. One study based on pyrosequencing of a mixed-tissue normalized cDNA library provided 976,904 raw sequence reads which were used to generate 33,105 unique transcripts with a mean length of 893 bases and an N50 of 870 (Trumbi et al., 2015). A second study used an expressed sequencing tag (EST) strategy to sequence several thousand ovary, testis and liver derived cDNAs (Chini et al., 2008). ABFT FASTQ files of interest were converted to FASTA files with *seqtk* and a searchable database using these FASTA files was created (via *makeblastdb*). We queried this database via blastn nucleotide searches using query sequences of interest from related fish species including *Dicentrarchus labrax*, *Sparus aurata* and *Danio rerio*. The output setting was set to zero to highlight the alignments of the various ABQT sequence hits and present the alignment regions. The sequences were used to guide RT-qPCR primer design as outlined below.

2.4.2. RNA extraction and cDNA synthesis

Liver tissues were collected from each fish and stored with RNA*later*™ solution (Invitrogen by Thermo Fisher Scientific) until used for RNA extraction.

Total RNA was extracted using RNAzol solution (Sigma-Aldrich) according to the manufacturer's instructions and then eluted with RNAse-free water. Final RNA concentrations were determined using a Nanophotometer TM PClass (Implem GmbH, Münich, Germany) while integrity was verified by GelRed staining of 28S and 18S ribosomal RNA bands on 1% agarose gel.

RNA was stored at -80°C until use. A total amount of 5 µg of RNA was used for cDNA synthesis with iSscript cDNA Synthesis Kit (Bio-Rad, Milano, Italy) and kept at -20°C until use.

2.4.3. RTqPCR assays

For determining expression of the target genes in liver, males and females fish for each experimental groups were sampled.

RT-qPCRs were performed for target genes with SYBR green method in an iQ5 iCycler thermal cycler (Bio-Rad) in triplicate as previously described by Maradonna et al. (Maradonna et al., 2013, 2014). The reactions were set up on a 96-well plate by mixing, for each sample, 1 µl of diluted cDNA (1/10), 5 µl of 2× concentrated iQ ™ SYBR Green Supermix (Bio-Rad), containing SYBR Green as a fluorescent intercalating agent, 0.3 µM of the forward primer and 0.3 µM of the reverse primer. The thermal profile for all reactions was 3 min at 95 °C followed by 45 cycles of 20 sec at 95 °C, 20 sec at 60 °C and 20 sec at 72 °C. Fluorescence was monitored at the end of each cycle. Dissociation curve analysis showed a single peak in all cases. *β- actin* (a*ctb*) and *elongation factor1a* (*ef1α*) were used as the reference genes to standardize the results by eliminating variation in mRNA and cDNA quantity and quality. Data were analyzed using Bio-Rad's iQ5 optical system software, version 2.0. Alterations in gene expression were reported with respect to the control sample. Primer sequences

for *igf1*, *igf1r* and *mTOR* were designed using Primer3 (210 v. 0.4.0) according to manufacturer's guidelines and purchased from SIGMA-ALDRICH (*igf-1*: 5'- GCACCTGCCAAGACTAGCAA-3'/5'-TCCGCTTTTTGTCCCGCT-3'; *igf-1r*: 5'- GGAGGACTCCTGGACAAACC-3'/5'-AGGGAGGATCCAGTTCATCG-3'; *mTOR*: 5'- GTGCAAGGAATGCAACAGCA-3'/5'-ACTGCAGAACCTTGGGGATG-3'). We validated the use of bluefin tuna *actb* and *ef*1α genes for normalization between different body tissues and then we applied both reference genes in this study. The real-time PCR primers sequences used were *actb* 5'- TATCCTGACCCTGAAGTA-3'/5'-CATTGTAGAAGGTGTTGATG-3' and *ef1α* 5'-ATGGTCGTCACCTTTGCTCC-3'/5'-CCACGTATCCACGACGGATT-3'.

2.4.4. Statistical analysis

Results related to mRNA expression obtained by RT q-PCR analysis were analyzed with GraphPad Prism 6 software (GraphPad Software, Inc., San Diego, CA, U.S.A.) and processed with a two-way ANOVA followed by Tukey's multiple comparisons test. All statistical data are shown as the mean ± SEM. Differences were considered statistically significant at $P < 0.05$.

2.5. Histology and lipid content in tuna liver

Liver samples were collected and fixed in Bouin and stored overnight at 4°C. Samples were then washed in PBS 0.1 M and dehydrated by subsequent washing in a graded series of alcohol concentrations (Et-OH 80% for 1 h, Et-OH 95% for 1 h, first wash Et-OH 100% for 30 min, second wash Et-OH 100% for 30 min). The dehydration was followed by a clearing agent (Xilene) wash and embedded in liquid paraffin (Bio-Optica, Italy).

From each sample, slides of 5 µm sections was obtained using microtome and stained with Mayer's hematoxylin and eosin Y (Sigma-Aldrich). Sections were examined using an optical microscope connected with a camera Canon EOS 6D.

Images were analyzed using ImageJ Software ver. 1.49 to estimate the lipid vacuoles (ACLV %) in each microphotograph that were used to cover different areas of the liver (n=5) in each specimen.

3. Results

3.1. Age estimation and age-group formation

Otolith age readings were performed to estimate the age of ABFT.

Transverse sections contained translucent and opaque zones, which appeared as alternating clear and dark zones, were analysed from otoliths. Translucent zones are formed annually during the life of ABFT, so the counting criteria provide a reliable method of estimating age from otoliths. Zones were counted on the dorsal side and increments of age were measured at the end of each opaque zone.

Age estimates were made from tuna fish ranged 149-270 cm CFL.Among our samples, the oldest fish were estimated to be 13 years old and the youngest were 5 years old. Based on the otolith reading procedure, three different tuna age groups (A, B and C) were formed: Group A (included fish from ages 5 to 7 years); Group B (fish from the ages 8 to 10 years); and Group C (fish from the ages 11 to 13 years).

3.2. Growth analysis

Morphometric data such as total round weight (RWT, kg) and length (CFL, cm) were provided for each group (Group A, B and C) in order to evaluate the growth rate. The length-weight relationship was determined for each group as shown in Figure 1. In Group A curved fork lengths (CFL) ranged from 149 cm to 228 cm while body weights (RWT) ranged from 54 to 195 kg; in Group B curved fork lengths (CFL) ranged from 222 cm to 252 cm while body weights (RWT) ranged from 216 to 268 kg; in Group C curved fork lengths (CFL) ranged from 244 cm to 270 cm while body weights (RWT) ranged from 305 to 408 kg.

As shown in Fig. 2a, Group A presented a high-growth respect to Group B and C in terms of length (CFL).

Male specimens tended to be at the top of the chart revealing a higher size (weight and length) with respect to females from the same group (Tab.2b).

Evidence of sexual dimorphism in length-at-age and weight-at-age in female and male of ABFT is provided in Fig. 2c,d,e,f. Considering the data set analyzed in this study, female specimens ranged from 149 to 255 cm CFL, with a CFL mean of 216,44 S.D. ± 32,7; while males specimens ranged from 158 to 269 cm with a mean CFL of 240, 47S.D. ± 30 (Fig. 2c and 2d). The weight-frequency data showed that female size, ranged from 54 to 323 kg, were smaller (196,83; S.D. ± 86,42) than male (279,76; S.D. ± 79,29) ranging from 93 to 379 kg (Fig. 2e and 2f).

Growth is faster from 5 to 8 years of age with a peak at about 8 years. After this age, ABFT grows more slowly in length throughout all the period analyzed (Fig.3).

Mean length for females from Group A was 163,00 cm (S.D. ± 14,17), Group B was 220,14 cm (S.D. ± 6,34) and Group C was 243,29 cm (S.D. ± 11,34). Mean of the length-at-age for males from group A was 185,67 cm (S.D. ± 32,87), group B was 246,20 cm (S.D. ± 8,79) and group C 255,56 cm (S.D. ± 9,34).

3.3. Molecular analysis of genes related to IGF system

The expression of mRNA coding for *igf1* showed a similar patterns in both male and female, although males seemed to have slightly higher expression but without a sex-specific statistical difference. Both males and females exhibited a significant increase in Group B ($p < 0,0001$), which remained high in Group C (Fig 4a).

Similarly, the gene expression of *igf1r* revealed the same trend between males and females demonstrating a significant increase in group B ($p = 0,0002$), and remaining high in Group C (Fig 4b).

3.4. Expression of mTOR gene

With regard to *mTOR* gene expression, males showed a significant increase in the three different groups ($p < 0,0001$) while females had an increase in gene expression between groups A and B, but not Group C where mRNA levels remained similar to that found in Group B (Fig 4c).

3.5. Histology and lipid content analysis in the liver

In order to investigate the accumulation of lipids in liver, we analysed histological sections from male and female liver of all individuals and quantified the area occupied by vacuoles (Fig. 5).

As evidenced by Figure 5b, both males and females from group A showed a significantly lower lipid percentage compared to groups B and C. In fact, liver tissues from individuals from group A exhibited a lipid percentage in males and females of 25% and 20,83% respectively. This percentage reached an average of 36,13% and 36,38% in males and females from group B and 40,90% and 37,10% respectively in males and females from group C.

4. Discussion

Despite the historical and socio-economic importance of ABFT, a comprehensive understanding of its biology remains to be fully elucidated. Regarding the growth rate of this species, captive rearing let us measure length and weight for all specimens analyzed. However, we need to take into consideration the fact that captive rearing conditions may differ from wild conditions (e.g. food supply, swimming range, stress, etc.), which might produce different growth rates to those from wild populations even in the limited period of captivity.
Individual length-at-age for ABFT is also due to individual variations in growth rate and it is often difficult to estimate the growth rate for the full life span of long-lived species such as tuna.

The otolith readings permitted us to create age-length and age-weight curves and obtain three Groups A, B and C, according to age class. Our data showed that ABFT growth was higher during the first 8 years of life after which the growth rate decreased in fish with greater size.

Regrettably, some of the age classes were not represented (tuna-age less than 5 years and greater than 13 years), since these individuals are less abundant in the fishery but in general, the age-length key is very representative of the length distribution of fish caught by the traps. For each individual, curved fork length (CFL) and wet weight were measured and a growth curve achieved.
Although the differences between male and female were not statistically significant, the larger sizes found in males were concordant with the molecular analysis. The insulin-like growth factor (IGF) system is the key promoter of growth in vertebrates (Glass, 2003; Wood et al., 2005; Velloso, 2008) . IGFs in fish stimulate muscle growth, myogenic cell proliferation, differentiation, and protein synthesis through the MAPK/ERK and PI3K/AKT/TOR signaling pathways.
The IGF system plays a key role in controlling growth not only in the early life, but also in adult individuals with different rate, by regulating the development and differentiation of muscle cells (Clemmons, 2009).

In this study, molecular analysis of genes belonging to IGF system revealed that genes involved in the growth including *igf1, igf1r* and *mTOR* were differentially expressed in relation with the ABFT age.

igf1 gene expression in males and females liver, tended to increase significantly from group A to group B according to size, while group C showed no difference in gene expression in comparison with group B, in spite of their greater size. The trend of *igf1r* gene expression agreed with that of *igf1*, the correlation between these two genes and the slight differences in expression between male and female in relation to growth as previously noted in Fathead minnow by Filby & Tyler's (Filby and Tyler, 2007).

Focusing on *mTOR*, the encoded protein is considered to be one of the main regulators of muscle growth and metabolism, acting by integrating different inputs such as growth factors (e.g. *igf1*), nutrients (e.g. amino acids) and energy status (e.g. AMP:ATP ratio)(Loewith and Hall, 2011; Fuentes et al., 2013). In the present study *mTOR* increase in relation with age in male and in female till they reach about 10 years old. This close linkage with growth factors, such as insulin or *igf1*, reflects *mTOR* gene expression; in addition, *mTOR* plays an important role in lipid metabolism and its expression increases during adipogenesis (Kim and Chen, 2004) suggesting its involvement in lipid accumulation as defined by the higher lipid contents in the liver of group B and C.

In conclusion, these data suggests that females have a slower growth rate than males; however, given the fact that the sample size for each age group it is small, it cannot be excluded that the smaller female fish represent the lower part of the natural size variation within their age classes. However, a gender differential rate may be due to a variance in reproductive energy cost, i.e., much more energy is used for reproduction in females than

males (Schaefer, 1983) leading to a slower growth rate in females after maturity. Several studies found sexual dimorphism in growth for other tuna, such as southern bluefin tuna *Thunnus maccoyii* (Gunn et al., 2008) and Pacific bluefin tuna *Thunnus orientalis* (Shimose et al., 2009) or differential growth parameters for bigeye tuna *Thunnus obesus* (Farley et al., 2006) and albacore *Thunnus alalunga* (Chen et al., 2012).

Another aspect of tuna energy metabolism concerns the link between metabolic rate and growth.
The liver is an essential metabolic organ and its activity is tightly controlled by insulin and other metabolic hormones. The metabolic processes such as maintenance, growth and reproduction requires energy to be used or mobilized from the reserve. The rate at which this happens is determined by the utilization or mobilization of energy. In the hepatocytes, fatty acids are incorporated in phospholipids, triacylglycerol, cholesterol and these complex lipids are stored in lipid droplets.
Histological analyses were conducted to evaluate the variation in the percentage of lipid droplets accumulated in the liver according to the age of all specimens.

There was a gradual increase in liver lipid concentration among groups, with significant increases only between groups A and both groups B and C. No gender differences were uncovered. This progressive increase suggested the onset of hepatic steatosis since fish after they reach 8 years old (group B) use their metabolic energies mainly for adding fat and not only for growth in length.

In our study, ABFT after they reached about 8 years of age and the relative length, increased storage of adipose tissue as supported by the increase of fat in the liver.
Additional studies are necessary to improve knowledge on tuna fish growth. This study highlights findings on differences in the IGF system during *T. thynnus* life and application of this basic insight may directly benefit the aquaculture industry.

One of the objectives of aquaculture facilities is to increase the fat content of tuna in order to satisfy mainly the eastern market (e.g. Japan). This goal can be achieved by focusing on food quality and quantity, reducing the stress of farming and harvest procedures and delaying the onset of rigor mortis. Here, we suggest that additionally differences in the IGF system associated with ABFT age can be one of the factors that needs to be taken into consideration for improving farming strategies.

Acknowledgements

We are grateful to the staff of Kurikoma vessel, Oceanis S.r.l. and Fish & Fish Co. Ltd, Malta for cooperating with sampling. We are especially grateful to Iman Busuttil and Rino Glorioso for help with otoliths sampling**.** Gratefully acknowledged to Dr. Kyne Krusic-Golub from Fish Ageing Service (FAS), Portarlington-Victoria Australia, for sectioning otoliths and providing age estimates.

Funding: this work was supported by Ministry of Agriculture, Food and Forestry Policies (MIPAAF), note 6775, Art.36 Paragraph 1 Reg (UE9 n 508/2014) to O.C.

References

Camacho, C., Coulouris, G., Avagyan, V., Ma, N., Papadopoulos, J., Bealer, K., Madden, T.L., 2009. BLAST + : architecture and applications. BMC Bioinformatics 10, 1–9.

Campana, S.E., 2001. Accuracy , precision and quality control in age determination , including a review of the use and abuse of age validation methods. J. Fish Biol. 59, 197–242.

Chen, K., Shimose, T., Tanabe, T., Chen, C., Hsu, C., 2012. Age and growth of albacore Thunnus alalunga in the North Pacific Ocean. J. Fish Biol. 80, 2328–2344.

Chini, V., Cattaneo, A.G., Rossi, F., Bernardini, G., Terova, G., Saroglia, M., Gornati, R., 2008. Genes expressed in Blue Fin Tuna (Thunnus thynnus) liver and gonads. Gene 410, 207–213.

Clemmons, D.R., 2009. Role of IGF-I in skeletal muscle mass maintenance. Trends Endocrinol. Metabol. 20, 349–356.

Farley, J.H., Clear, N.P., Leroy, B., Davis, T.L.O., McPherson G., 2006. Age, growth and preliminary estimates of maturity of bigeye tuna , Thunnus obesus, in the Australian region. Mar. Freshwater Res. ,57, 713–724.

Filby, A.L., Tyler, C.R., 2007. Cloning and characterization of cDNAs for hormones and/or receptors of growth hormone, insulin-like growth factor-I, thyroid hormone, and corticosteroid and the gender-, tissue-, and developmental-specific expression of their mRNA transcripts in fathead minnow (Pimephales promelas). Gen. Comp. Endocrinol. 150,151–163.

Fromentin, J., Powers, J.E., 2005. Atlantic bluefin tuna : population dynamics , ecology , fisheries and management. Fish Fish. 6, 281–306.

Fuentes, E.N., Safian, D., Eir, I., Antonio, J., Elorza, A.A., Molina, A., Thrandur, B., 2013. Nutritional status modulates plasma leptin , AMPK and TOR activation , and mitochondrial biogenesis : Implications for cell metabolism and growth in skeletal muscle of the fine flounder. Gen. Comp. Endocrinol. 186, 172–180.

Glass, D.J., 2003. Molecular mechanisms modulating muscle mass. Trends Mol. Med. 9, 344–350.

Gunn, J.S., Clear, N.P., Carter, T.I., Rees, A.J., Stanley, C.A., Farley, J.H., Kalish, J.M., 2008. Age and growth in southern bluefin tuna , Thunnus maccoyii (Castelnau): Direct estimation from otoliths, scales and vertebrae. Fish. Res. 92, 207–220.

Kim, J.E., Chen, J., 2004. Regulation of peroxisome proliferation-activated receptor-activity by mammalian target of rapamycin and amino acids in adipogenesis. Diabetes 53, 2748-2756.

Kitagawa, T., Shingo, K., 2015. Biology and Ecology of Bluefin Tuna. CRC Press Taylor & Francis Group.

Koutnikova, H., Auwerx J. 2001.Regulation of adipocyte differentiation. Ann. Med. 33, 556–561.

Liebert, M.A., Zhang, Z., Schwartz, S., Wagner, L., Miller, W., 2000. A Greedy Algorithm for Aligning DNA Sequences. J. Comput. Biol. 7, 203–214.

Loewith, R., Hall, M.N., 2011. Target of rapamicyn (TOR) in nutrient signaling and growth control. Genetics 189, 1177–1201.

Maradonna, F., Gioacchini, G., Falcinelli, S., Bertotto, D., Radaelli, G., Olivotto, I., Carnevali, O., 2013. Probiotic supplementation promotes calcification in Danio rerio larvae: a molecular study. PLoS One 8, 1–10.

Maradonna, F., Nozzi, V., Dalla, L., Traversi, I., Gioacchini, G., Benato, F., Colletti, E., Gallo, P., Di, I., Pisciottano, M., Mita, D.G., Hardiman, G., Mandich, A., Carnevali, O., 2014. A developmental hepatotoxicity study of dietary bisphenol A in Sparus aurata juveniles. Comp. Biochem. Physiol. Part C 166, 1–13.

Mesa, M.L.A., Sinopoli, M., Andaloro, F., 2005. Age and growth rate of juvenile bluefin tuna Thunnus thynnus from the Mediterranean Sea (Sicily , Italy). Sci. Mar. 69, 241–249.

Quelle, P., Ruiz, M., Luque, P.L., 2016. Standardized age- length key for east atlantic and mediterranean bluefin tuna based on otoliths readings. Collect. Vol. Sci. Pap. ICCAT. 72, 1365–1375.

Santamaria, B.N., Bello, G., Corriero, A., Deflorio, M., Bo, T., 2009. Age and growth of Atlantic bluefin tuna , Thunnus thynnus (Osteichthyes : Thunnidae), in the Mediterranean Sea J. Appl. Ichthyol. 25, 38–45.

Schaefer, K.M., 2001. Reproductive biology of tunas.Fish Physio.19, 225–270.

Shimose, T., Tanabe, T., Chen, K., Hsu, C., 2009. Age determination and growth of Pacific bluefin tuna , Thunnus orientalis , off Japan and Taiwan Fish Res.100, 134–139.

Trumbi, Ž., Bekaert, M., Taggart, J.B., Bron, J.E., Gharbi, K., Mladineo, I., 2015. Development and validation of a mixed- tissue oligonucleotide DNA microarray for Atlantic bluefin tuna, Thunnus thynnus (Linnaeus , 1758). BMC Genomics 16, 1–17.

Velloso, C.P., 2008. Regulation of muscle mass by growth hormone and IGF-1. Br. J. Pharmacol. 154, 557–568.

Wood, A.W., Duan, C., Bern, H.A., 2005. Insulin-like growth factor signaling in fish. Int. Rev. Cytol. 243, 215–285.

Figures

Fig.1 Example of ABFT otolith illuminated with transmitted light at 25x magnification. A transverse section of sagitta showing the ventral ridge (longer arm) and the dorsal ridge (shorter arm). Zone count=10

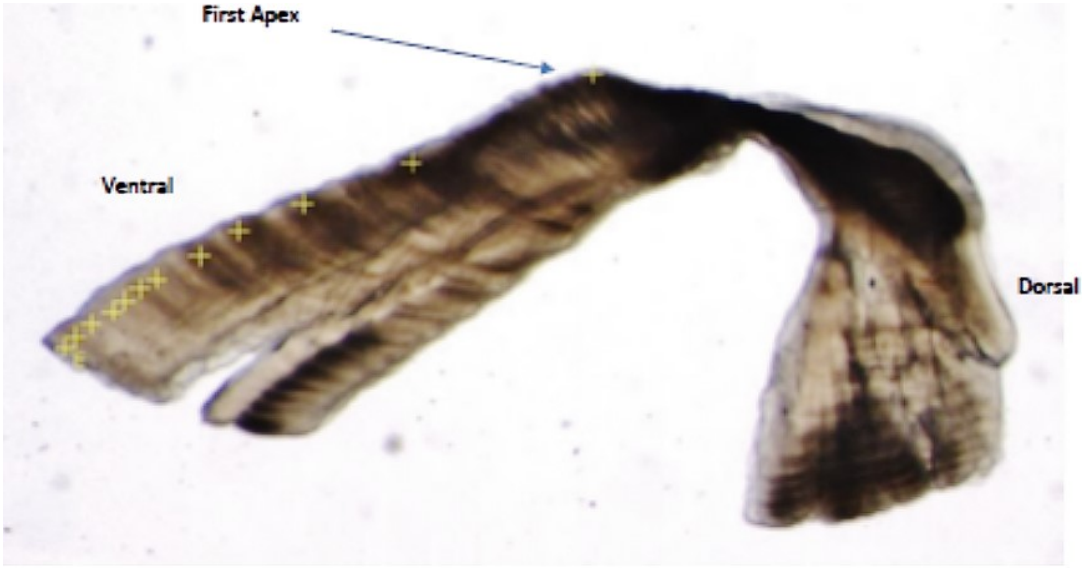

Fig. 2 Growth curves. Relationship between length (CFL) and weight in male and female (a) Group A curved fork lengths (CFL) ranging from 149 cm to 228 cm (y=1,726x – 198; R^2 = 0,9011), Group B curved fork lengths (CFL) ranging from 222 cm to 252 cm (y= 2,7954x – 409,37; R^2 = 0,7443), Group C curved fork lengths (CFL) ranging from 244 cm to 270 cm (y= 3,5284x – 571,1; R^2 = 0,805). **Comparison between weight and CFL (b)** male were represented by ▲ and female as •. **Comparison between length-at-age in female (c). Comparison between length-at-age in male (d). Comparison between weight-at-age in female (e). Comparison between weight-at-age in male (f).**

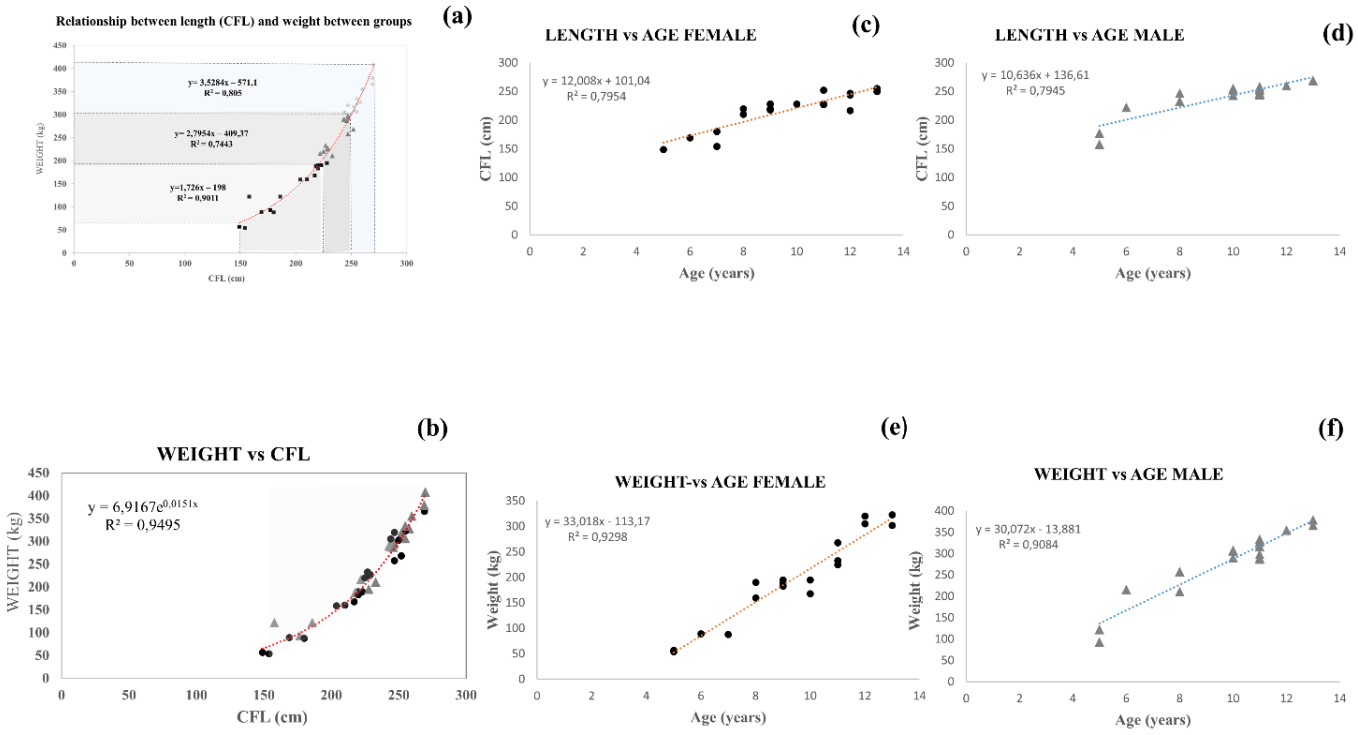

Fig. 3 Growth curves rate: (a) relationship between age estimated from otolith bands and CFL of all specimens; (b) comparison between female (red) and male (blue) growth.

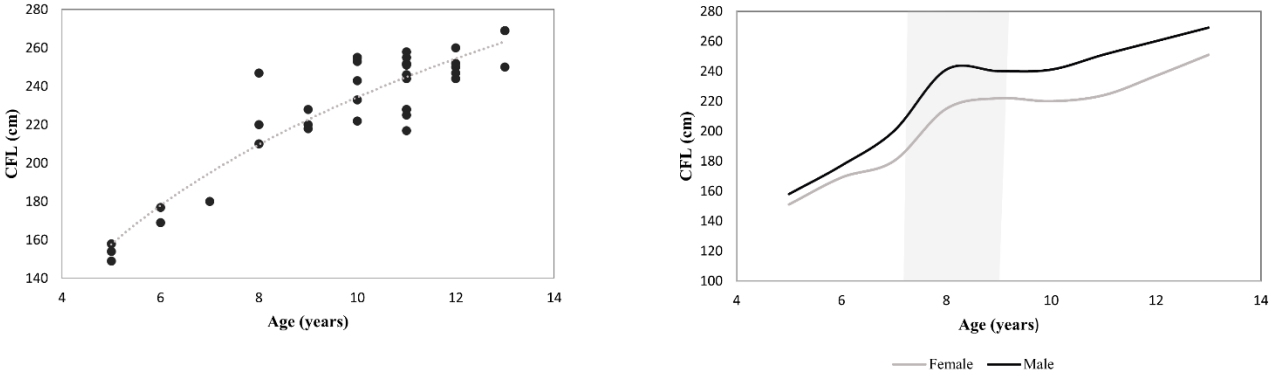

Fig. 4 Gene expression quantification in the liver of male and female from group A, group B and group C of: *igf1* (a), *igf1-r* (b) and *mtor* (c). Error bars indicate mean ± S.D. Letters symbolize the statistical difference within the same experimental group and among the three groups. Confidence interval set at 95% ($p<0.05$).

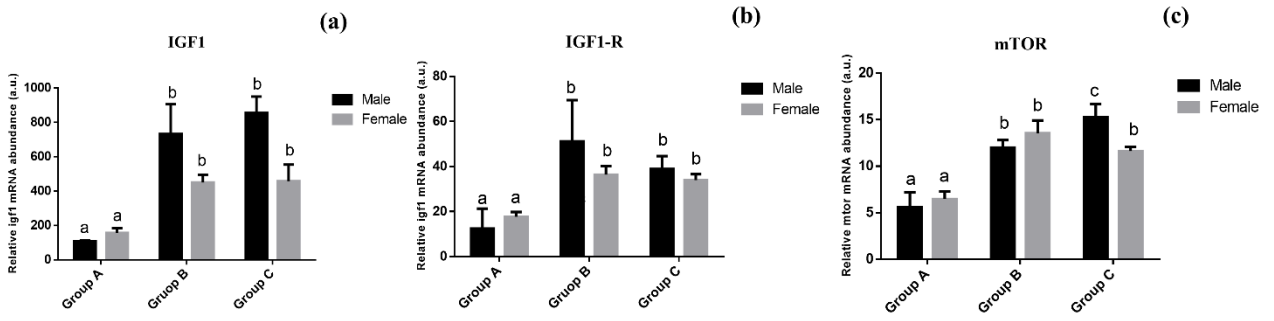

Fig. 5 Histological sections of male and female liver from the three groups (a) Scale bar 100 µM. **Lipid content in male and female liver (b)** Percentage of area covered with lipid vacuoles (ACLV %) in male and female *Thunnus thynnus* liver. Letters symbolize the statistical difference within the same experimental group and among the three groups. Confidence interval set at 95% ($p<0.05$).

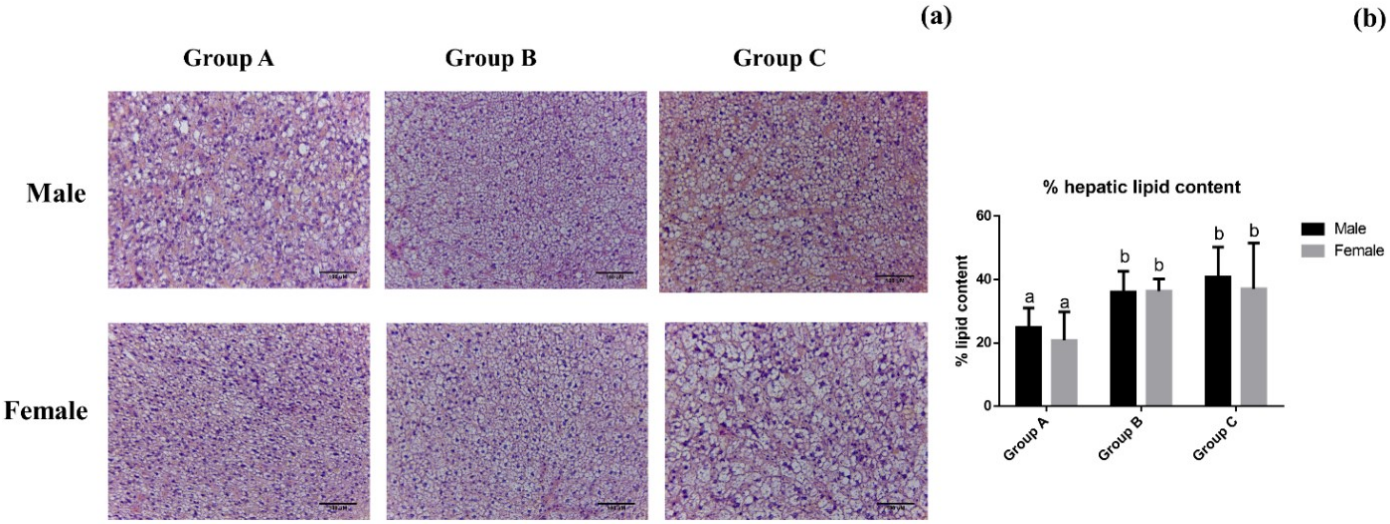

Chapter 5

Published by SCRS/2016/190 Collect. Vol. Sci. Pap. ICCAT, 73(7): **2333-2339 (2017)**

AN UPDATE ON THE LENGTH/WEIGHT RELATIONSHIP FOR BLUEFIN TUNA CAUGHT BY LONGLINERS IN MEDITERRANEAN SEA

Francesco Lombardo[a], Pasquale Baiata[b], Paolo Pignalosa[b], Martina Api[a], Francesca Maradonna[a], Oliana Carnevali[a]

[a] Department of Life and Environmental Sciences (DiSVA)-Università Politecnica delle Marche, Via Brecce Bianche, 60131 Ancona, Italy

[b] OCEANIS Srl, Ercolano (NA), Italy

Corresponding Author: Prof. Oliana Carnevali, Dipartimento di Scienze della Vita e dell'Ambiente, Università Politecnica delle Marche, Via Brecce Bianche, 60131 Ancona, Italy email: o.carnevali@univpm.it tel +390712204990, fax +390712204650

KEYWORDS: *Thunnus thynnus*, length-weight relationship, CFL, SFL, Mediterranean Sea, longliners.

SUMMARY

The present paper represents a continuity of data collection work that started in 2013. Our attempt is to provide a valid length-weight equation to be used for the next stock assessment of the eastern Atlantic and Mediterranean Bluefin tuna (Thunnus thynnus).

Biometric analyses of Curved Fork Length (CFL), Straight Fork Length (SFL) and Round Weight (RWT) were performed in order to update the conversion factors used by ICCAT. Data from 345 specimens were collected by scientific observers aboard the Italian longliner vessels in the Mediterranean during the fishing season of 2016. The length and weight measurements were used for a new CFL/SFL conversion factor, as follows:

$$\mathbf{SFL = 0.9596*CFL+2.0985} \quad (R^2 = 0.9961)$$

Moreover, updated length-weight (SFL-RWT and CFL-RWT) relationships for the Bluefin tuna caught in the central Mediterranean Sea are presented as follow:

$$\mathbf{RWT = 5E^{-05}*SFL^{2.7609}} \quad (R^2 = 0.9828)$$

$$\mathbf{RWT = 6E^{-05}*CFL^{2.7349}} \quad (R^2 = 0.9841)$$

1.Introduction

Bluefin tuna (BFT) stock assessment requires the acquisition and analysis of catch-at-size and catch-at-age data from all BFT fishing industry; such analysis is carried out by the Scientific Committee on Research and Statistics (SCRS) which symbolise the scientific arm of the International Commission for the Conservation of Atlantic Bluefin Tuna (ICCAT).

Biometric studies of length and weight measurements are therefore important for empirical estimates of the catches during the BFT stock assessment.

Stock assessments made by the ICCAT-SCRS for the Atlantic and Mediterranean Bluefin tuna (ABFT) apply different L–W relationship (Parrack and Phares, 1979; Rey & Cort, unpublished; Arena, unpublished).

In recent SCRS Species Group meetings, these equations have been questioned and several new equations have been proposed to the SCRS Working Group (Santos et al., 2004; Aguado-Gimenez & Garcia-Garcia, 2005; Tzoumas et al., 2010; Deguara et al., 2010 and 2012; Galaz, 2012; Cort et al., 2013; Lombardo et al., 2016). Cort et al. (2015) demonstrated that the Arena equation clearly underestimates the weight of the East Atlantic and Mediterranean BFT at specific periods of the year, at different K and in particular during the spawning season.

In view of the above considerations, the authors of the present paper propose an update on the L-W relationship for the Mediterranean Bluefin tuna, caught by Italian longliners in the Mediterranean Sea during the fishing season 2016, suggesting a new conversion factor (SFL-CFL) and two different L-W equations for both Fork Length and Curved Fork Length.

2. Materials and Methods

Data collection was carried out by the scientific staff of OCEANIS Srl and Univpm within a data collection programme started in 2013. The area of study covers the fisheries of BFT in waters around Strait of Sicily, Ionian and Tyrrhenian Sea as well as in authorised landing docks. A total of 345 specimens were sampled and different biometric measurements were collected as: Curved fork length (CFL), Strait Fork Length (SFL) and Round Weight (RWT).

This data were used to work out a new SFL-CFL conversion factor that has been compared to the conversion factor adopted by the ICCAT-SCRS for Atlantic BFT: FL = 0.955*CFL (Parrack et al., 1979).

The Allometric equation was used to fit the SFL/RWT relationship, $W = aL^b$, where W (weight) and L (length) are variables and a and b are parameters. The coefficient of determination (R^2) was used as index of the quality of the estimates.

3. Results and Discussion

It is clear that BFT stock assessment requires the acquisition and analysis of catch-at-size and catch-at-age data from all BFT fisheries.

Figure 1 presents a linear SFL-CFL relationship showing a qualitatively better conversion factor, as indicated by the coefficient of determination, than the equation approved by ICCAT (SFL = 0.955*CFL; Parrack et al., 1979). The authors suggest to take into consideration the new equation for further stock assessments:

$$\boldsymbol{SFL = 0.9596*CFL+2.0985} \quad (R^2 = 0.9961)$$

Figure 2 presents the SFL-RWT relationship for the 2016 dataset used in this study showing better estimates of the data compared to the Arena equation ($RWT = 1.9607E^{-05} *SFL^{3.0092}$) which overestimated the total catches:

$$\boldsymbol{RWT = 5E^{-05}*SFL^{2.7609}} \quad (R^2 = 0.9828)$$

Figure 3 presents the CFL-RWT relationship for the same dataset as follows:

$$\mathbf{RWT = 6E^{-05}*CFL^{2.7349}} \quad (R^2 = 0.9841)$$

Figure 4 shows a comparison of the total BFT biomass, related to the dataset included in this study, calculated applying the Arena equation ($RWT = 1.9607E^{-05} * SFL^{3.0092}$) and the Italian equation ($RWT = 5E^{-05} * SFL^{2.7609}$) compared to the real total biomass caught.

4. Conclusions

These data and equations can be a valuable contribution to the advancement of knowledge in the evaluation of BFT population in the Mediterranean and can be incorporated into the catch-at-size analysis and database to be used at future BFT stock assessment sessions.

It should be noted that the utilization of the length-weight relationship adopted by the ICCAT-SCRS seems to overestimate the real BFT biomass caught by Italian longliners by up to 24.2% while the italian equation underestimated it by 10.5%. This can greatly impact future BFT stock assessments.

5. Acknowledgments

The authors wish to thank those persons and groups who made possible the data collection included and analysed in the present work.
The Masters and National Observers of Longliner Vessels.

References

Aguado-Gimenez, F. and Garcia-Garcia, B. 2005. Changes in some morphometric relationships in Atlantic bluefin tuna (*Thunnus thynnus thynnus* Linnaeus, 1758) as a result of fattening process. Aquaculture, 249: 303-309.

Arena, P. Unpublished. In: Length-weight relationships adopted by the SCRS for major species. http://iccat.int/Documents/SCRS/Manual/Appendices/Appendix%204%20III%20Length-weight.pdf

Cort, J.L., Deguara, S., Galaz, T., Mèlich, B., Artetxe, I., Arregi, I., et al. 2013. Determination of Lmax for Atlantic Bluefin Tuna, *Thunnus thynnus* (L.), from Meta-Analysis of Published and Available Biometric Data, Reviews in Fisheries Science, 21: 2, 181-212.

Cort, J. L., V. D. Estruch, M. N. Santos, A. Di Natale, N. Abid, J. M. de la Serna. 2015. On the variability of the length-weight relationship for Atlantic bluefin tuna, *Thunnus thynnus* (L.). Reviews in Fisheries Science & Aquaculture 23:1, 23–38.

Deguara, S., Caruana, S. and Agius, C. 2010. An appraisal of the use of length-weight relationships to determine growth in fattened Atlantic bluefin tuna, *Thunnus thynnus* L.. Collect. Vol. Sci. Pap. ICCAT, 65(3): 776- 781.

Deguara, S., Gatt, M., Caruana, S., Agius, C. 2012. Changes in length-weight relationships of atlantic bluefin tuna, *Thunnus thynnus*, caught by maltese longliners during the years 2008-2011. Collect. Vol. Sci. Pap. ICCAT, 68(1): 223-229.

Galaz, T. 2012. Eleven years –1995-2005- of experience on growth of bluefin tuna (Thunnus thynnus) in farms. Collect. Vol. Sci. Pap. ICCAT, 68 (1): 163-175.

Lombardo, F., Baiata, P., Oliveri, A., and Pignalosa, P. 2016. Length/weight relationship for bluefin tuna caught by longliners in central Mediterranean Sea. Collect. Vol. Sci. Pap. ICCAT, 72 (7): 1815-1822.

Parrack, M. and Phares, P. 1979. Aspects of the growth of Atlantic bluefin tuna determined from mark-recapture data. Collect. Vol. Sci. Pap. ICCAT, 8 (2): 356-366.

Rey, J.C. and Cort, J. L. Unpublished. In: Length-weight relationships adopted by the SCRS for major species. http://iccat.int/Documents/SCRS/Manual/Appendices/Appendix%204%20III%20Length-weight.pdf

Santos dos, M.N., Garcia, A., Lino, P.G. and Hirofumi, M. 2004, Length-weight relationships and weight conversion factors for bluefin tuna (*Thunnus thynnus thynnus*) from the Algarve: prior to and after fattening. Collect. Vol. Sci. Pap. ICCAT, 56 (3): 1089-1095.

Tzoumas, A., Ramfos, A, De Metrio, G., Corriero, A., Spinos, E., Vavassis, C., and Katselis G. 2010. Weight growth of Atlantic bluefin tuna (*Thunnus thynnus*, L. 1758) as a result of a 6-7 months fattening process in central Mediterranean. Collect. Vol. Sci. Pap. ICCAT, 65(3): 787-800.

Figures

Figure 1. SFL-CFL relationship (*SFL = 0.9596*CFL+2.0985*; $R^2 = 0.9961$) for Mediterranean Bluefin tuna.

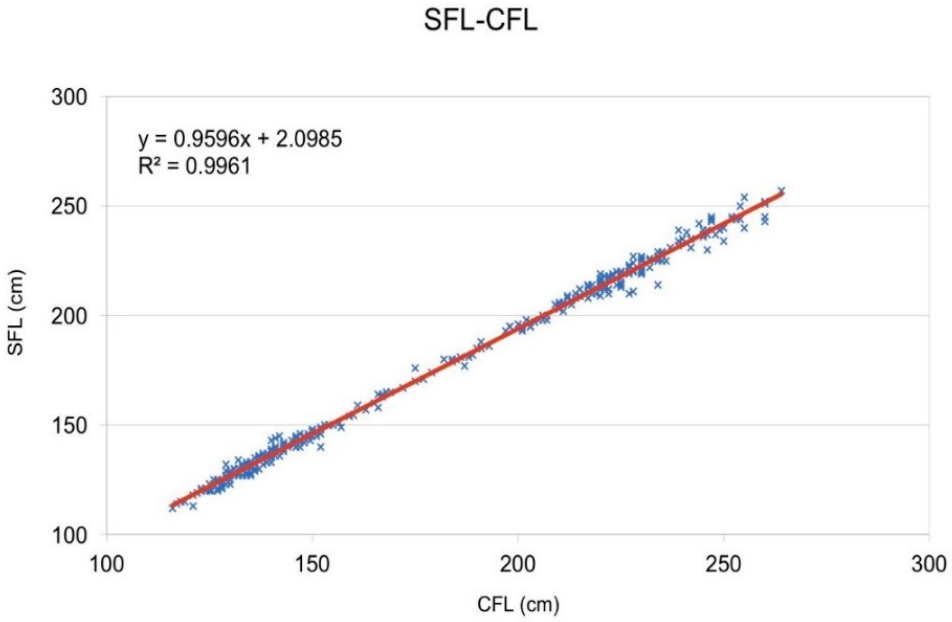

Figure 2. SFL-RWT relationship (*RWT = 5E-05*SFL^2.7609*; $R^2 = 0.9828$) for the Mediterranean Bluefin tuna.

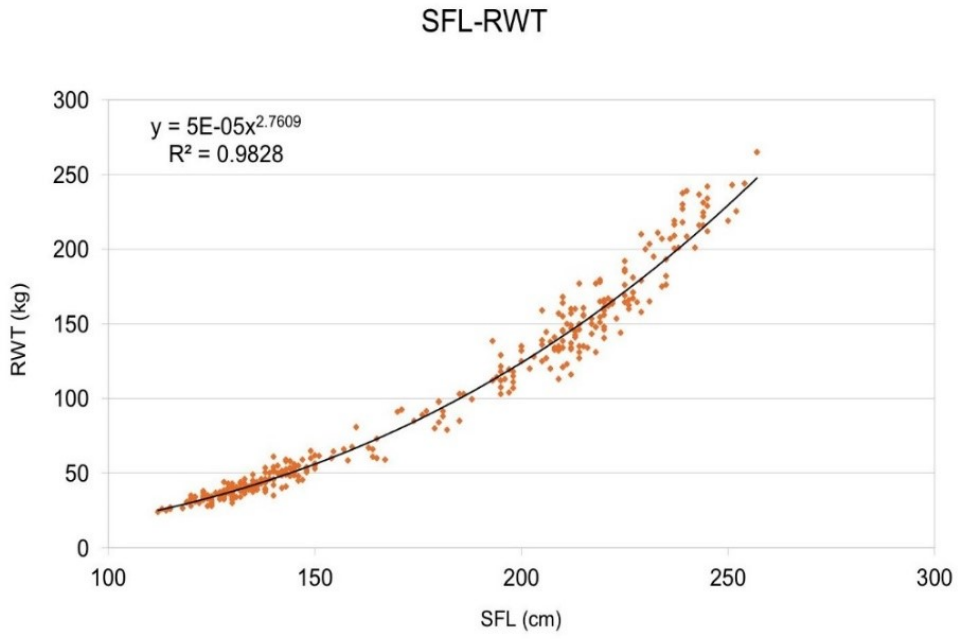

Figure 3. CFL-RWT relationship ($RWT = 6E^{-05} * CFL^{2.7349}$; $R^2 = 0.9841$) for the Mediterranean Bluefin tuna.

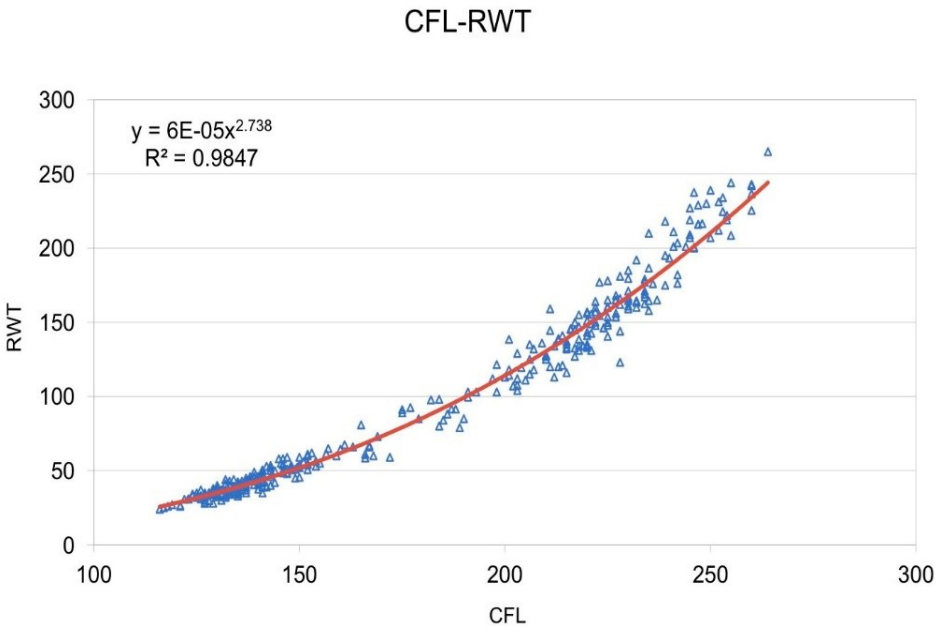

Figure 4. Biomass comparison when using different L-W relationships for Mediterranean Bluefin tuna. Arena equation ($RWT = 1.9607E^{-05} * SFL^{3.0092}$) and the Italian equation ($RWT = 5E^{-05} * SFL^{2.7609}$).

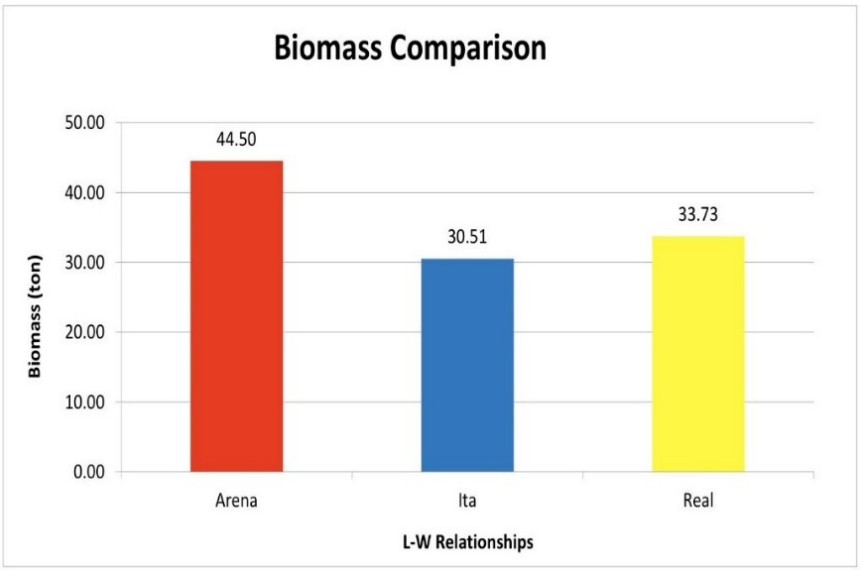

Conclusions and final remarks

This thesis aimed to investigate the effects of aging on growth and reproduction in two experimental models: *Nothobranchius furzeri* , a small freshwater fish whose lifespan is very short and peculiar life cycle, considered one of the best model for aging study, and a marine fish model, *Thunnus thynnus* a long-life pelagic marine species of high commercial value whose conservation is indispensable due overfishing.

The data presented in **Chapter 1** demonstrated that phenotypic plasticity during embryogenesis in *N. furzeri* is influenced by parental aging, underlying that diapause II occurs in most embryos from old parents, slowing their developmental time course. The remarkable phenotypic differences related to the embryonic development from different-age parents, evidenced in this chapter, could be linked to a different epigenetic effects that occur in embryos. Moreover, our results underline that the developmental plasticity could affects growth process during adult life in a gender-specific manner. Results evidenced that growth was more pronounced in females than males. In **Chapter 2** we also demonstrated that F1 females from young parents reached sexual maturity before than F1 females from old parents. These parental-age effects on offspring growth and sexual maturity were probably due to different maternal energy allocation regulated via germ cell. At this purpose, in **Chapter 3** we investigated macromolecular composition differences in not fertilized oocytes between old and young females using Raman micro spectroscopy technique**.** Results obtained showed clear differences related to protein composition, lipid and carotenoids content, suggesting a lack in the proper oocyte content that could affect the embryonic development, underlying the age-induced decline in oocyte quality from old females. These findings reflect age-specific breeder differences in reproductive performance illustrated in **Chapter 2**. Maternal-age contribution was relevant in terms of fecundity and embryo quality, resulting in best success of embryonic survival and hatching rate from young females.

Taking all these together, this work using *N. furzeri* revealed the transgenerational influence that parental aging reflect to offspring traits is a result of evolutionary strategy to hostile habitats and support survival across multiple generations.

Considering that recent genome sequencing data highlights several common signaling pathways between *N. furzeri* and mammals; this model represents a valid alternative to human cells and can consequently avoid any related ethical issue.

Future works are needed to understand molecular and epigenetic mechanisms that can promote phenotypic plasticity related to parental age to better understand the factors transmitted via germ cell to progeny and improve the knowledge on the complex mechanism of aging.

The second part of my PhD thesis involved studies on catch-at-size and catch-at-age of *Thunnus thynnus* within the framework of the "observer program" supported by MIPAAF (Ministry of Agricultural, Food and Forestry Policies, Italy).

In **Chapter 4**, focus was addressed to growth studies related to aging in ABFT. It is established that ABFT growth rate was higher during the first 8 years of life after which their growth decreased. In fact, after this age, tunas use their metabolic energies mainly for adding fat. Moreover, gender growth differences emerged. Molecular analysis revealed that genes involved in growth including *igf1, igf1r* and *mTOR* were differentially expressed in relation with the ABFT age.

Finally, a valuable contribution for tuna stock assessment emerged in **Chapter 5.** New equation updated to growth (length-weight relationships) for the Bluefin tuna was presented.

In conclusion, the second part of this PhD project, which deals with the practical aspect of fisheries and aquaculture, we foresee to find benefit in aquaculture industry and in fishery organization involved in tunas species.

One of the objectives of aquaculture facilities is to increase the fat content of tuna in order to satisfy mainly the eastern market (e.g. Japan). Here, we suggest the "ideal age" and the related size by which tuna reach the best fattening and the additionally differences in the IGF system associated with ABFT age can be one of the factors that needs to be taken into consideration for improving farming strategies.

Finally, we proposed a new equation that was then adopted by ICCAT (International Commission for the Conservation of Atlantic Tunas), the most important organization for tuna management, in 2016. With the introduction of our equation, we intend to estimate the real BFT biomass as the past equation used overestimates the real biomass and this can greatly impact future BFT stock assessments.

In conclusion, these results could represent an enlarged set of basic and applied research opportunities from shedding light on evolutionary biology to limit the recent ABFT tuna overfishing increasing trend.

List of publications

- ✓ Api M., Bonfanti E., Lombardo F., Pignalosa P., Hardiman G., Carnevali O. (2018) Effects of age on growth in Atlantic Bluefin tuna *(Thunnus thynnus*). Gen Comp Endocr *In press:* **doi.org/10.1016/j.ygcen.2018.01.010**

- ✓ Api M., Biondi P., Olivotto I., Terzibasi E., Cellerino A., Carnevali O. (2017) Effects of Parental Aging During Embryo Development and Adult Life: The Case of *Nothobranchius furzeri.* Zebrafish, vol.0, No.0 **doi.org/10.1089/zeb.2017.1494**

- ✓ Lombardo F., Baiata P., Pignalosa P., Api M., Maradonna F., Carnevali O. (2017) An Update on the Length/Weight Relationship for Bluefin tuna Caught by Longliners in Mediterranean Sea. **SCRS/2016/190 Collect. Vol. Sci. Pap. ICCAT, 73(7): 2333-2339**

- ✓ Api M., Notarstefano V., Olivotto I., Cellerino A., Carnevali O. (2018) Breeders age affects reproductive success in *Nothobranchius furzeri.*
  Submitted to Aging Cell Journal: **ID ACE-18-0036 under *Review***

- ✓ "Molecular differences in *Nothobranchius furzeri* oocytes: influence of maternal age"
  Paper in preparation